Appendix C
Dipole Calibration Certificate

Calibration File No: DC-596
Project Number: APREL-ALSAS10U

CERTIFICATE OF CALIBRATION

It is certified that the equipment identified below has been calibrated in the **NCL CALIBRATION LABORATORIES** by qualified personnel following recognized procedures and using transfer standards traceable to NRC/NIST.

APREL Validation Dipole

Manufacturer: APREL Laboratories
Part number: ALS-D-2450-S-2
Frequency: 2450 MHz
Serial No: 2450-220-00754

Customer: APREL

Calibrated: 4th March 2005
Released on: 4th March 2005

Released By: _____

NCL CALIBRATION LABORATORIES

51 SPECTRUM WAY
NEPEAN, ONTARIO
CANADA K2R 1E6

Division of APREL Lab.
TEL: (613) 820-4988
FAX: (613) 820-4162

Conditions

Dipole 2450-220-00754 was new and taken from stock prior to calibration.

Ambient Temperature of the Laboratory: 22 °C +/- 0.5°C
Temperature of the Tissue: 21 °C +/- 0.5°C

We the undersigned attest that to the best of our knowledge the calibration of this device has been accurately conducted and that all information contained within this report has been reviewed for accuracy.

Stuart Nicol

Director Product Development

D. Brooks

Member of Engineering Staff

(Calibration Engineer)

51 Spectrum Way
Ottawa ON Canada K2R 1E6
www.aprel.com
info@aprel.com
Phone (613) 820-2730
Fax (613) 820-4161

Calibration Results Summary

The following results relate the Calibrated Dipole and should be used as a quick reference for the user.

Mechanical Dimensions

Length: 51.5 mm
Height: 30.4 mm

Electrical Specification

SWR: 1.16 U
Return Loss: -22.7 dB
Impedance: 48.7 Ω

System Validation Results

Frequency	1 Gram	10 Gram	Peak
2450 MHz	5.31	2.44	10.18

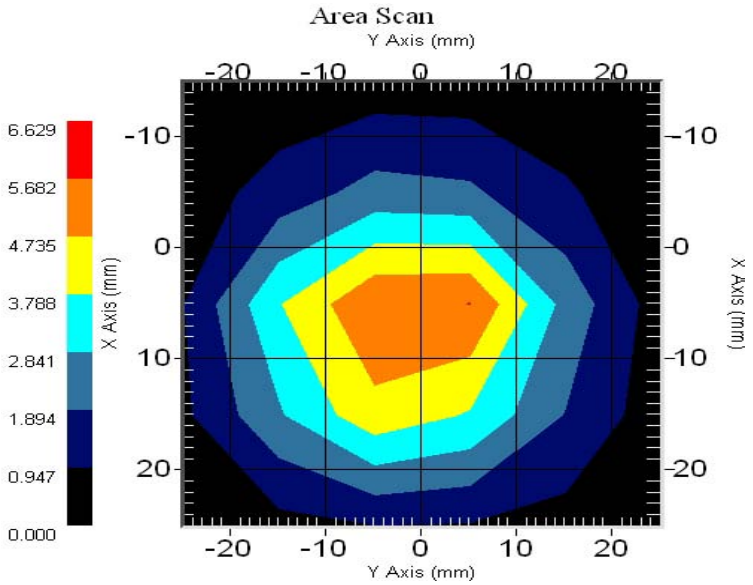

Introduction

This Calibration Report has been produced in line with the SSI Dipole Calibration Procedure SSI-TP-018-ALSAS. The results contained within this report are for Validation Dipole 2450-220-00754. The calibration routine consisted of a three-step process. Step 1 was a mechanical verification of the dipole to ensure that it meets the mechanical specifications. Step 2 was an Electrical Calibration for the Validation Dipole, where the SWR, Impedance, and the Return loss were assessed. Step 3 involved a System Validation using the ALSAS-10U, along with APREL E-020 130 MHz to 26 GHz E-Field Probe Serial Number 212.

References

SSI-TP-018-ALSAS Dipole Calibration Procedure
SSI-TP-016 Tissue Calibration Procedure
IEEE 1528 “Recommended Practice for Determining the Peak Spatial-Average Specific Absorption Rate (SAR) in the Human Body Due to Wireless Communications Devices: Experimental Techniques”

Conditions

Dipole 2450-220-00754 was new taken from stock.

Ambient Temperature of the Laboratory: 22 °C +/- 0.5°C
Temperature of the Tissue: 20 °C +/- 0.5°C

Dipole Calibration Results

Mechanical Verification

APREL Length	APREL Height	Measured Length	Measured Height
51.5 mm	30.4 mm	52.1 mm	30.6 mm

Tissue Validation

Head Tissue 2450 MHz	Measured
Dielectric constant, ε_r	39.2
Conductivity, σ [S/m]	1.80

Electrical Calibration

Test	Result
S11 R/L	-22.7 dB
SWR	1.16 U
Impedance	48.7 Ω

The Following Graphs are the results as displayed on the Vector Network Analyzer.

S11 Parameter Return Loss

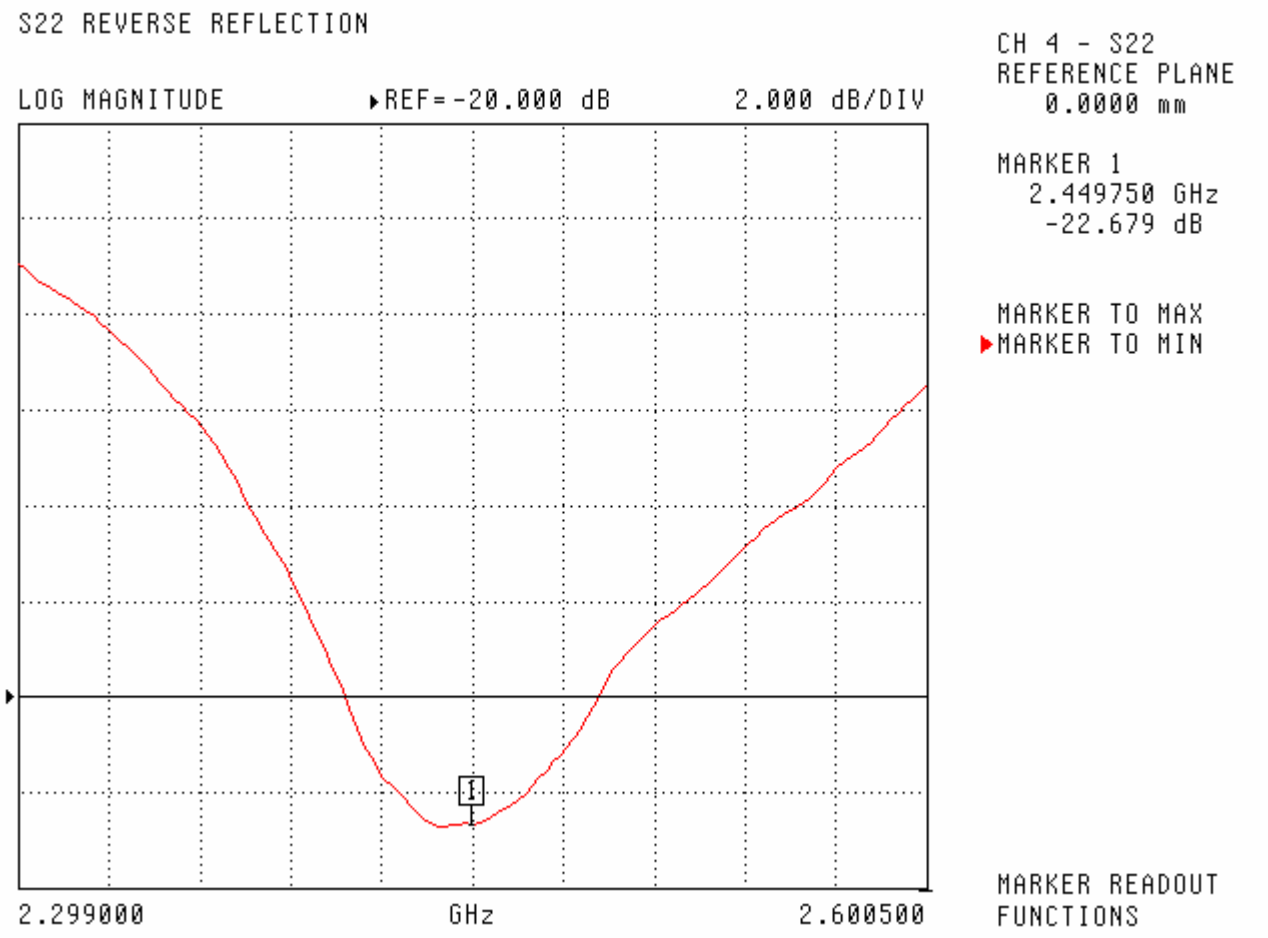

SWR

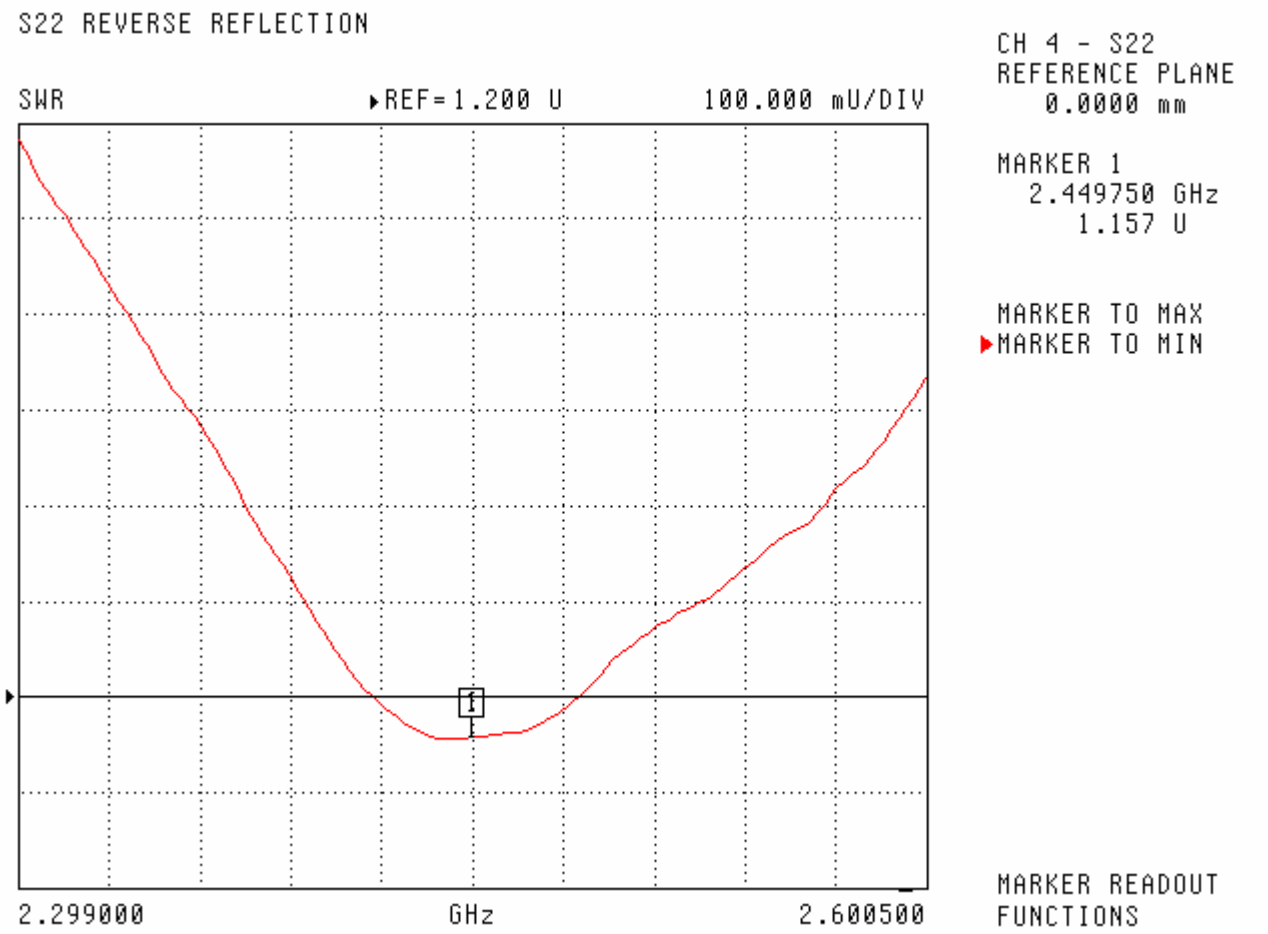

Smith Chart Dipole Impedance

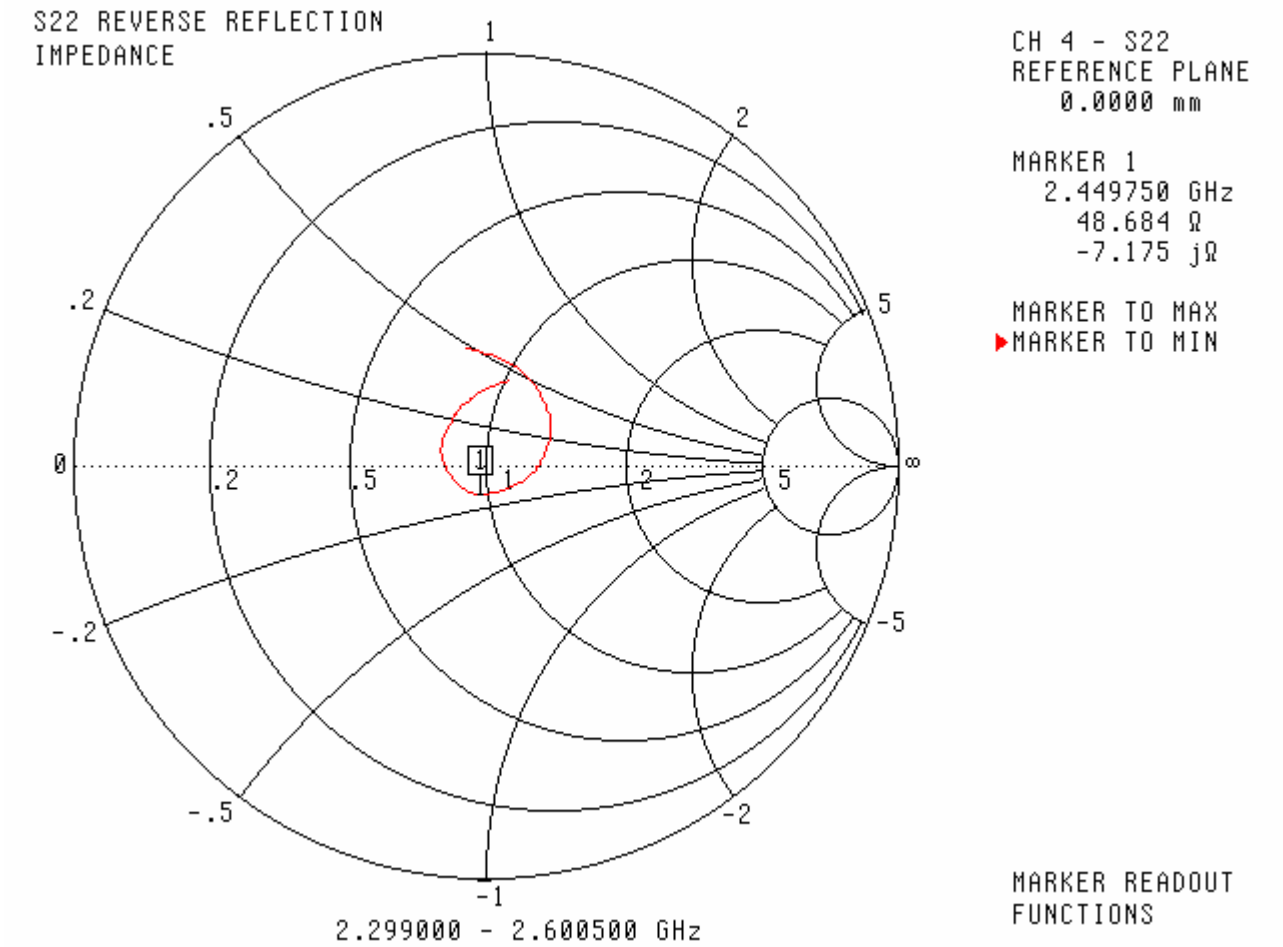

System Validation Results Using the Electrically Calibrated Dipole

Head Tissue Frequency	1 Gram	10 Gram	Peak Above Feed Point
2450 MHz	5.31	2.44	10.18

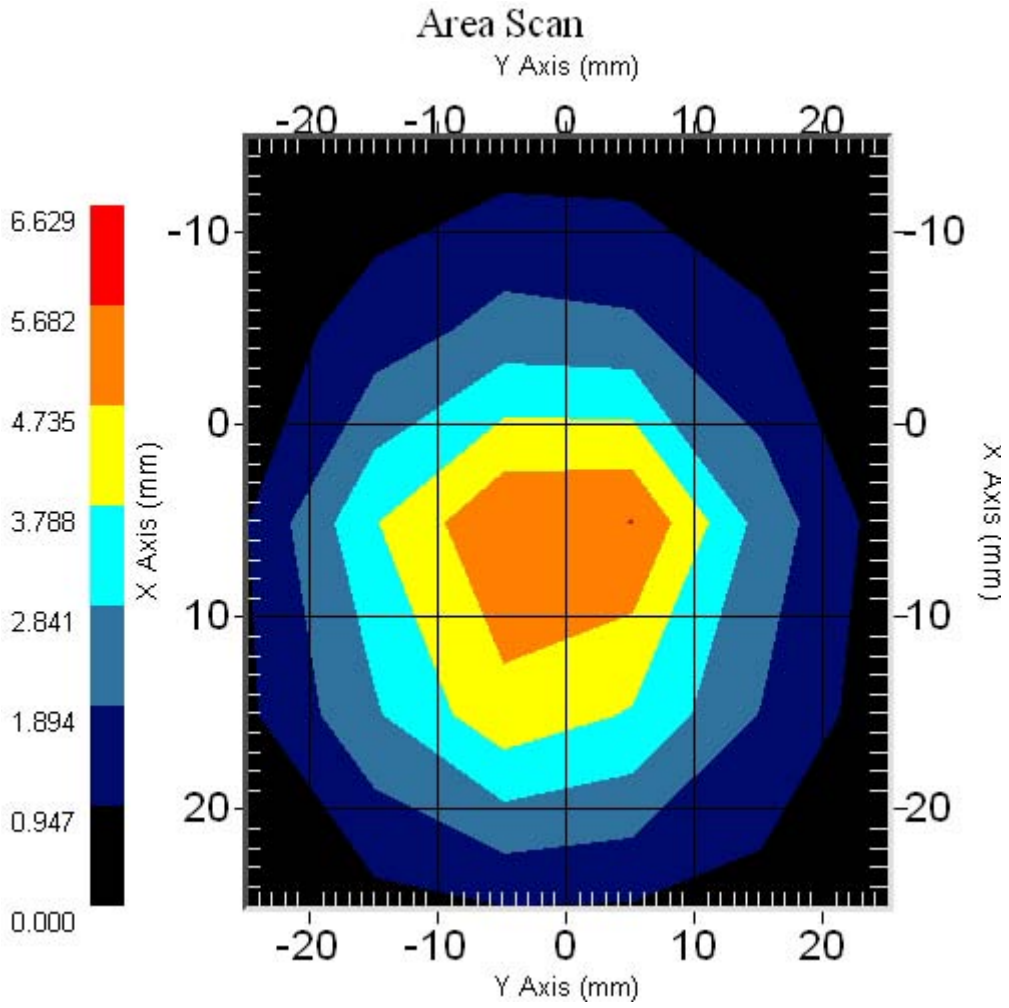

Test Equipment

The test equipment used during Probe Calibration, manufacturer, model number and, current calibration status are listed and located on the main APREL server R:\NCL\Calibration Equipment\Instrument List May 2005

NCL CALIBRATION LABORATORIES

Calibration File No: DC-599
Project Number: APREL-ALSAS 10U

CERTIFICATE OF CALIBRATION

It is certified that the equipment identified below has been calibrated in the **NCL CALIBRATION LABORATORIES** by qualified personnel following recognized procedures and using transfer standards traceable to NRC/NIST.

APREL Validation Dipole

Manufacturer: APREL Laboratories
Part number: ALS-D-5258-S-2
Frequency: 5.2GHz to 5.8GHz
Serial No: 5258-235-00802

Customer: APREL

Calibrated: 24th May 2005
Released on: 24th May 2005

Released By: _____

NCL CALIBRATION LABORATORIES
51 SPECTRUM WAY
NEPEAN, ONTARIO
CANADA K2R 1E6
Division of APREL Lab.
TEL: (613) 820-4988
FAX: (613) 820-4162

Conditions

Dipole 5258-235-00802 was new and taken from stock prior to calibration.

Ambient Temperature of the Laboratory: 22 °C +/- 0.5°C
Temperature of the Tissue: 21 °C +/- 0.5°C

We the undersigned attest that to the best of our knowledge the calibration of this device has been accurately conducted and that all information contained within this report has been reviewed for accuracy.

Stuart Nicol

Director Product Development

D. Brooks

Member of Engineering Staff

(Calibration Engineer)

51 Spectrum Way
Ottawa ON Canada K2R 1E6
www.aprel.com
info@aprel.com
Phone (613) 820-2730
Fax (613) 820-4161

Calibration Results Summary

The following results relate the Calibrated Dipole and should be used as a quick reference for the user.

Mechanical Dimensions

Length: 23.3 mm
Height: 20.3 mm

Electrical Specification

SWR: 1.22 U
Return Loss: -20.0 dB
Impedance: 50.0 Ω

System Validation Results

Frequency	1 Gram	10 Gram	Peak
5200 MHz	62.9	17.9	223.1

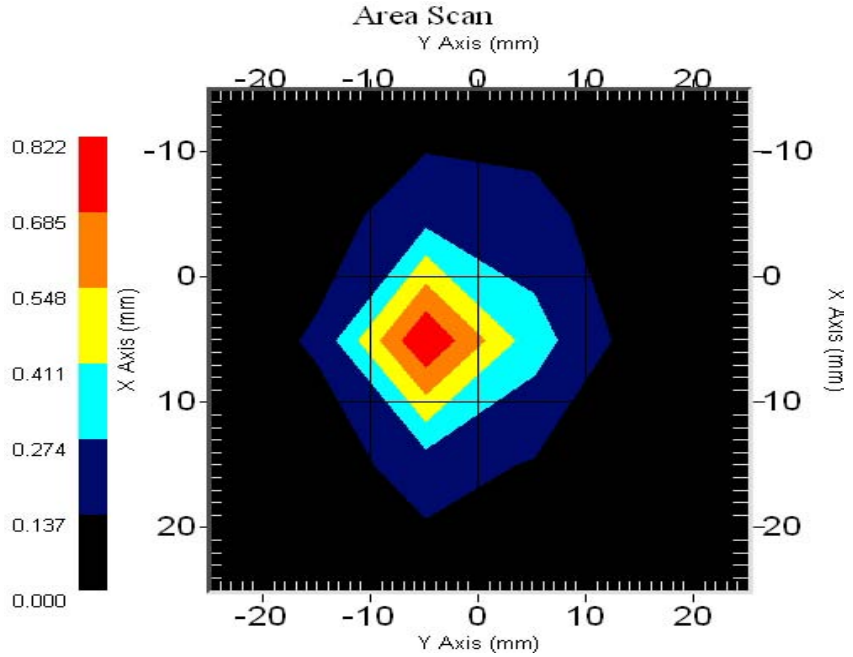

Frequency	1 Gram	10 Gram	Peak
5800 MHz	58.3	18	207.1

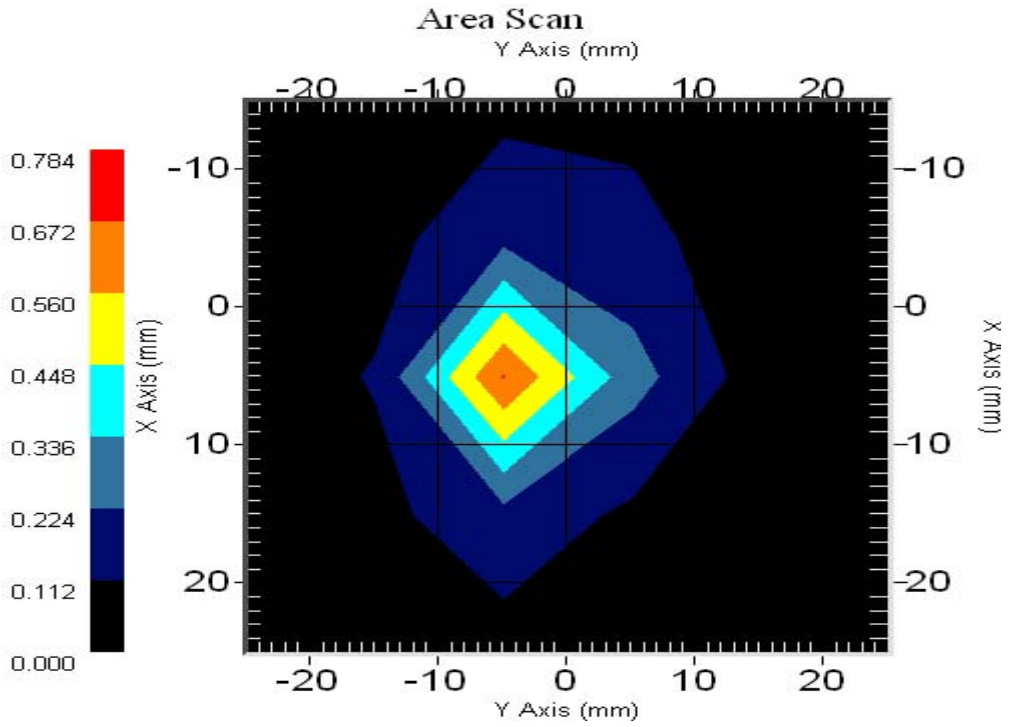

Introduction

This Calibration Report has been produced in line with the SSI Dipole Calibration Procedure SSI-TP-018-ALSAS. The results contained within this report are for Validation Dipole 5258-235-00802. The calibration routine consisted of a three-step process. Step 1 was a mechanical verification of the dipole to ensure that it meets the mechanical specifications. Step 2 was an Electrical Calibration for the Validation Dipole, where the SWR, Impedance, and the Return loss were assessed. Step 3 involved a System Validation using the ALSAS-10U, along with APREL E-020 130 MHz to 26 GHz E-Field Probe Serial Number 212.

References

SSI-TP-018-ALSAS Dipole Calibration Procedure
SSI-TP-016 Tissue Calibration Procedure
IEEE 1528 “Recommended Practice for Determining the Peak Spatial-Average Specific Absorption Rate (SAR) in the Human Body Due to Wireless Communications Devices: Experimental Techniques”

Conditions

Dipole 5258-235-00802 was new taken from stock.

Ambient Temperature of the Laboratory: 22 °C +/- 0.5°C
Temperature of the Tissue: 20 °C +/- 0.5°C

Dipole Calibration Results

Tissue Validation

Head Tissue 5200 MHz	Measured
Dielectric constant, ε_r	35.3
Conductivity, σ [S/m]	5.30

Head Tissue 5800 MHz	Measured
Dielectric constant, ε_r	35.3
Conductivity, σ [S/m]	5.30

Mechanical Verification

APREL Length	APREL Height	Measured Length	Measured Height
23.1 mm	20.7 mm	23.3 mm	20.3 mm

Electrical Calibration

S11	5200MHz	5800MHz
RL (dB)	-21.16	-22.34
SWR	1.2	1.17
Impedance (ohms)	51.38	43.92

The Following Graphs are the results as displayed on the Vector Network Analyzer.

S11 Parameter Return Loss

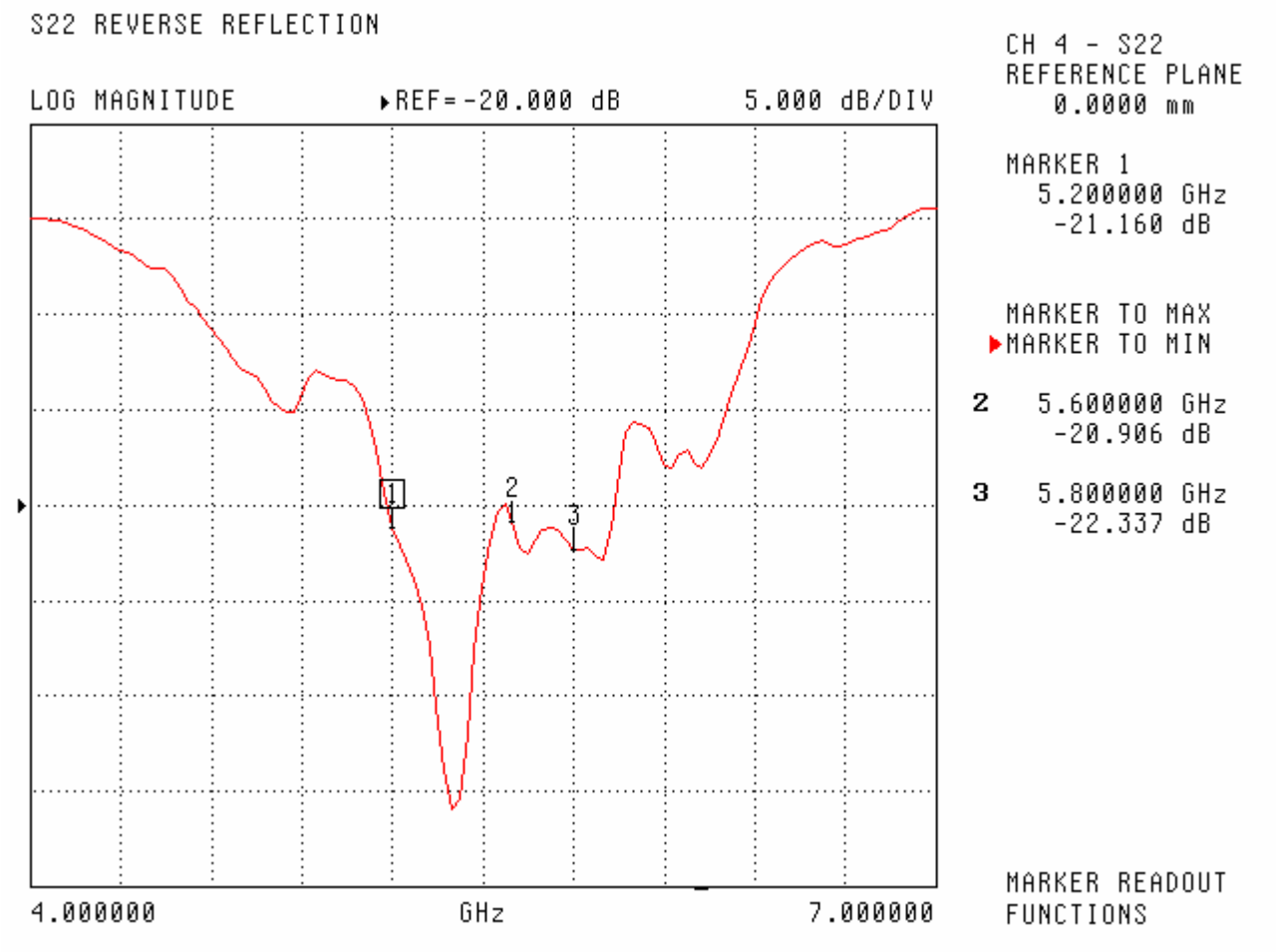

SWR

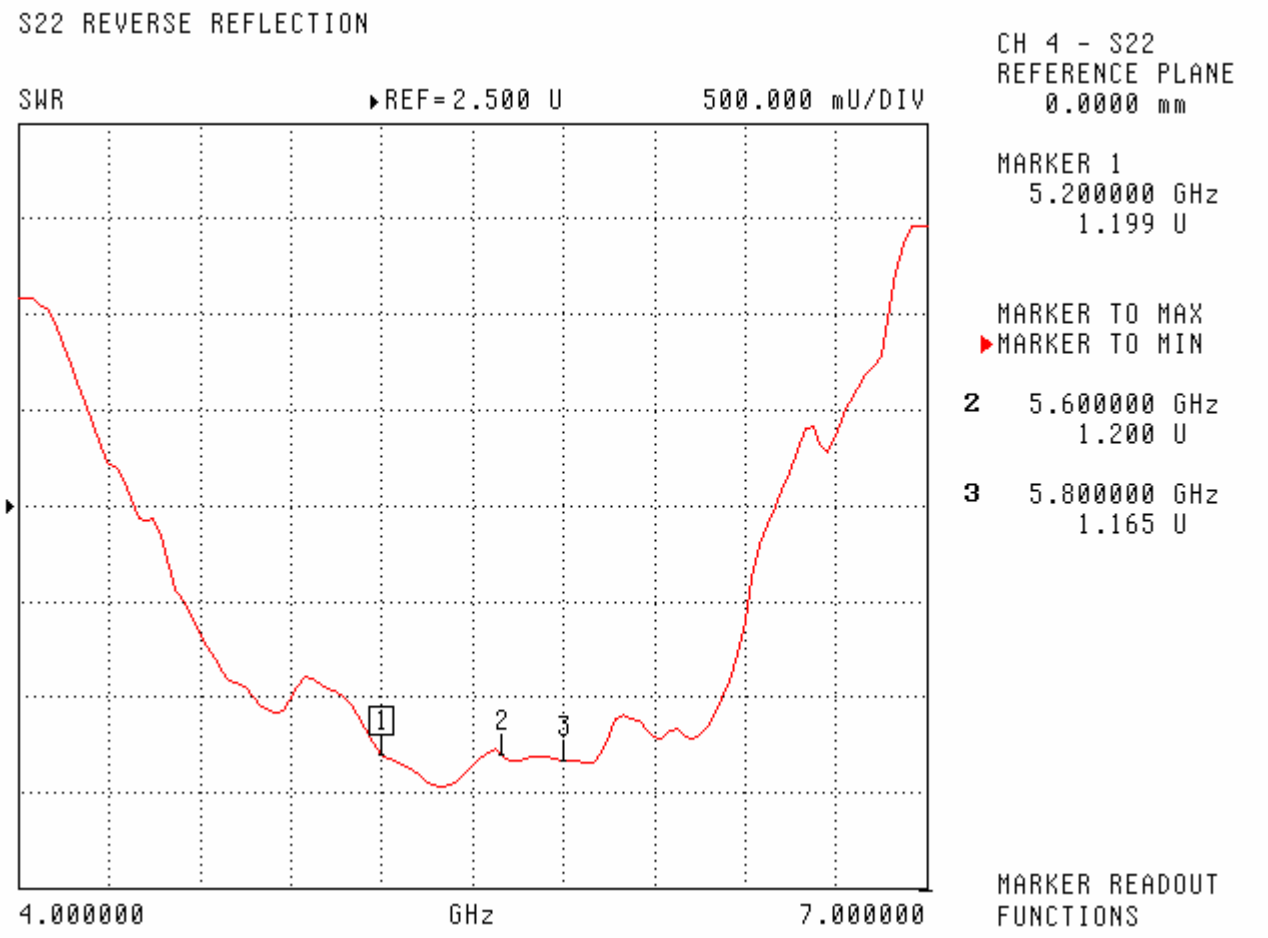

Smith Chart Dipole Impedance

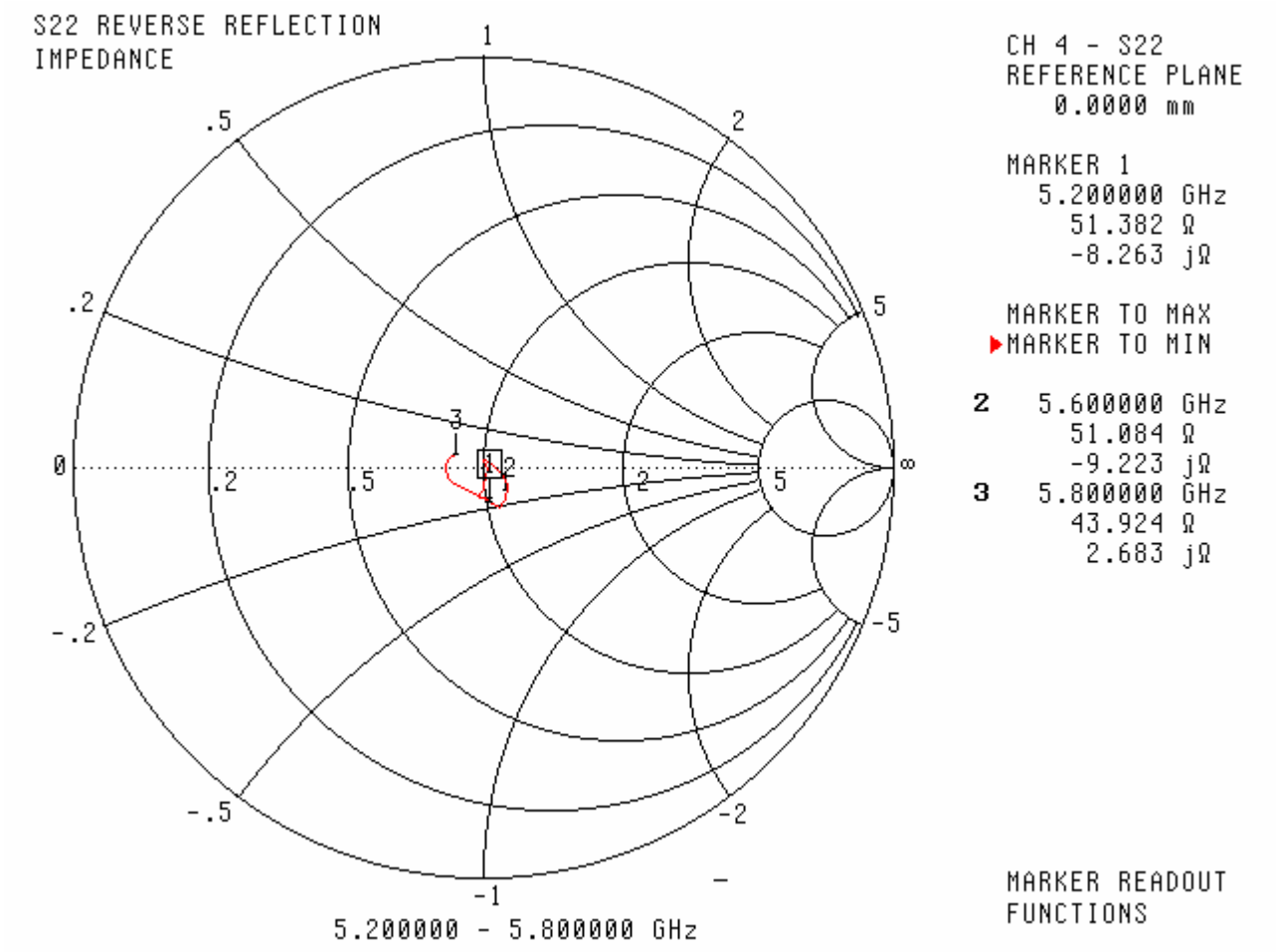

Test Equipment

The test equipment used during Probe Calibration, manufacturer, model number and, current calibration status are listed and located on the main APREL server R:\NCL\Calibration Equipment\Instrument List May 2004

Appendix D
Probe Calibration Certificate

NCL CALIBRATION LABORATORIES

Calibration File No.: CP-616

Client.: APREL

CERTIFICATE OF CALIBRATION

It is certified that the equipment identified below has been calibrated in the **NCL CALIBRATION LABORATORIES** by qualified personnel following recognized procedures and using transfer standards traceable to NRC/NIST.

Equipment: Miniature Isotropic RF Probe 2450 MHz

Manufacturer: APREL Laboratories
Model No.: E-020
Serial No.: 209

BODY Calibration

Calibration Procedure: SSI/DRB-TP-D01-032-E020
Project No: Internal

Calibrated: 10th March 2005
Released on: 10th March 2005

This Calibration Certificate is Incomplete Unless Accompanied with the Calibration Results Summary

Released By: _____

***NCL* CALIBRATION LABORATORIES**
51 SPECTRUM WAY
NEPEAN, ONTARIO
CANADA K2R 1E6

Division of APREL Lab.
TEL: (613) 820-4988
FAX: (613) 820-4161

Introduction

This Calibration Report reproduces the results of the calibration performed in line with the SSI/DRB-TP-D01-032-E020-V2 E-Field Probe Calibration Procedure. The results contained within this report are for APREL E-Field Probe E-020 260.

References

SSI/DRB-TP-D01-032-E020-V2 E-Field Probe Calibration Procedure
IEEE 1528 “Recommended Practice for Determining the Peak Spatial-Average Specific Absorption Rate (SAR) in the Human Head Due to Wireless Communications Devices: Experimental Techniques”
SSI-TP-011 Tissue Calibration Procedure

Conditions

Probe 260 was a new probe taken from stock prior to calibration.

Ambient Temperature of the Laboratory: 22 °C +/- 0.5°C
Temperature of the Tissue: 21 °C +/- 0.5°C

We the undersigned attest that to the best of our knowledge the calibration of this probe has been accurately conducted and that all information contained within this report has been reviewed for accuracy.

Stuart Nicol

Y. Pan

Calibration Results Summary

Probe Type:	E-Field Probe E-020
Serial Number:	260
Frequency:	5800 MHz
Sensor Offset:	1.56 mm
Sensor Length:	2.5 mm
Tip Enclosure:	Ertalyte*
Tip Diameter:	<4.9 mm
Tip Length:	60 mm
Total Length:	290 mm

*Resistive to recommended tissue recipes per IEEE-1528

Sensitivity in Air

Channel X:	1.2 $\mu V/(V/m)^2$
Channel Y:	1.2 $\mu V/(V/m)^2$
Channel Z:	1.2 $\mu V/(V/m)^2$
Diode Compression Point:	95 mV

Sensitivity in Body Tissue

Frequency: 2450 MHz

Epsilon: 50.6 (+/-5%) **Sigma:** 1.98 S/m (+/-10%)

ConvF

Channel X: 5.0

Channel Y: 5.0

Channel Z: 5.0

Tissue sensitivity values were calculated using the load impedance of the APREL Laboratories Daq-Paq.

Boundary Effect:

Uncertainty resulting from the boundary effect is less than 2% for the distance between the tip of the probe and the tissue boundary, when less than 2.4mm.

Spatial Resolution:

The measured probe tip diameter is 5 mm (+/- 0.01 mm) and therefore meets the requirements of SSI/DRB-TP-D01-032 for spatial resolution.

Receiving Pattern 2450 MHz (Air)

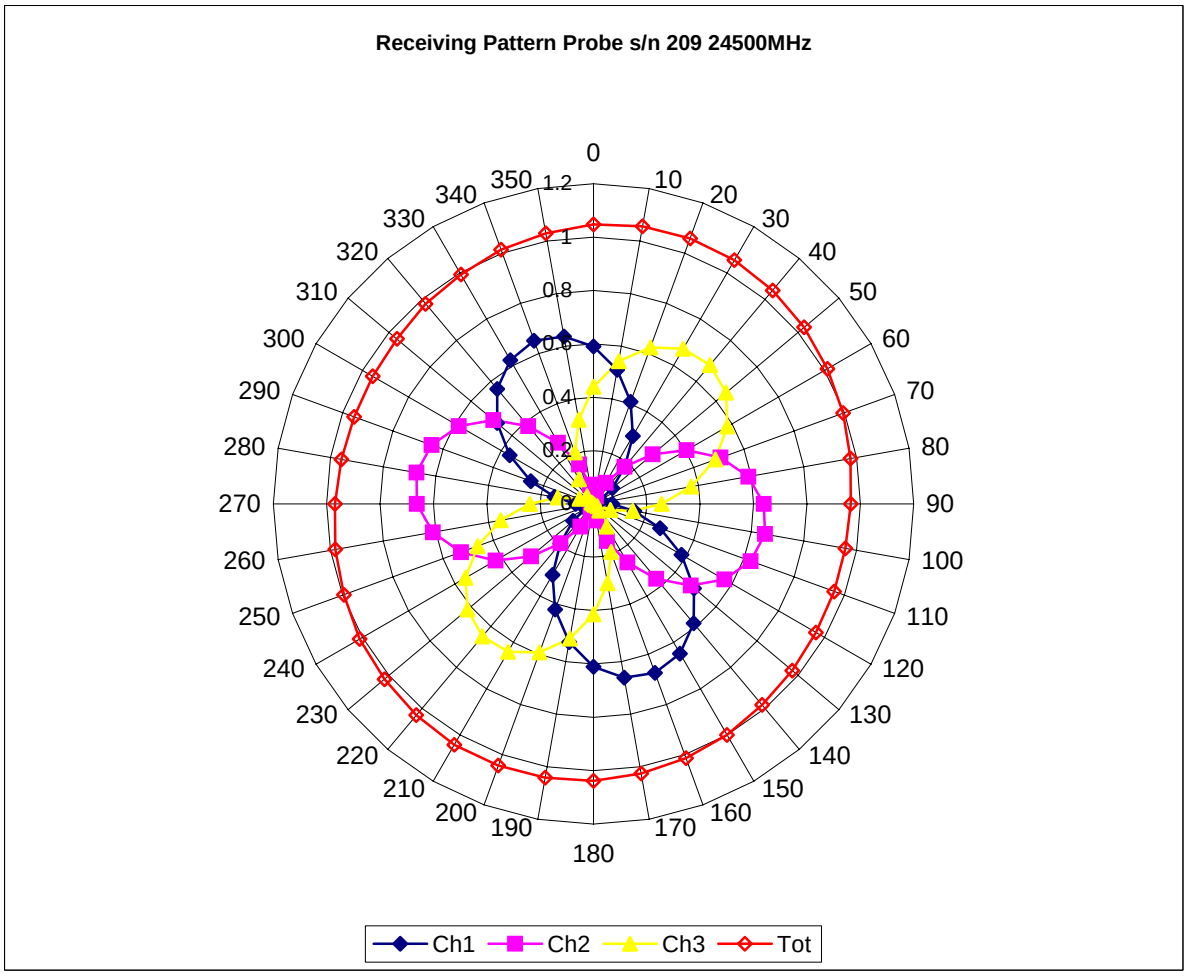

Isotropy Error 2450 MHz (Air)

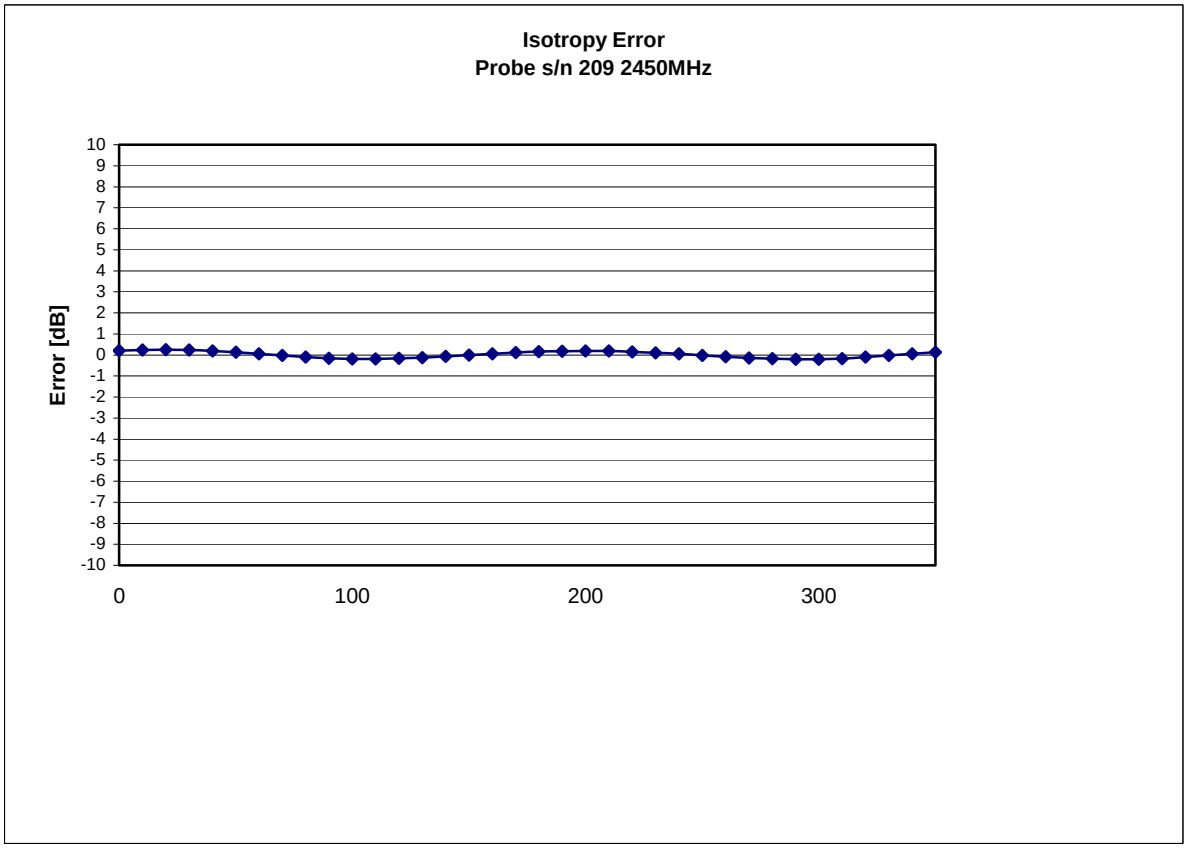

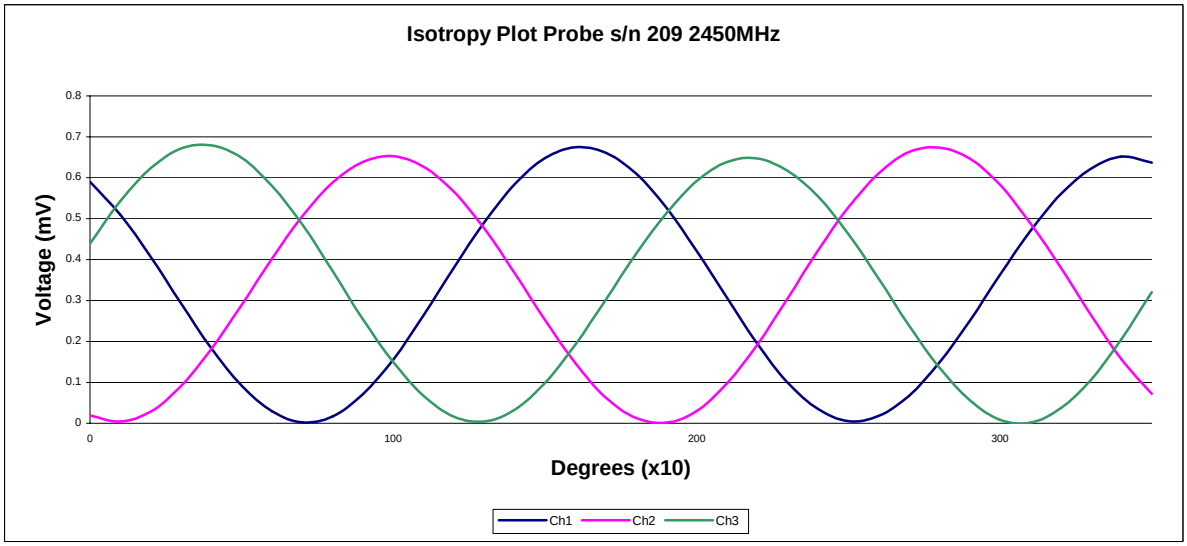

Isotropicity: 0.10 dB

Dynamic Range

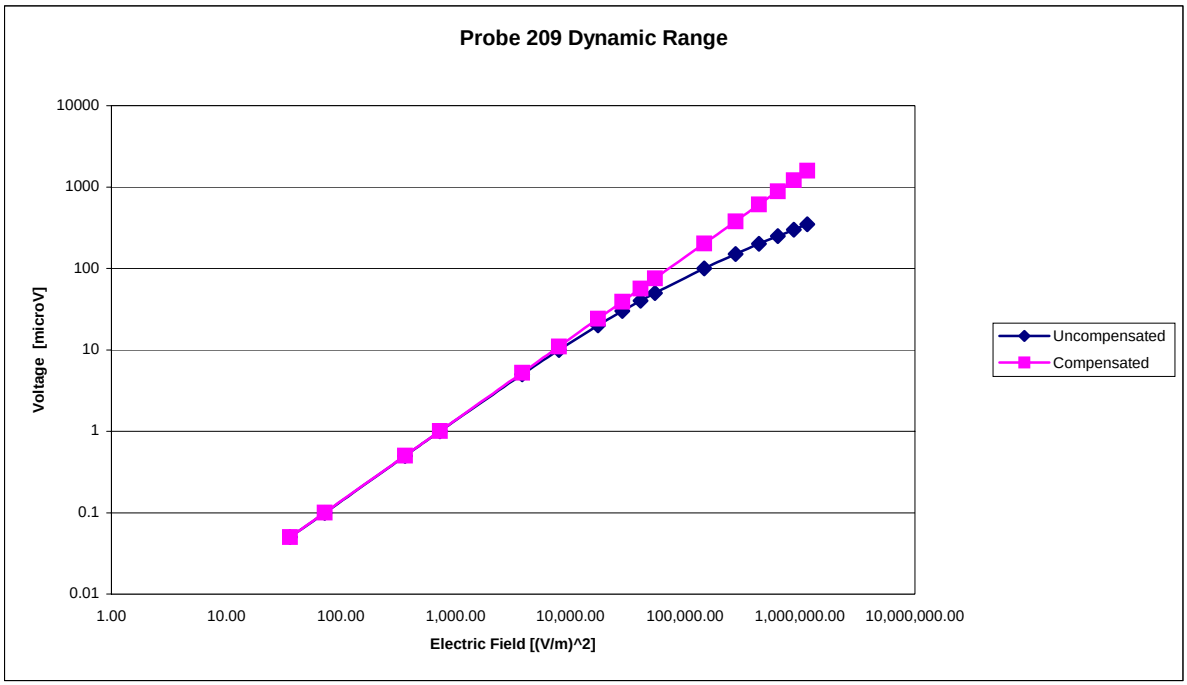

Video Bandwidth

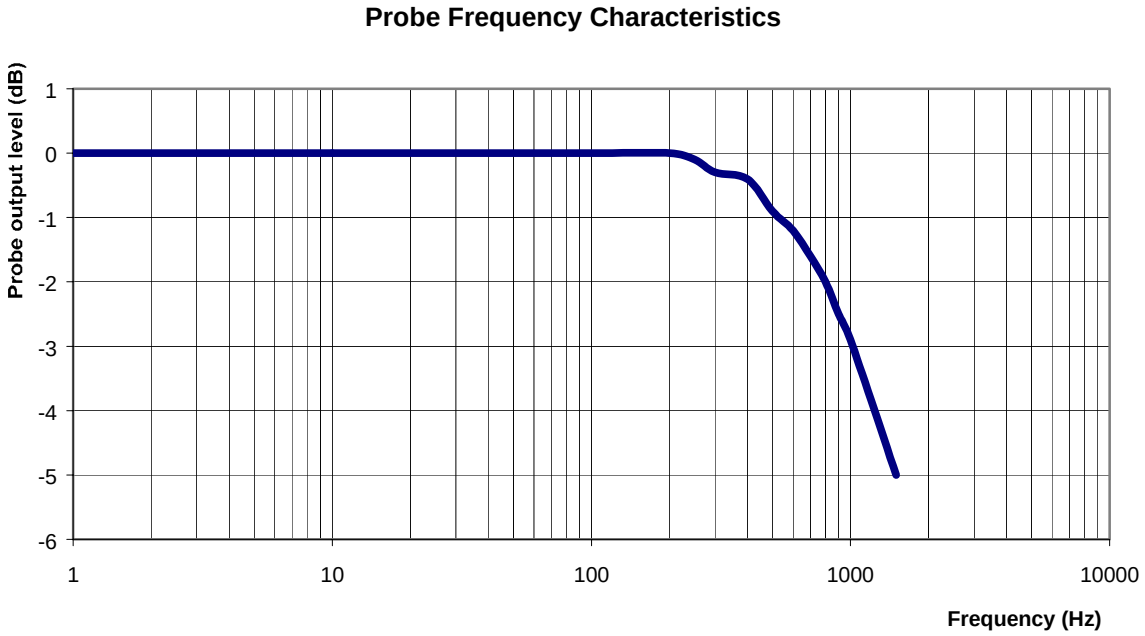

Video Bandwidth at 500 Hz 1 dB
Video Bandwidth at 1.02 KHz: 3 dB

Conversion Factor Uncertainty Assessment

Frequency:		2450MHz	
Epsilon:	50.6 (+/-5%)	**Sigma:**	1.98 S/m (+/-10%)

ConvF

Channel X:	5.0	7%(K=2)
Channel Y:	5.0	7%(K=2)
Channel Z:	5.0	7%(K=2)

To minimize the uncertainty calculation all tissue sensitivity values were calculated using a load impedance of 5 MΩ.

Boundary Effect:

For a distance of 2.4mm the evaluated uncertainty (increase in the probe sensitivity) is less than 2%.

Test Equipment

The test equipment used during Probe Calibration, manufacturer, model number and, current calibration status are listed and located on the main APREL server R:\NCL\Calibration Equipment\Instrument List May 2005.

NCL CALIBRATION LABORATORIES

Calibration File No.: CP-617

Client.: APREL

CERTIFICATE OF CALIBRATION

It is certified that the equipment identified below has been calibrated in the **NCL CALIBRATION LABORATORIES** by qualified personnel following recognized procedures and using transfer standards traceable to NRC/NIST.

Equipment: Miniature Isotropic RF Probe 5200 MHz

Manufacturer: APREL Laboratories
Model No.: E-020
Serial No.: 212

Head Calibration

Calibration Procedure: SSI/DRB-TP-D01-032-E020-V2
Project No: Internal

Calibrated: 10th March 2005
Released on: 10th March 2005

This Calibration Certificate is Incomplete Unless Accompanied with the Calibration Results Summary

Released By: _____

***NCL* CALIBRATION LABORATORIES**
51 SPECTRUM WAY
NEPEAN, ONTARIO
CANADA K2R 1E6

Division of APREL Lab.
TEL: (613) 820-4988
FAX: (613) 820-4161

Introduction

This Calibration Report reproduces the results of the calibration performed in line with the SSI/DRB-TP-D01-032-E020-V2 E-Field Probe Calibration Procedure. The results contained within this report are for APREL E-Field Probe E-020 260.

References

SSI/DRB-TP-D01-032-E020-V2 E-Field Probe Calibration Procedure
IEEE 1528 “Recommended Practice for Determining the Peak Spatial-Average Specific Absorption Rate (SAR) in the Human Head Due to Wireless Communications Devices: Experimental Techniques”
SSI-TP-011 Tissue Calibration Procedure

Conditions

Probe 260 was a new probe taken from stock prior to calibration.

Ambient Temperature of the Laboratory: 22 °C +/- 0.5°C
Temperature of the Tissue: 21 °C +/- 0.5°C

We the undersigned attest that to the best of our knowledge the calibration of this probe has been accurately conducted and that all information contained within this report has been reviewed for accuracy.

Stuart Nicol

Y. Pan

51 Spectrum Way
Ottawa ON Canada K2R 1E6
www.aprel.com
info@aprel.com
Phone (613) 820-2730
Fax (613) 820-4161

Calibration Results Summary

Probe Type:	E-Field Probe E-020
Serial Number:	260
Frequency:	5800 MHz
Sensor Offset:	1.56 mm
Sensor Length:	2.5 mm
Tip Enclosure:	Ertalyte*
Tip Diameter:	<4.9 mm
Tip Length:	60 mm
Total Length:	290 mm

*Resistive to recommended tissue recipes per IEEE-1528

Sensitivity in Air

Channel X:	1.2 $\mu V/(V/m)^2$
Channel Y:	1.2 $\mu V/(V/m)^2$
Channel Z:	1.2 $\mu V/(V/m)^2$
Diode Compression Point:	95 mV

Sensitivity in Head Tissue

Frequency: 5200 MHz

Epsilon: 36.0 (+/-5%) **Sigma:** 4.65 S/m (+/-10%)

ConvF

Channel X: 6.4

Channel Y: 6.4

Channel Z: 6.4

Tissue sensitivity values were calculated using the load impedance of the APREL Laboratories Daq-Paq.

Boundary Effect:

Uncertainty resulting from the boundary effect is less than 2% for the distance between the tip of the probe and the tissue boundary, when less than 2.4mm.

Spatial Resolution:

The measured probe tip diameter is 5 mm (+/- 0.01 mm) and therefore meets the requirements of SSI/DRB-TP-D01-032 for spatial resolution.

51 Spectrum Way
Ottawa ON Canada K2R 1E6
www.aprel.com
info@aprel.com
Phone (613) 820-2730
Fax (613) 820-4161

Receiving Pattern 5200 MHz (Air)

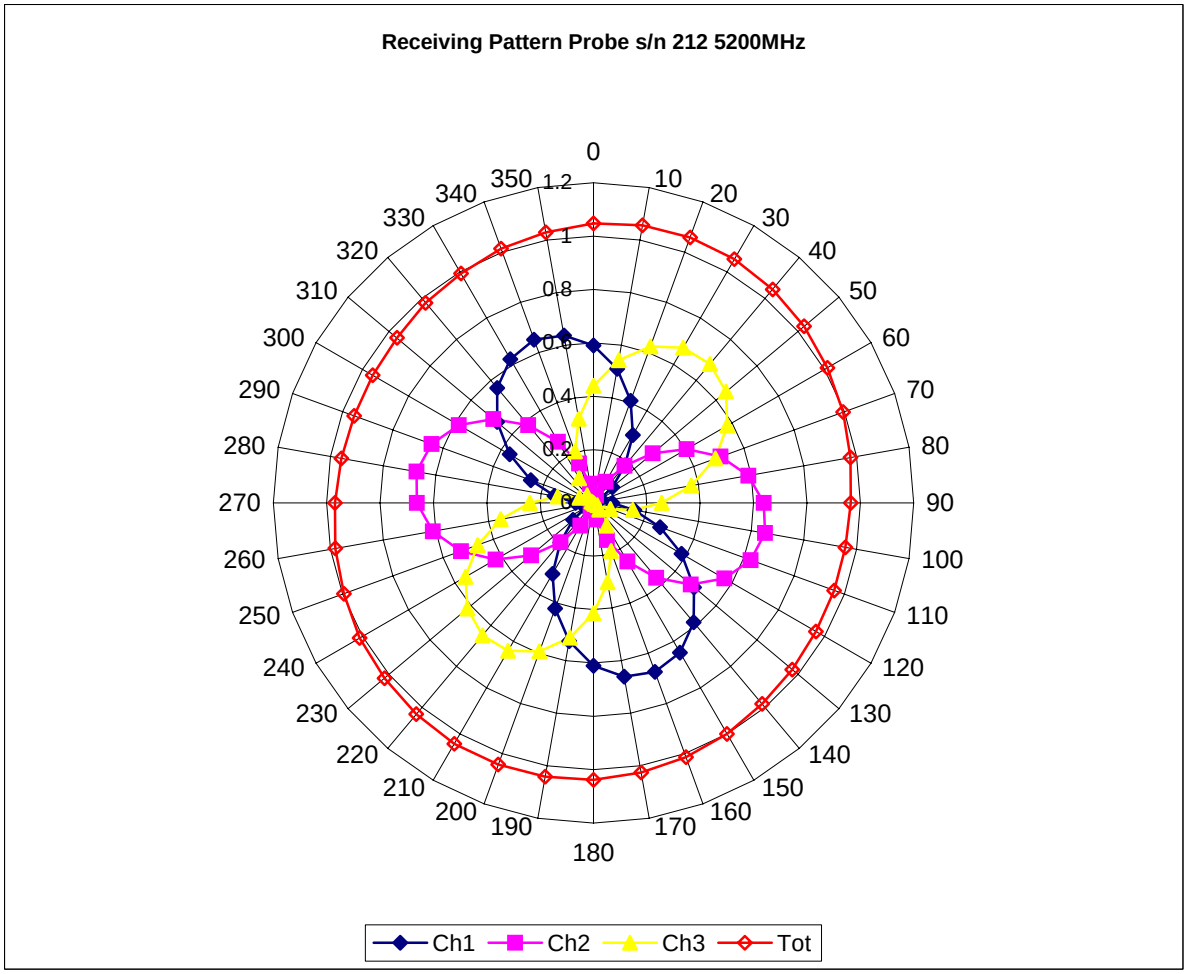

Isotropy Error 5200 MHz (Air)

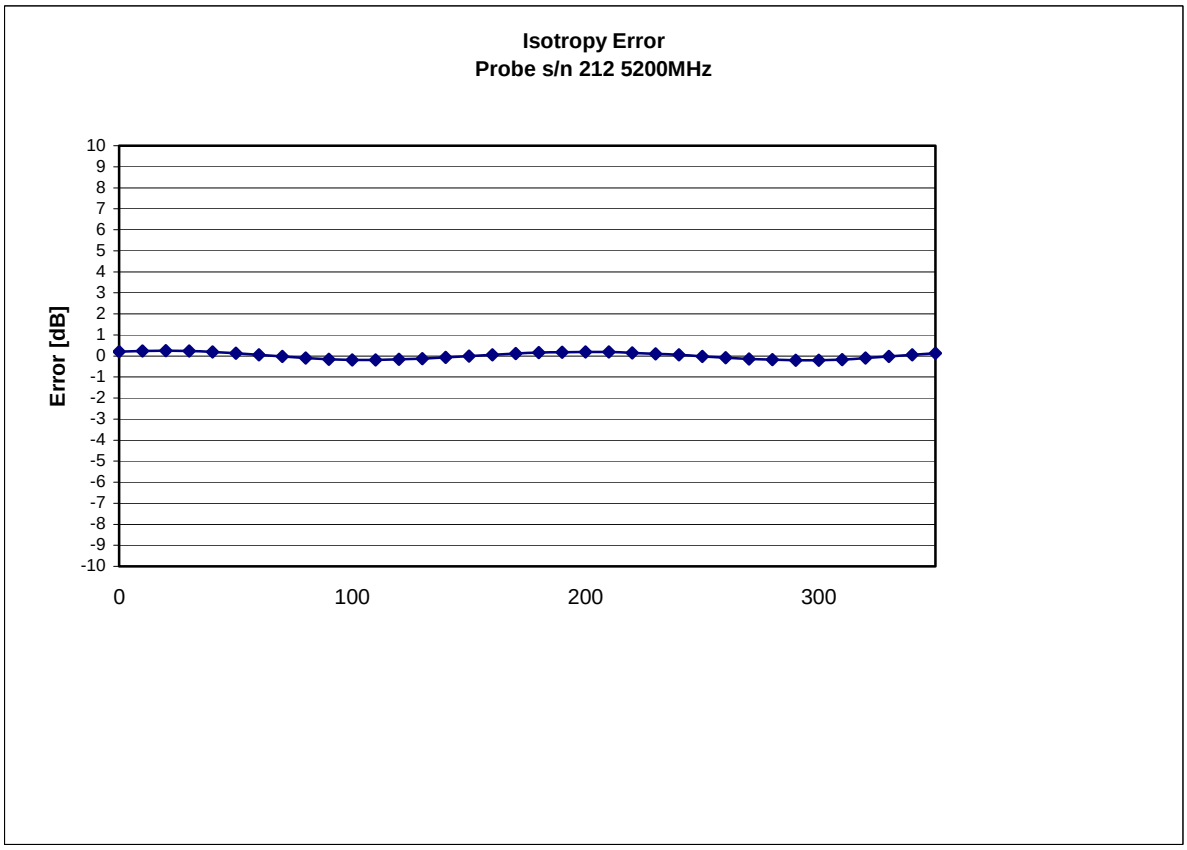

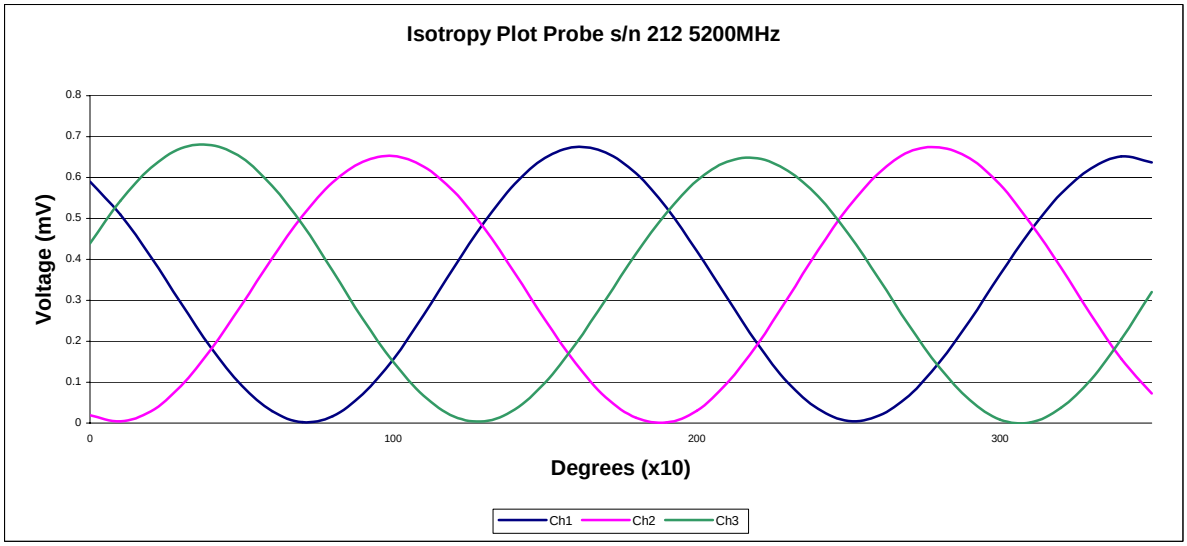

Isotropicity: 0.10 dB

Dynamic Range

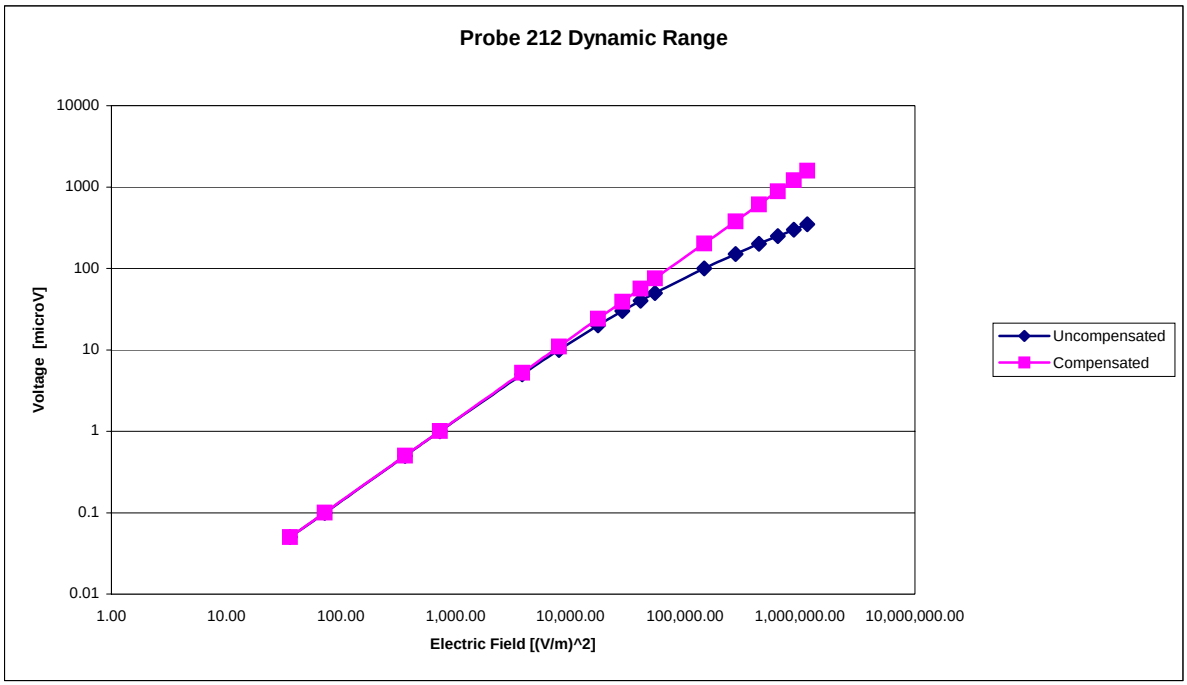

Video Bandwidth

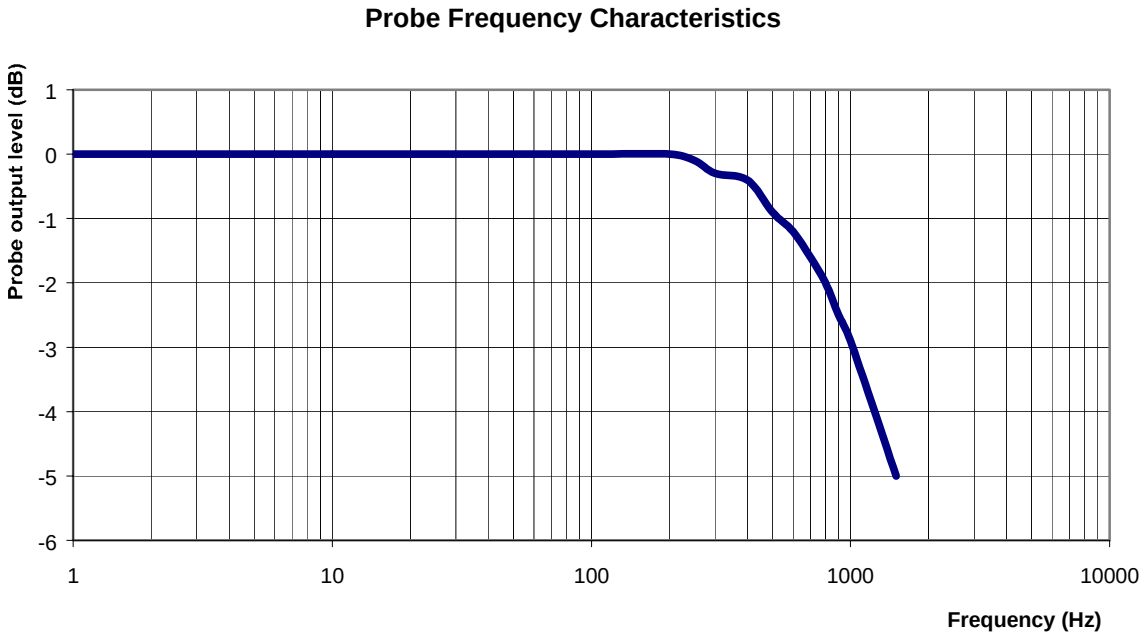

Video Bandwidth at 500 Hz 1 dB
Video Bandwidth at 1.02 KHz: 3 dB

Conversion Factor Uncertainty Assessment

Frequency: 5200MHz

Epsilon: 36.0 (+/-5%) **Sigma:** 4.65 S/m (+/-10%)

ConvF

Channel X: 6.4 7%(K=2)

Channel Y: 6.4 7%(K=2)

Channel Z: 6.4 7%(K=2)

To minimize the uncertainty calculation all tissue sensitivity values were calculated using a load impedance of 5 MΩ.

Boundary Effect:

For a distance of 2.4mm the evaluated uncertainty (increase in the probe sensitivity) is less than 2%.

Test Equipment

The test equipment used during Probe Calibration, manufacturer, model number and, current calibration status are listed and located on the main APREL server R:\NCL\Calibration Equipment\Instrument List May 2005.

NCL CALIBRATION LABORATORIES

Calibration File No.: CP-618

Client.: APREL

CERTIFICATE OF CALIBRATION

It is certified that the equipment identified below has been calibrated in the **NCL CALIBRATION LABORATORIES** by qualified personnel following recognized procedures and using transfer standards traceable to NRC/NIST.

Equipment: Miniature Isotropic RF Probe 5800 MHz

Manufacturer: APREL Laboratories
Model No.: E-020
Serial No.: 212

Head Calibration

Calibration Procedure: SSI/DRB-TP-D01-032-E020-V2
Project No: Internal

Calibrated: 10th March 2005
Released on: 10th March 2005

This Calibration Certificate is Incomplete Unless Accompanied with the Calibration Results Summary

Released By: _____

***NCL* CALIBRATION LABORATORIES**
51 SPECTRUM WAY
NEPEAN, ONTARIO
CANADA K2R 1E6

Division of APREL Lab.
TEL: (613) 820-4988
FAX: (613) 820-4161

Introduction

This Calibration Report reproduces the results of the calibration performed in line with the SSI/DRB-TP-D01-032-E020-V2 E-Field Probe Calibration Procedure. The results contained within this report are for APREL E-Field Probe E-020 260.

References

SSI/DRB-TP-D01-032-E020-V2 E-Field Probe Calibration Procedure
IEEE 1528 “Recommended Practice for Determining the Peak Spatial-Average Specific Absorption Rate (SAR) in the Human Head Due to Wireless Communications Devices: Experimental Techniques”
SSI-TP-011 Tissue Calibration Procedure

Conditions

Probe 260 was a new probe taken from stock prior to calibration.

Ambient Temperature of the Laboratory: 22 °C +/- 0.5°C
Temperature of the Tissue: 21 °C +/- 0.5°C We the undersigned attest that to the best of our knowledge the calibration of this probe has been accurately conducted and that all information contained within this report has been reviewed for accuracy.

Stuart Nicol

Y. Pan

Calibration Results Summary

Probe Type:	E-Field Probe E-020
Serial Number:	260
Frequency:	5800 MHz
Sensor Offset:	1.56 mm
Sensor Length:	2.5 mm
Tip Enclosure:	Ertalyte*
Tip Diameter:	<4.9 mm
Tip Length:	60 mm
Total Length:	290 mm

*Resistive to recommended tissue recipes per IEEE-1528

Sensitivity in Air

Channel X:	1.2 $\mu V/(V/m)^2$
Channel Y:	1.2 $\mu V/(V/m)^2$
Channel Z:	1.2 $\mu V/(V/m)^2$
Diode Compression Point:	95 mV

Sensitivity in Head Tissue

Frequency: 5800 MHz

Epsilon: 35.4 (+/-5%) **Sigma:** 5.27 S/m (+/-10%)

ConvF

Channel X: 5.9

Channel Y: 5.9

Channel Z: 5.9

Tissue sensitivity values were calculated using the load impedance of the APREL Laboratories Daq-Paq.

Boundary Effect:

Uncertainty resulting from the boundary effect is less than 2% for the distance between the tip of the probe and the tissue boundary, when less than 2.44mm.

Spatial Resolution:

The measured probe tip diameter is 5 mm (+/- 0.01 mm) and therefore meets the requirements of SSI/DRB-TP-D01-032 for spatial resolution.

51 Spectrum Way
Ottawa ON Canada K2R 1E6
www.aprel.com
info@aprel.com
Phone (613) 820-2730
Fax (613) 820-4161

Receiving Pattern 5800 MHz (Air)

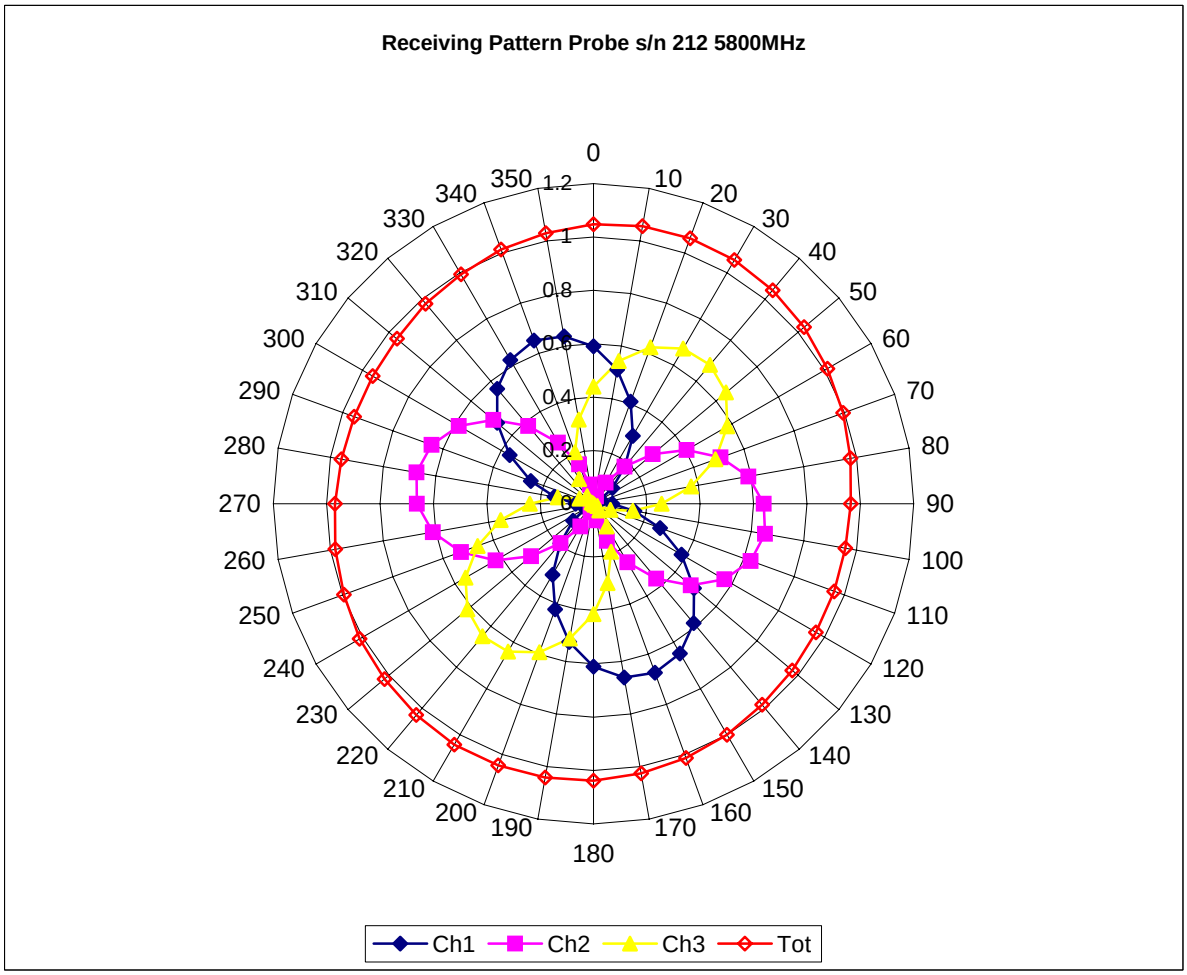

Isotropy Error 5800 MHz (Air)

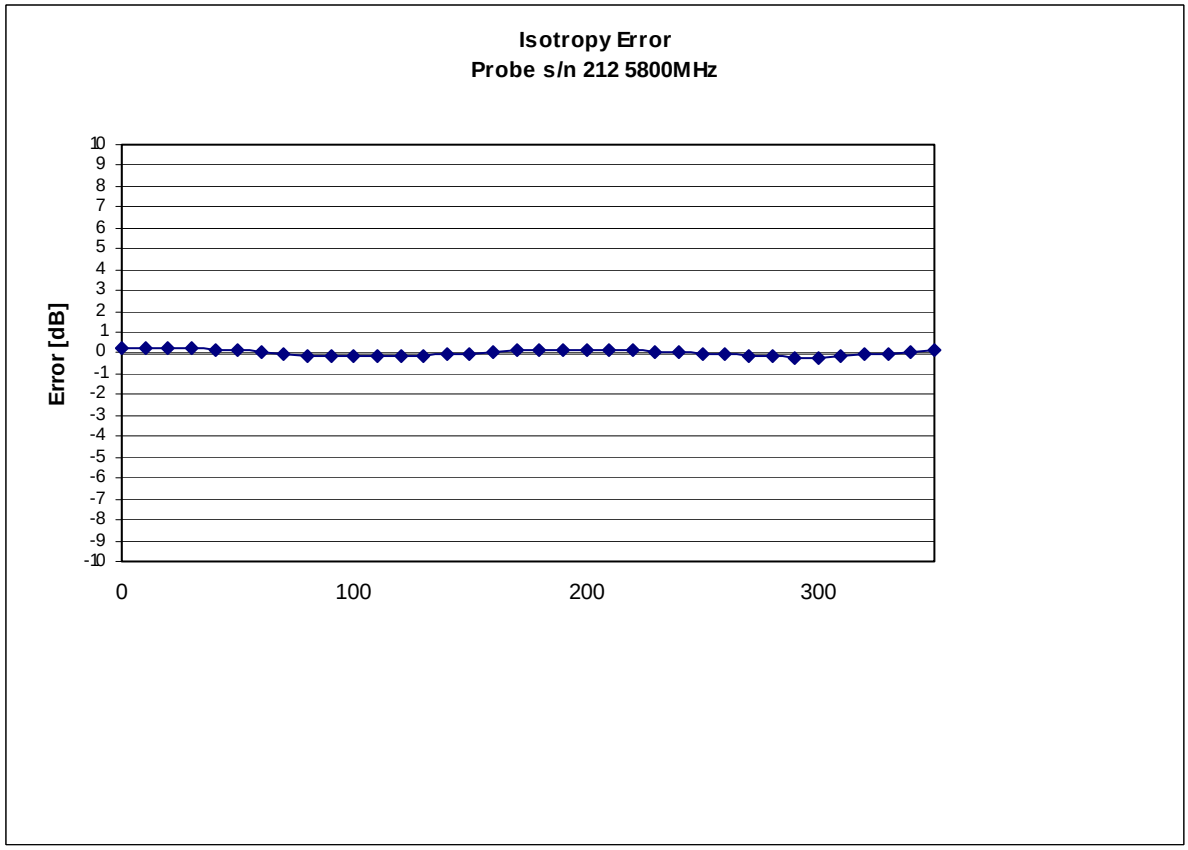

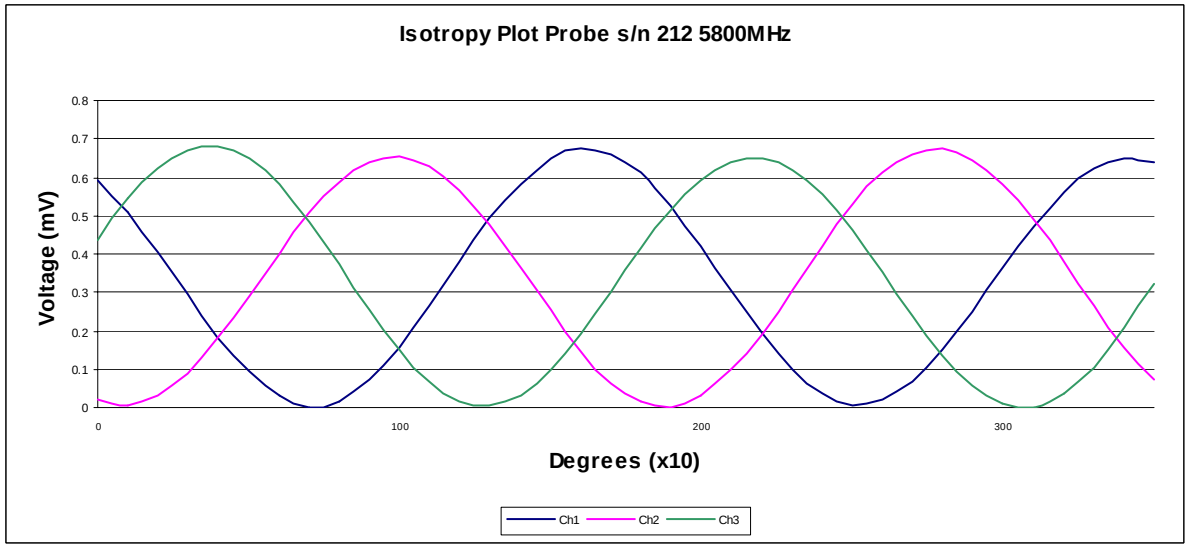

Isotropicity: 0.10 dB

Dynamic Range

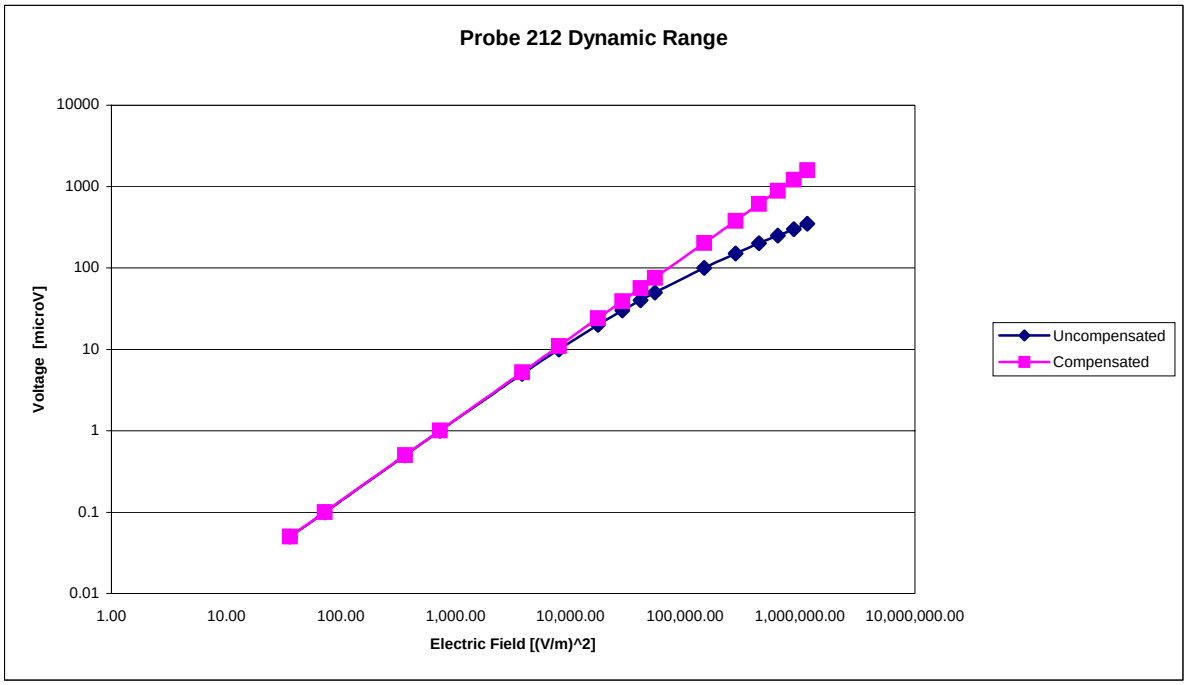

Video Bandwidth

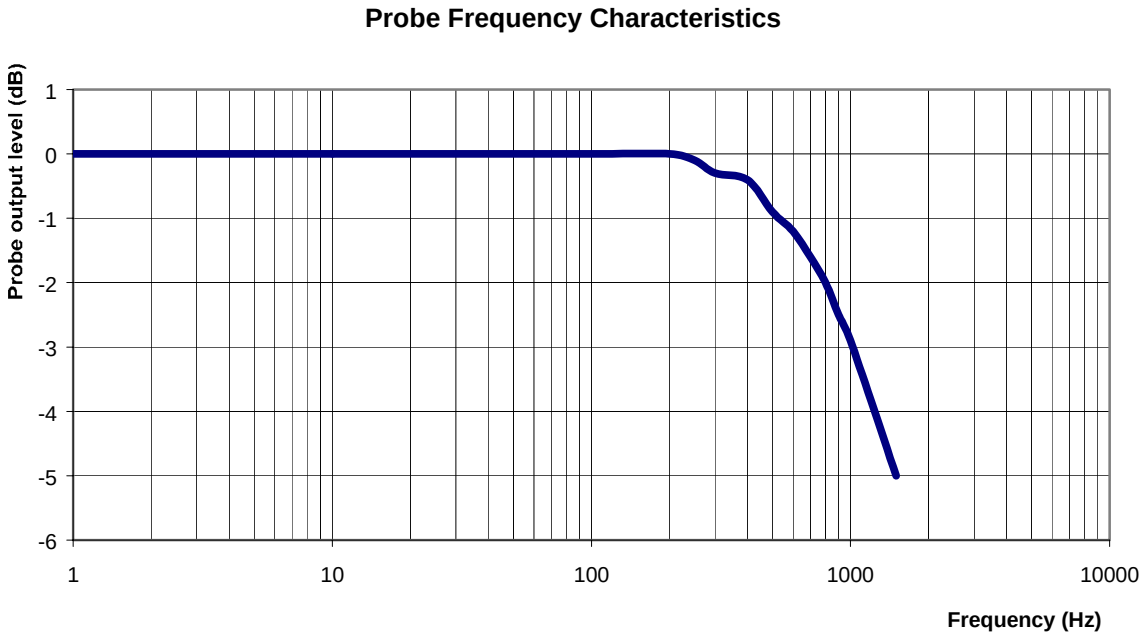

Video Bandwidth at 500 Hz 1 dB
Video Bandwidth at 1.02 KHz: 3 dB

Conversion Factor Uncertainty Assessment

Frequency: 5800MHz

Epsilon: 35.4 (+/-5%) **Sigma:** 5.27 S/m (+/-10%)

ConvF

Channel X: 5.9 7%(K=2)

Channel Y: 5.9 7%(K=2)

Channel Z: 5.9 7%(K=2)

To minimize the uncertainty calculation all tissue sensitivity values were calculated using a load impedance of 5 MΩ.

Boundary Effect:

For a distance of 2.4mm the evaluated uncertainty (increase in the probe sensitivity) is less than 2%.

Test Equipment

The test equipment used during Probe Calibration, manufacturer, model number and, current calibration status are listed and located on the main APREL server R:\NCL\Calibration Equipment\Instrument List May 2005.

51 Spectrum Way
Ottawa ON Canada K2R 1E6
www.aprel.com
info@aprel.com
Phone (613) 820-2730
Fax (613) 820-4161

NCL CALIBRATION LABORATORIES

Calibration File No: DC-599
Project Number: APREL-ALSAS 10U

CERTIFICATE OF CALIBRATION

It is certified that the equipment identified below has been calibrated in the **NCL CALIBRATION LABORATORIES** by qualified personnel following recognized procedures and using transfer standards traceable to NRC/NIST.

APREL Validation Dipole

Manufacturer: APREL Laboratories
Part number: ALS-D-5258-S-2
Frequency: 5.2GHz to 5.8GHz
Serial No: 5258-235-00802

Customer: APREL

Calibrated: 24th May 2005
Released on: 24th May 2005

Released By: _____

NCL CALIBRATION LABORATORIES

51 SPECTRUM WAY
NEPEAN, ONTARIO
CANADA K2R 1E6

Division of APREL Lab.
TEL: (613) 820-4988
FAX: (613) 820-4162

Conditions

Dipole 5258-235-00802 was new and taken from stock prior to calibration.

Ambient Temperature of the Laboratory: 22 °C +/- 0.5°C
Temperature of the Tissue: 21 °C +/- 0.5°C

We the undersigned attest that to the best of our knowledge the calibration of this device has been accurately conducted and that all information contained within this report has been reviewed for accuracy.

Stuart Nicol

Director Product Development

D. Brooks

Member of Engineering Staff

(Calibration Engineer)

Calibration Results Summary

The following results relate the Calibrated Dipole and should be used as a quick reference for the user.

Mechanical Dimensions

Length: 23.3 mm
Height: 20.3 mm

Electrical Specification

SWR: 1.22 U
Return Loss: -20.0 dB
Impedance: 50.0 Ω

System Validation Results

Frequency	1 Gram	10 Gram	Peak
5200 MHz	62.9	17.9	223.1

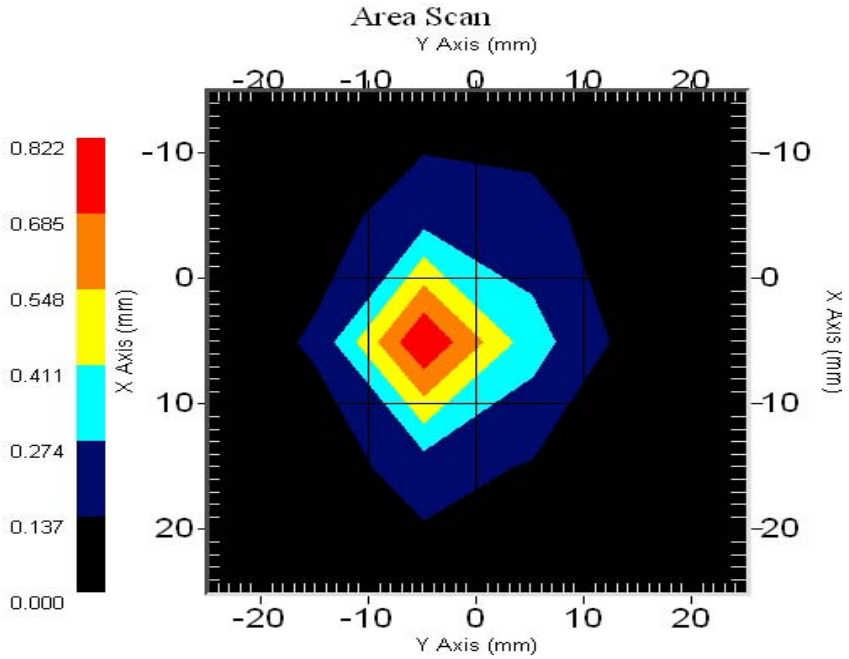

Frequency	1 Gram	10 Gram	Peak
5800 MHz	58.3	18	207.1

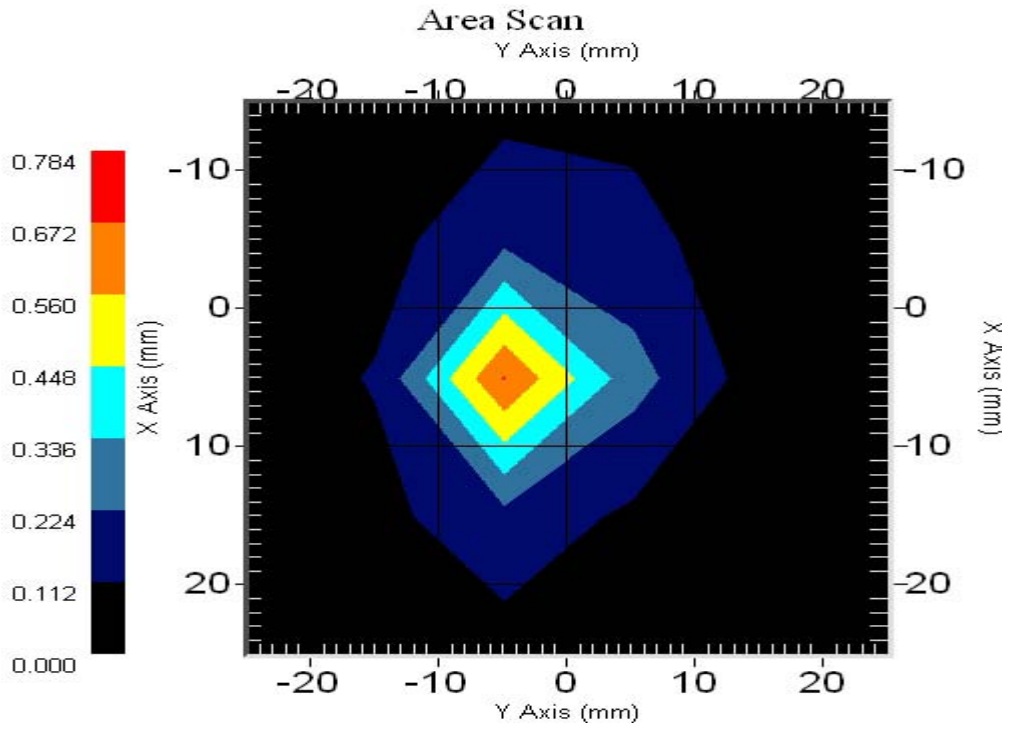

Introduction

This Calibration Report has been produced in line with the SSI Dipole Calibration Procedure SSI-TP-018-ALSAS. The results contained within this report are for Validation Dipole 5258-235-00802. The calibration routine consisted of a three-step process. Step 1 was a mechanical verification of the dipole to ensure that it meets the mechanical specifications. Step 2 was an Electrical Calibration for the Validation Dipole, where the SWR, Impedance, and the Return loss were assessed. Step 3 involved a System Validation using the ALSAS-10U, along with APREL E-020 130 MHz to 26 GHz E-Field Probe Serial Number 212.

References

SSI-TP-018-ALSAS Dipole Calibration Procedure
SSI-TP-016 Tissue Calibration Procedure
IEEE 1528 “Recommended Practice for Determining the Peak Spatial-Average Specific Absorption Rate (SAR) in the Human Body Due to Wireless Communications Devices: Experimental Techniques”

Conditions

Dipole 5258-235-00802 was new taken from stock.

Ambient Temperature of the Laboratory: 22 °C +/- 0.5°C
Temperature of the Tissue: 20 °C +/- 0.5°C

Dipole Calibration Results

Tissue Validation

Head Tissue 5200 MHz	Measured
Dielectric constant, ε_r	35.3
Conductivity, σ [S/m]	5.30

Head Tissue 5800 MHz	Measured
Dielectric constant, ε_r	35.3
Conductivity, σ [S/m]	5.30

Mechanical Verification

APREL Length	APREL Height	Measured Length	Measured Height
23.1 mm	20.7 mm	23.3 mm	20.3 mm

Electrical Calibration

S11	5200MHz	5800MHz
RL (dB)	-21.16	-22.34
SWR	1.2	1.17
Impedance (ohms)	51.38	43.92

The Following Graphs are the results as displayed on the Vector Network Analyzer.

S11 Parameter Return Loss

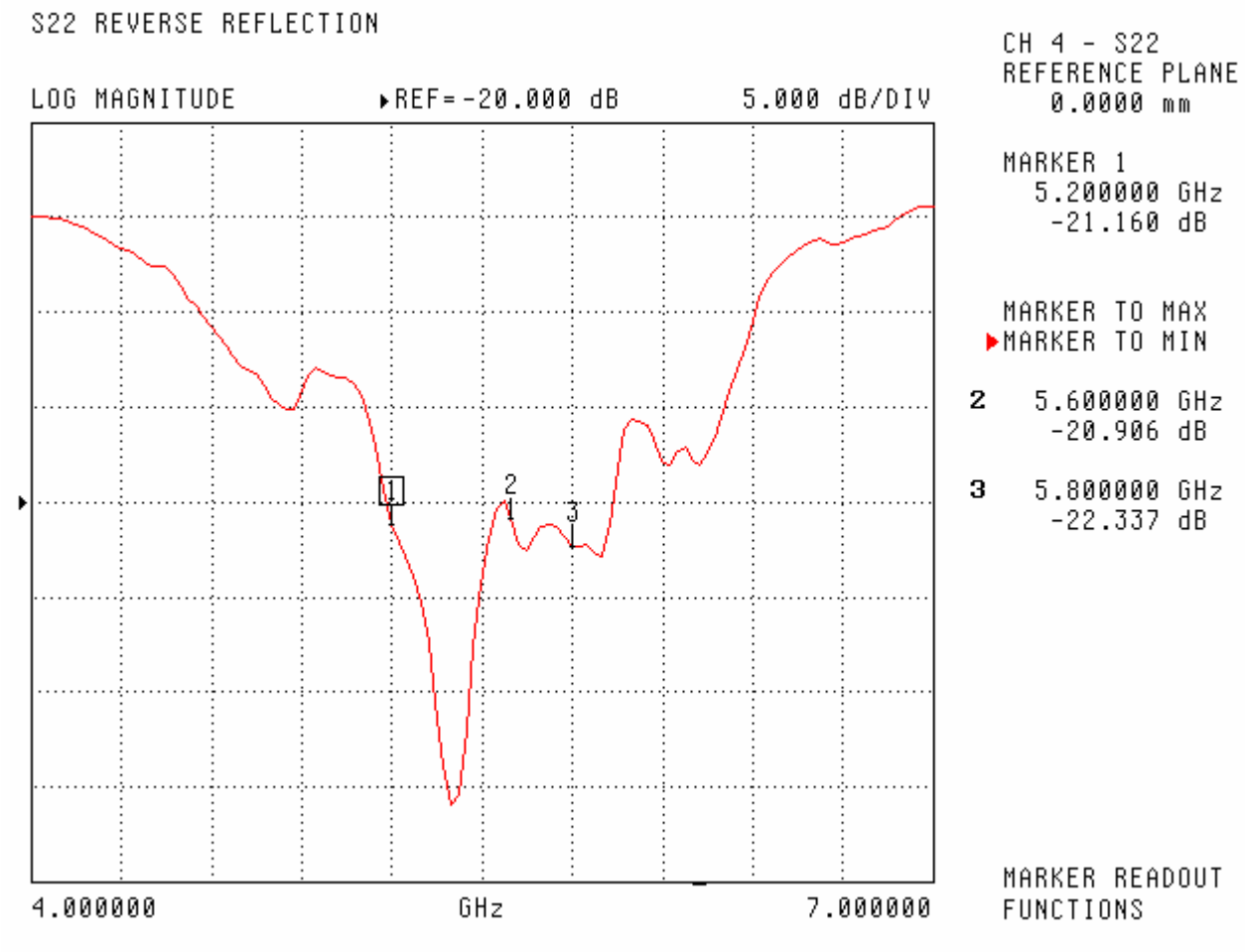

SWR

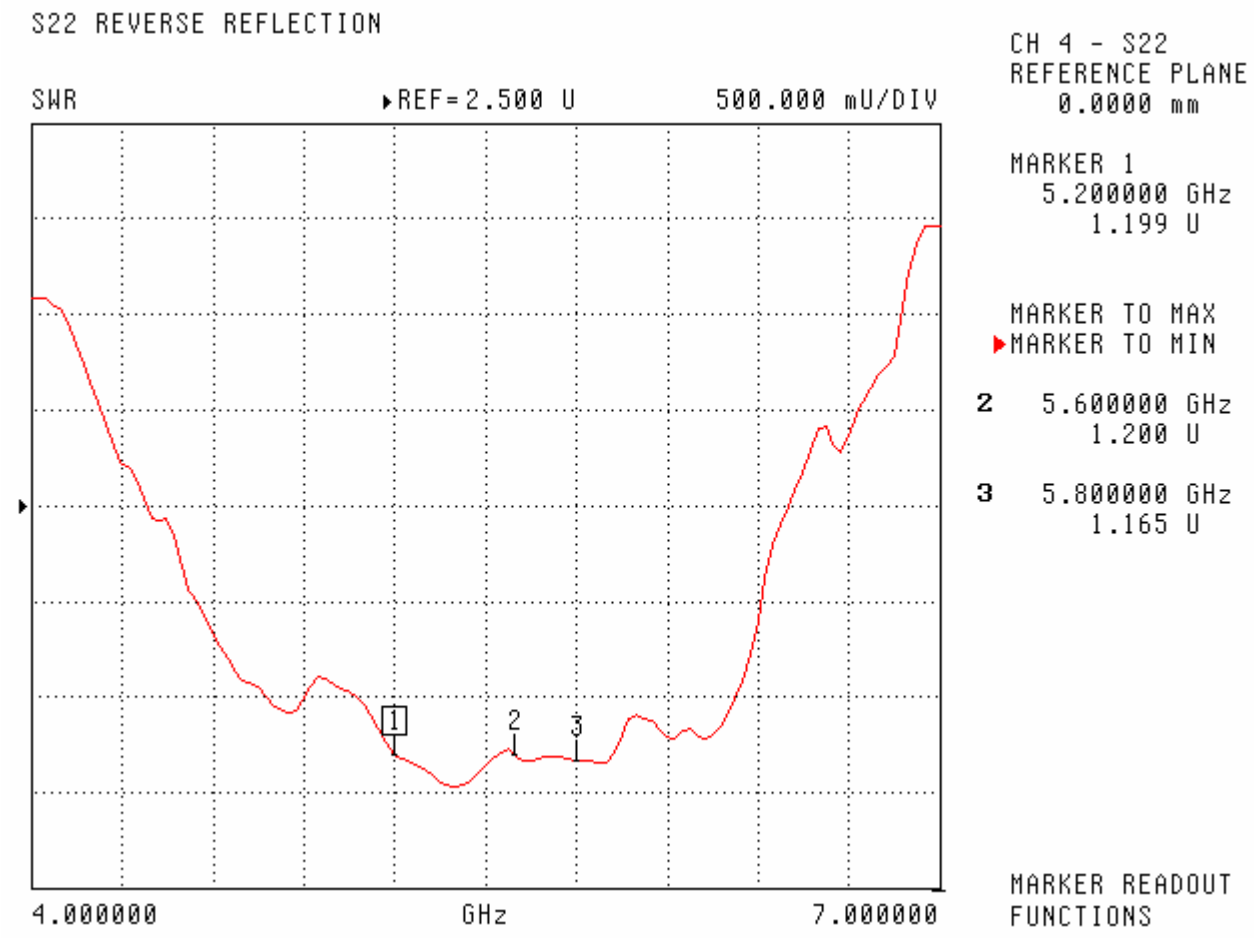

Smith Chart Dipole Impedance

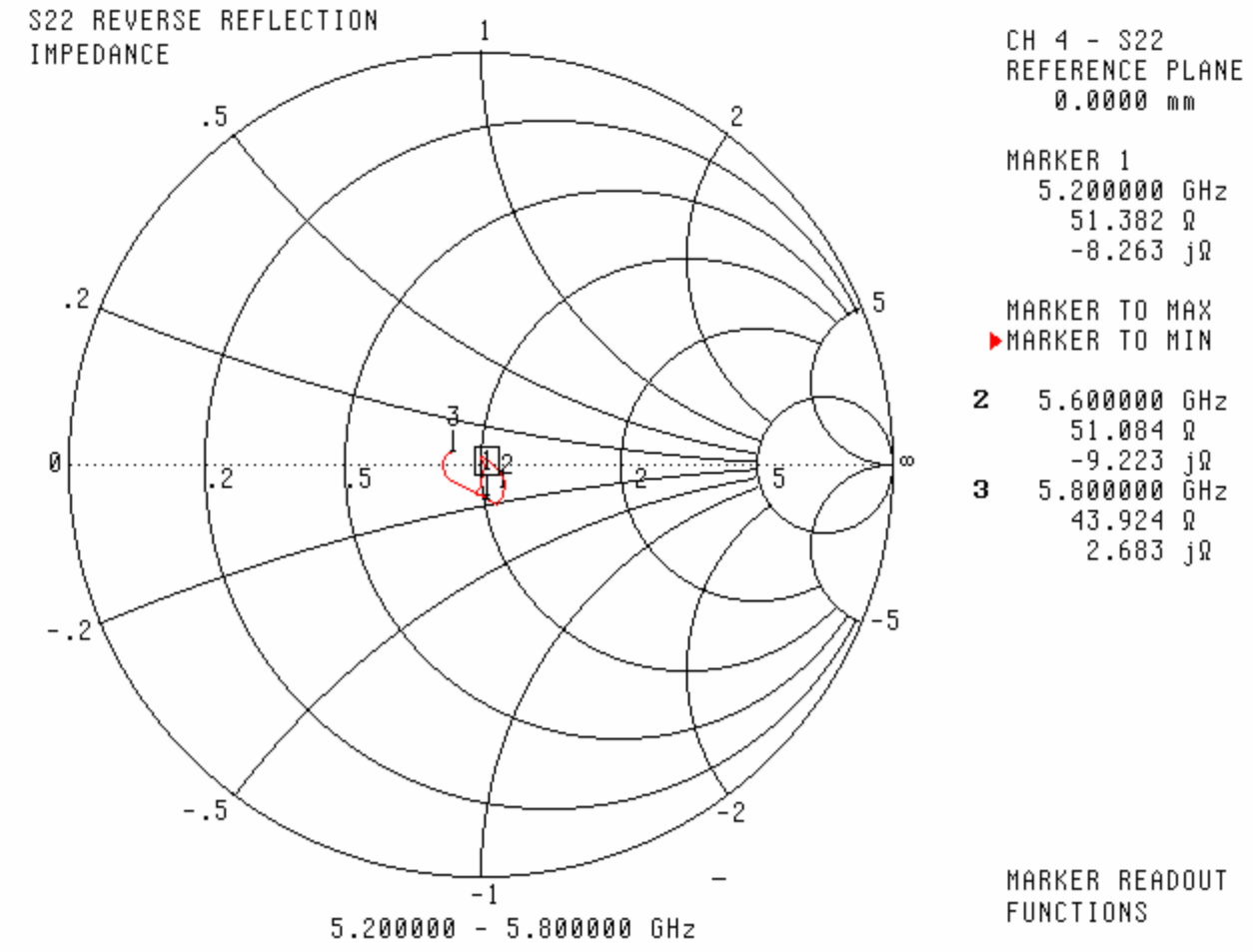

51 Spectrum Way
Ottawa ON Canada K2R 1E6
www.aprel.com
info@aprel.com
Phone (613) 820-2730
Fax (613) 820-4161

Test Equipment

The test equipment used during Probe Calibration, manufacturer, model number and, current calibration status are listed and located on the main APREL server R:\NCL\Calibration Equipment\Instrument List May 2004

Appendix E
Published Scientific Papers

51 Spectrum Way
Ottawa ON Canada K2R 1E6
www.aprel.com
info@aprel.com
Phone (613) 820-2730
Fax (613) 820-4161

Comparative study of the effects of dosimetric E-field sensor size on the detected field intensity, at 5.2 GHz and 5.8 GHz

Alain Tran[1], Stuart Nicol[2], Jacek Wojcik[3], Mustapha C.E. Yagoub[1].

[1] School of Information Technology and Engineering, Ottawa University, Ottawa ON, K1N 6N5 Canada.
[2] APREL Laboratories, Ottawa, ON, K2R 1E6 Canada, [3] Spectrum Sciences Institute, Ontario, Canada.

ABSTRACT: Numerical and experimental characterizations of the dosimetric E-field probe sensor size has been performed at 5.2 GHz and 5.8 GHz. Also investigated is the, 2.8mm and 4.9mm tip-diameter probes which have been designed and validated against international regulations' and standards. Numerical characterizations show that smaller probe-sensors have lower sensitivity than longer probe-sensors. Lab measurement results show that both of the fabricated probes (3mm and 4.9mm diameter) yield SAR values in line with the FDTD (finite-difference-time-domain) derived target SAR values within +/-5%. When the probe is in immediate proximity of the phantom boundary, probe positioning uncertainty becomes a major factor. Probe positioning uncertainty, as well as boundary effect, can be reduced by keeping this distance to at least 0.6mm from the probe tip. Since the difference in SAR between the two probes is less than 13%, we conclude that the 4.9mm and 2.8mm probes are both equally suitable to be used for dosimetric assessment in the 5.2 - 5.8 GHz frequency range.

Index Terms: Dosimetry, SAR, SAM, radio frequency exposure, dipole-sensor, handset.

I. Introduction

It had been claimed that a reduced probe diameter at frequencies greater than 2GHz would increase the experimental SAR accuracy, due to the improved spatial resolution and boundary effect. Also, current IEC draft standard [3] recommends as a "rule of thumb" that the maximum probe-tip diameter be 16 / (freq in GHz) millimeters; this means that the largest tip-diameter for 5.8 GHz SAR evaluation is 2.8mm and largest tip-diameter for 5.2 GHz SAR evaluation is 3.1mm. It is also recommended that the maximum sensor displacement (in mm) from the bottom of the probe be 8 / (freq in GHz); this means the maximum sensor displacement should be 1.4mm for 5.8 GHz and 1.5 for 5.2GHz.

The purpose of this paper is to discuss and present results which can question those claims. The paper will demonstrate that the proposed recommendation for smaller probe-tip diameter is not required for frequencies above 5 GHz, and that a smaller probe-tip displacement (distance from the sensor to the tip) does not significantly improve the measurement accuracy. Instead of the probe diameter sizes, other factors such as mechanical positioning and distance from the phantom surface have a greater effect on SAR.

This paper will also show that smaller probes are not necessarily better than slightly larger probes. The negative effect of reducing the probe size on its sensitivity has been analytically investigated by Smith [4]. It was found that when the physical dimensions of the probe are reduced by the scale factor k ($k < 1$), the minimum-detectable incident electric field, for a fixed transmitted field, increased by approximately the factor k^{-2}. Thus reducing the dipole length by half would increase the minimum-detectable field by 4.

II. Background

Miniaturized dosimetric electric field (E-field) probes are used to measure radio-frequency E-fields induced in biological bodies by relatively low-level exposures that cannot be detected by thermal detector methods. This exposure is formally defined as the rate of energy absorbed (Specific Absorption Rate or SAR) by biological bodies exposed to emissions from cellular phones and other radiators. SAR is defined as follows:

$$SAR = \frac{\sigma |E|^2}{\rho} \ (W/kg) \ where: \qquad (1)$$

where σ is the electrical conductivity, |E| is the rms magnitude of the electric field strength vector, and ρ is the mass density of the medium. Various radiation safety standards require the maximum SAR to not exceed a specified value at any point within the body of a person exposed to microwave fields [l], [2].

Generally, dosimetric E-field probe measurement systems consist of an array of three orthogonal electrically short dipole sensors. Each dipole sensor has the following components [1]: a diode detector, a dielectric substrate (mechanical support), a highly resistive balanced transmission line, a differential amplifier, and a detected-signal processor. Dosimetric E-field probes high-sensitivity enables the measurement of local SAR using physically low-power radiation sources such as a handheld cellular phone. By mechanically scanning the surface of a model (or phantom) filled with tissue-simulating liquids, the spatial distribution of the local SAR can be obtained.

To make them implantable in tissue or tissue-simulating liquid, the probes are housed within a protective cylindrical tube. The tube electrically and mechanically protects the fragile dipole-sensors. A beam-lead Schottky (metal barrier) diode is placed across the gap of each dipole to detect the E-field of the order of 1 mV per mW/cm^2 in free space. These diodes may produce erroneous readings when illuminated by sunlight or strong incandescent light [2]; however, the opaque protective tube eliminates this effect.

The protective tube, however, causes a small field distortion inside the probe. The field distortion is due to the difference between the low-loss low-dielectric-constant material of the tube and the high-dielectric-constant of the

surrounding lossy tissue (ε_r 30-40). This field distortion is magnified when the probe is in immediate vicinity of the phantom boundary (air and tissue-simulating liquid). This coupling effect is referred to as the boundary effect [3].

We have fabricated two dosimetric probes for use in experimental studies. These probes are called isotropic since they comprise of three dipoles approximately orthogonal to each other. One has outer probe tip diameter of 2.8mm and the other of 4.9mm.

III. Numerical Analysis

Probes with tip-diameters of 2.8mm and 4.9mm were assessed at frequencies of 5.2 and 5.8 GHz. Numerical tools such as Remcom's XFDTD was used to calculate the field intensity, peak, 1g and 10g average SAR and Ansoft's HFSS software tool was used to determine the filed strength within the sensor. SAR was assessed and recorded at 0.3mm intervals at the centre of the mass average cube volume in the Z-axis, as well as in X and Y-axis. The APREL broadband dipole [5] was used as a field-radiating source with power normalized to the feed. IEC dielectric tissue-simulating liquid for frequency of 5.2 GHz was used [3].

Numerical simulations have been done for various scenarios: probe-tip(s) exposed to fields in a homogeneous tissue by positioning the probe-tip against the inner phantom boundary (zero separation); and probe-tips exposed to fields in homogeneous tissues by positioning the probe at 0.3mm, 0.6mm, 0.9mm and 1.2mm above the phantom boundary.

From the simulations, we observed that the zoom scan step resolution volume can remain constant for both probes. The simulations ran on XFDTD also provided optimal scanning requirements which would be used on the ALSAS-10U (APREL Laboratories SAR Assessment System) for experimental verification. The optimized zoom scan variables are 4mm steps in X and Y-axis and 2mm in Z-axis up to a height of 10mm where the resolution can be reduced. When variable step routines are used, measurement time is reduced. The positional step uncertainty must be maintained at less than 0.1mm for positions close to the phantom boundary to reduce uncertainty.

When comparing experimental results form the ALSAS-10u (using the broad band dipole [5]) with simulated results, the following observations were made:

1) Equally strong gradient fields were detected by both probes at the surface of the inner phantom. The difference in sensitivity between the two probes at a given input power varies approximately between 0 and 13% (see Figure 1) and by identifying the area of uncertainty compensation routines can be employed.

2) The distance from the phantom boundary significantly influences the SAR value. For both probes, the optimal distance must be at 1.6 where additional measurement points can be defined up to 10mm between the phantom shell and the probe-tip.

3) Probe positioning uncertainty becomes the predominant source of errors when the probe touches the phantom boundary. This is due to positioning uncertainty and boundary effect. Positioning uncertainty is larger for a 3mm probe (up to 5%) than for 5mm probe (~2.5%). The boundary effect could be eliminated if a minimum distance of 0.6mm from the inner phantom surface is observed.

4) SAR measurements beyond 10mm from the phantom surface are subjected to ambient conditions.

5) Both the 3mm and 5mm probes yield experimental SAR values within +/-5% (see Figure 2).

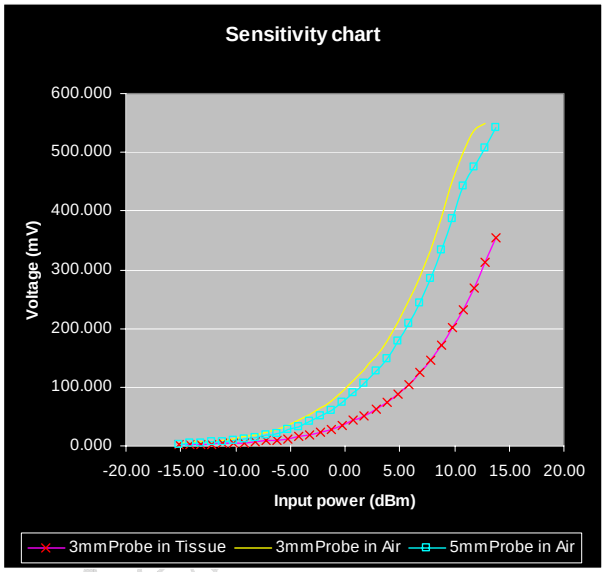

Figure 1: Sensitivity of the 3mm and 5mm probes.

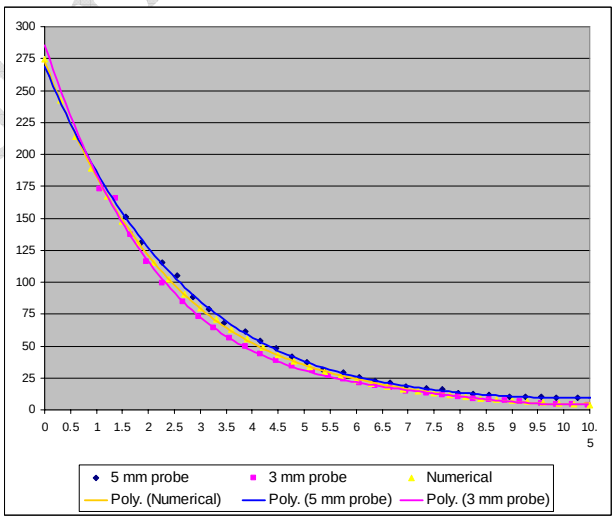

Figure 2: SAR in function of Z axis distance from phantom.

In this part of our investigation, we simulated various lengths of the dipole-sensor to see how this affects the field intensity which the sensor captures. Figure 3 illustrates our simulation set up. On top is a closed-end dielectric cylinder (εr=4.6) which surrounds the substrate and the sensor. The substrate is a thin dielectric strip (εr=2.2) on which the sensor rests. The sensor is composed of two perfectly balanced-electric-conductor strips, each having dimension of (0.3mm x1.2mm). The thickness of the sensor is 0.1mm. For the purpose of simulation, the two arms are separated by a lumped-port with a length of 0.4mm. The source-dipole is composed of two perfectly-electric-conductor cylinders of radius 1.8mm and length 14.4mm (for the 5.2GHz case) or 12.9mm (for the 5.8GHz case). The two arms are separated

by an 11.3mm-long lumped-port. The structure is immerged in a liquid (εr=35, σ=0.9S/m).

Simulations were performed for the 5.2GHz and 5.8GHz cases; then followed by a third simulation where the dipole length is reduced by 0.5mm each side. Results presented in Figure 4 show that the smaller and shorter dipole does not improve the sensitivity, and also that the field-intensity is reduced with a 0.5mm-shorter dipole.

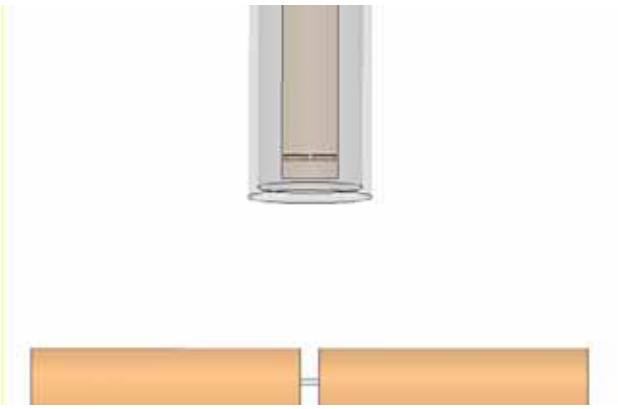

Figure 3: Sensor (top) and source (bottom) dipoles.

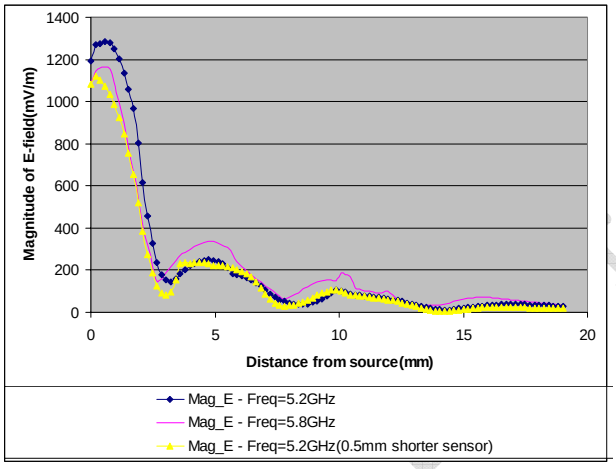

Figure 4: Field intensity captured by the sensors.

IV. Experimental Measurement Inside a Waveguide

In this part of our investigation, we experimentally measured the fabricated probe(s) output voltages in air and tissue-equivalent material. The incident field is emitted by a rectangular waveguide. The approach is based on the waveguide calibration technique outlined in [6]. A 1.590 inch x 0.795 inch rectangular waveguide was used, with its axis of propagation (z-axis) oriented vertically.

A dielectric septum separates the upper and lower parts of the waveguide, allowing the tissue simulating solution to be filled from the top.

The resulting transverse field distribution in the lossy tissue-liquid exponentially decays in the vertical direction (z-axis). The liquid is filled to a depth of about 3 cm, ensuring that reflections from the liquid/air interface (top surface) do not affect the calibration field.

Analytically, the SAR in the waveguide can be determined from the waveguide dimensions and the measured forward and reflected power. The SAR along the waveguide axis (z-axis) in the liquid is given by:

$$SAR = \frac{4(P_{fwd} - P_{ref})}{ab\,\delta\,\rho} e^{-2z/\delta} . \quad (2)$$

Where ab is the cross-sectional area of the waveguide, δ is the penetration depth, ρ is the mass density of the tissue-liquid, P_{fwd} and P_{ref} are the forward and reflected power in the lossless section of the waveguide.

The penetration depth is given by:

$$\delta = \left[(\pi / a)^2 + j\omega\mu_o(\sigma + j\omega\mu_o\varepsilon_r)\right]^{-1/2} . \quad (3)$$

Where ω is the radian frequency, μ_o is the tissue permeability, σ is the tissue conductivity, ε_o is the free-space permittivity, and ε_r is the tissue relative permittivity.

V. Results from the Waveguide Test

The waveguide technique described in section IV was used to compare the fabricated 5mm-diameter probe and the 3mm-diameter probe in air and in tissue. Both probes have the same dipole-sensor length. The only difference is that the 3mm-diameter probe has the three substrates inverted in such a way that the three dipoles are now on the inner side of the triangular cross-section formed by those three substrates, rather than on the outer side, this effectively reduces the distances between the three sensors. Also, compared to the 5mm probe, the 3mm probe has its sensors 0.5mm closer to the tip of the probe. Thus all measuring data had to be adjusted accordingly, so that both probes are compared at the same height and the same power level in the waveguide. The waveguide test results, presented in Figure 5, show that at distance further than 30mm from the dielectric septum, both probes have similar characteristics and that the difference is most noticeable around 20mm.

Thus it has also been observed that:

1) The penetration depth greatly diminishes in tissue, which is in agreement with Equation 2. In air, the field intensity in the vicinity of the waveguide septum is sinusoidal and has a constant mean; whereas in tissue, it exponentially decays.

2) The sensitivity of the 3mm probe is higher than the 5mm probe, both in air and in tissue. In tissue, it is about 2 times higher. In air, it is about 1.4 times higher.

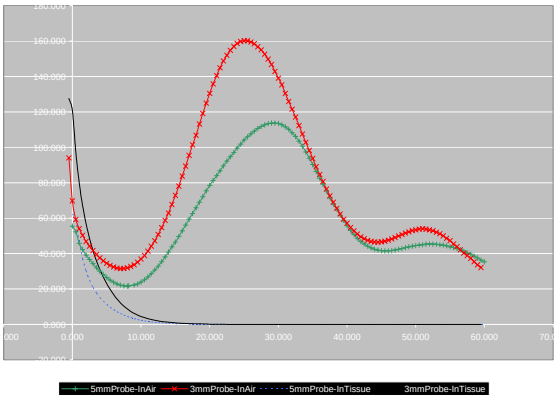

Figure 5: Comparison between the 2.8mm and 4.9mm probes in air and liquid-tissue with the WR159 waveguide.

V. Conclusion and Further Research

We have presented preliminary investigations of two fabricated probes (3mm and 5mm diameter probe) at 5.2 GHz, as well as a preliminary numerical investigation of two dipole-sensor sizes. The findings show that the fabricated probes yield good results in SAR measurements and that smaller sensor probes reduce the sensitivity of the probe, thus increasing the probe's uncertainty margins.

It has also been found that both mechanical positioning and optimum distance from the phantom surface will significantly affect SAR.

As part of our on-going work, we will investigate other factors affecting the dosimetric probe sensitivity at high-frequency, such as: sensor width, thickness, feed impedance, protective cylinder size and material, etc.

Acknowledgment

The authors would like to thank Mr. Dan Brooks, Mr. Atif Shamim-Khan and Mr. Paul Salem for their expertise in the numerical simulations, and Mrs. Yi Pan, for her experimental measurements.

References

[1] H. Bassen and G. Smith, "Electric Field Probes-A Review", IEEE Transactions on Antennas and Propagation, vol. AP-31, no. 5, Sept. 1983, pp. 710-718.

[2] ANSI/IEEE, "IEEE recommended practice for the measurement of potentially hazardous electromagnetic fields, 3kHz to 300GHz", ANSI/IEEE C95.3-1992.

[3] IEEE, "IEEE Recommended Practice for Determining the Peak Spatial-Average Specific Absorption Rate (SAR) in the Human Head from Wireless Communications Devices: Measurement Techniques" IEEE Std 1528-2003.

[3] IEC 62209-2 (Draft), "Human Exposure to Radio Frequency Fields from Hand-Held and Body-Mounted Wireless Communication Devices—Human Models, Instrumentation, and Procedures—Part 2: Procedure to Determine the Specific Absorption Rate (SAR) in the Head and Body for 30 MHz to 6 GHz Hand-Held and Body-Mounted Devices Used in Close Proximity to the Body" (Geneva: International Electrotechnical Commission, unpublished).

[4] Glenn S. Smith, "Limitations on the size of miniature electric-field probes", vol. MTT-32, no. 6, June 1984, pp. 594-600.

[5] D. Brooks, S. Nicol, J. Wojcik, "Wideband Complex Dipole Antenna Design for Reference measurements in the Human Body from RF Frequencies in the 5-6GHz Band," *EMC Zurich*, 2005, p 97-102.

[6] IEEE, "IEEE recommended practice for measurements and computations of radio frequency electromagnetic fields with respect to human exposure to such fields, 100 kHz-300 GHz", IEEE Std C95.3 (2002).

Wideband Complex Dipole Antenna Design for Reference Measurements in the Human Body from Radio-Frequencies in the 5-6GHz Band

Daniel R. Brooks, Stuart Nicol, Jacek Wojcik,
APREL Laboratories

ABSTRACT – Finite Difference Time Domain (FDTD) techniques were employed to design a complex half-wavelength dipole antenna model with a characteristic equal-ripple reflection coefficient across a frequency band. We will show how the Chebychev polynomial matching method discussed by Collin [1] Saad [2] and Oltman [3] has been implemented to increase the operational bandwidth of a dipole antenna design. This design method created an optimum wideband antenna used in the near-field of a phantom shell filled with a biological tissue simulation fluid *figure 7*. This setup can be used to determine the effects of peak and average Specific Absorption Rate (SAR) for system validation or for reference measurements and calculations. Numerical evaluations have been validated using experimental techniques, which involve electrical measurements, and SAR assessments using the ALSAS-10U, while the dipole is coupled to a dielectric which simulates the human body (simulation fluid) *figure 7* (Universal Phantom Model with dipole) at the frequencies under consideration. Numerically and experimentally derived peak and average SAR values have not been included in this paper.

Chebychev Polynomial Matching Method

The phase and amplitude of the antenna feedpoint reflection coefficient and impedance characteristics may be compared under different operating configurations to verify the response of our dipole model. The equal-ripple characteristic is obtained by making the reflection coefficient behave according to a Chebychev polynomial as shown in (1).

$$\Gamma = e^{-jN\theta}\frac{Z_A - Z_0}{Z_A + Z_0}\frac{T_N(\sec\theta_m \cos\theta)}{T_N(\sec\theta_m)} \qquad (1)$$

In the passband the maximum value of $T_N(\sec\theta_m \cos\theta)$ is unity $T_N(\sec\theta_m \cos\theta)\big|_{\theta=\theta m} = 1$, when $\theta = \theta_m$ the maximum allowable coefficient ρ_m occurs at the edges of the passband as shown in (2).

$$\rho_m = \frac{Z_A - Z_0}{Z_A + Z_0}\frac{1}{T_N(\sec\theta_m)} \qquad (2)$$

Numerical calculations are made to determine the optimum antenna dimensions required in creating the equal-ripple reflection coefficient response as shown in figure.1.

Equal-Ripple Reflection Coefficient

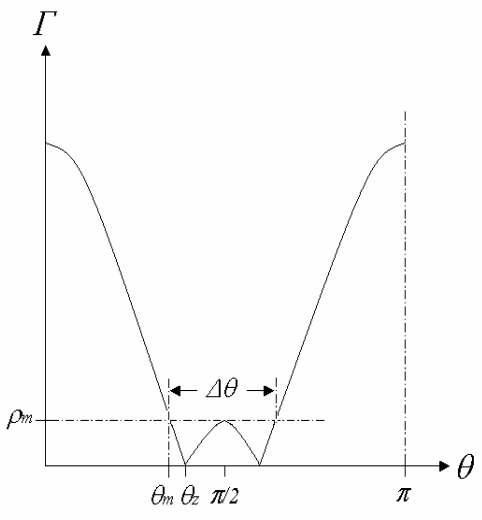

figure.1

The number of sections in the design determines the number of times the reflection coefficient ρ_m reaches the maximum value, within the passband. The tolerance of ρ_m is fixed, and the angle θ_m gives rise to the fractional bandwidth obtained from the relation described in (3).

$$\frac{\Delta\theta}{\pi/2} = \frac{\Delta f}{f_0} = 2 - \frac{4\theta_m}{\pi} \qquad (3)$$

A wide fractional bandwidth, Faraone [4], can be realized with rigorous control of the dipole antenna geometry. Numerical optimization is used to locate and then by adjusting the geometry, correctly position the upper and lower reactive zero θ_z resonant points. The optimum match is achieved when the reactive zeros θ_z align with points of minimum return loss or reflection coefficient *figure 10.* With the electrical characteristics attributed to the feed point of the antenna located close to the presence of the phantom that is filled with biological tissue simulation fluid.

Complex Dipole Antenna Model

FDTD provides the flexibility for modeling complex structures with the high degree of fidelity needed to evaluate antenna performance in near-field exposure conditions. Amplifier source matching is sensitive to antenna performance where output loading and power reflection are closely related to the antenna-matching components of the equivalent model in *figure 3*. Since SAR can be highly dependent on the surface current distribution on the device (resonant area) every effort was made to model the antenna and critical radiating structures of the circuit with optimized accuracy of the antenna matching components. The geometry and fine features of the complex dipole antenna in *figure 2* require special consideration so as to define the optimal cell size (discussed later) and object orientation that would reduce errors (known) to a minimum.

Complex Dipole Antenna (FDTD) Model

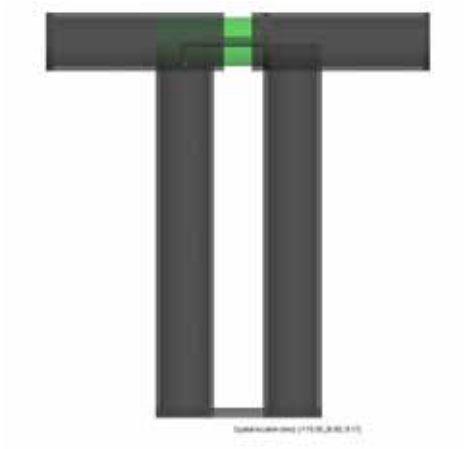

figure.2

Equivalent Model of Dipole

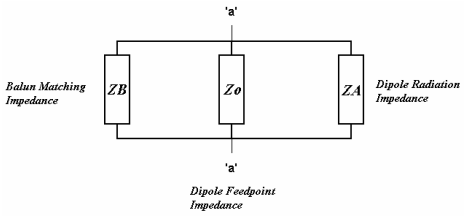

figure.3

Antenna impedance matching components and all other elements within the circuit that can potentially change the current distribution must be modeled correctly. While it may not be possible to model the exact shape and size of all the RF current contributing components, their effects on the near-field distribution produced by the overall device must be correctly represented and accounted for. The thickness and dielectric properties of the phantom plastic, its shape and size should be modeled *figure 7* to allow the dipole to be positioned precisely, ensuring correct energy distribution and coupling onto the phantom. The antenna must also resonate to ensure correct antenna current distribution. Mismatched antenna impedance will result in incorrect current distribution on the rest of the device test configuration. The electric and magnetic field distributions that can be expected are shown in *figures 4 & 5* respectively.

Electric Field Distribution

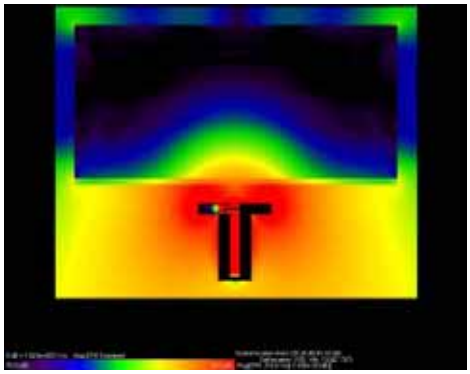

figure.4

Magnetic Field Distribution

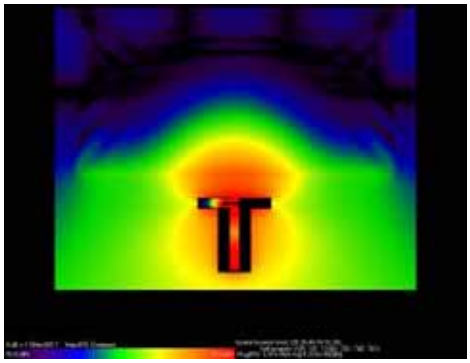

Figure.5

Geometry (Problem) Formulation

In our study, a numerical model of the complex half wavelength dipole antenna is placed near the numerical phantom (APREL Laboratories Universal Phantom) *figure 7* and is filled with a simulation liquid meeting the permitivity and conductivity requirements for the applicable frequencies. Application of the FDTD method requires determination of spatial and temporal aspects before commencing the calculation where the cell size should be λ/10 or less at the highest frequency of interest. For validation calculations, λ/20 or smaller cells are appropriate where the minimum cell size for 6.0 GHz in a medium with a relative permitivity of 40 should be;

$$Cell\ Size \le \frac{1}{20}\frac{c_0}{\sqrt{\varepsilon_r}\ f} \le 0.4\,mm$$

The FDTD method is applied to determine the electric and magnetic fields calculated inside the phantom together with the electrical characteristics of the dipole antenna and feed point. The dipole remains at a fixed distance of S=10mm between the dipole radial center and the tissue equivalent liquid of the model. The phantom shell is made from a low relative permitivity and conductivity material (ε_r = 3.7, σ = 0.008 S/m) and is T=2mm thick. The interior of the phantom is filled with a tissue equivalent liquid to a depth of 100mm with frequency dependant dielectric properties for the frequencies 5.2GHz (ε_r = 36.0, σ = 4.7 S/m) and 5.8GHz (ε_r = 35.3, σ = 5.3 S/m). The electrical geometric dimensions using 0.3mm size FDTD cell is (100 x 50 x 50)mm as presented in *Figure 6*. Although the phantom dimensions are significantly larger, to simplify the problem areas outside of the electrical geometry are excluded.

Problem Geometry

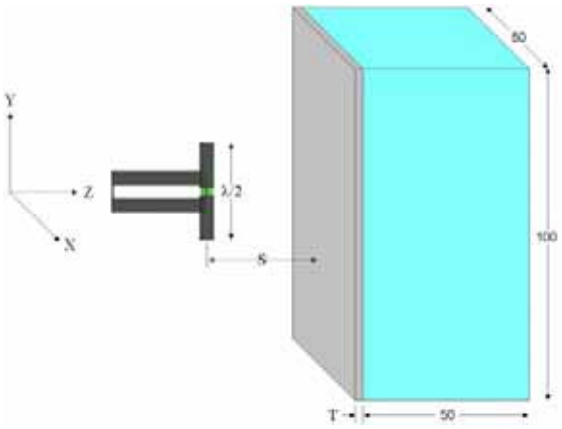

figure.6

The complex (balun included) half wavelength dipole antenna is placed parallel to the length side of the model and is oriented along the y-axis as shown in *figures 6 & 7*. Our dipole and electrical geometry is meshed using a cubic cell size of 0.3mm and is surrounded with a LIAO absorbing boundary with 20 cells of separation from all geometry facets. This expands the total electrical geometry solution space to a dimension of (115.5x62.7x112.5) FDTD cells of interest (electrical geometry) total 2.7 million. These calculations were performed using a Pentium Dual-XEON workstation and Remcom XFDTD software. The electrical geometry (including the complete Universal Phantom *figure 7*), cell size and separation distance remain fixed and do not change for all calculations presented. The only degrees of freedom permitted for changes to the model are with respect to the stimulus frequency 5.2GHz and 5.8GHz, and the tissue simulant parameters.

Universal Phantom Model

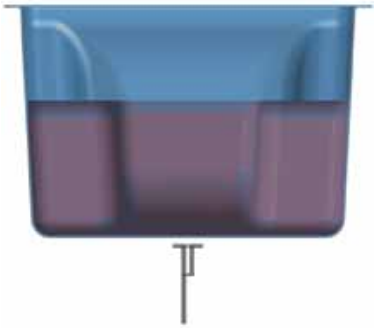

figure.7

The feed-point is excited with both Gaussian and sinusoidal waveforms of more than 20 cycles. This equates to 8000dt time-steps and allows courant stability to ensure steady state is reached, for proper calculation. The duration of the input signal has to be chosen so as to give steady state the number of steps necessary for the wave to propagate throughout the whole of the electrical geometry. The bandwidth of this source waveform is small and normally poses no problems to grid step and distance from boundaries. The SAR (*W/kg*) can be determined (measured or calculated) at any point from the electric field within the electrical geometry. Where *E* is the electric field in (*V/m*), σ is the conductivity (S/m), and ρ is its mass density ($1.0\ kg/m^3$) of the tissue in which the measurement is made. The calculated results of the dipole electrical characteristic parameters and the calculated SAR values are normalized to 1watt of input power and this shall be discussed in a future paper.

Theoretical and Measurement Results

The theoretical calculations of the model in *figure 2* are compared with experimental measurements of the actual dipole construction following the same physical dimensions as what was used and optimized within the FDTD model. The theoretical calculations in *figure 8* are derived from the impulse response and are verified with experimental measurements on our first physical model *figure 9.*

Calculated Return Loss

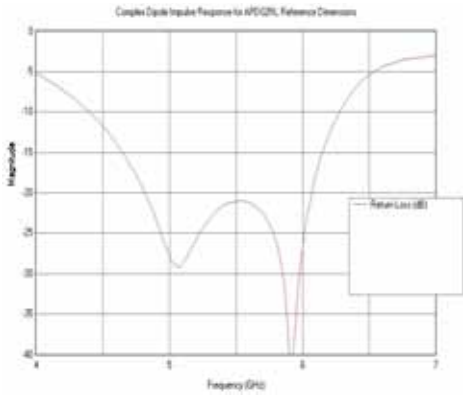

figure.8

Measured Return Loss

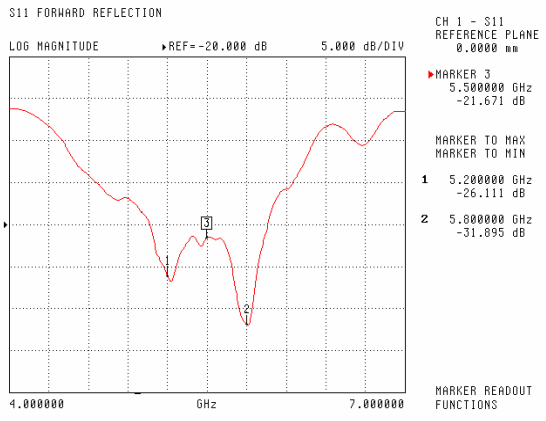

figure.9

The impulse response electrical performance relative to tissue and air is represented in *figures 10 & 11* respectively. Several production dipoles were constructed and measured; the physical dimensions and respective VNA results are presented in *figure 12.*

Impulse Response in Tissue

figure.10

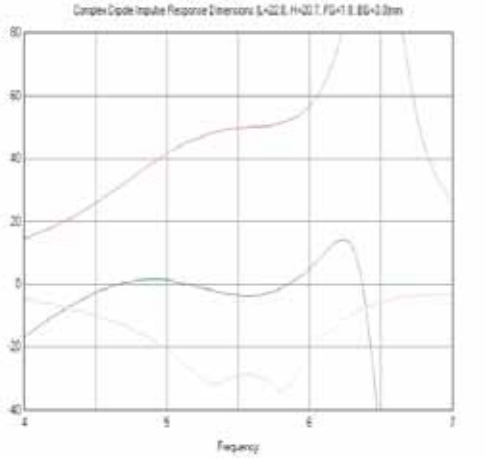

Impulse Response in Air of FDTD Model

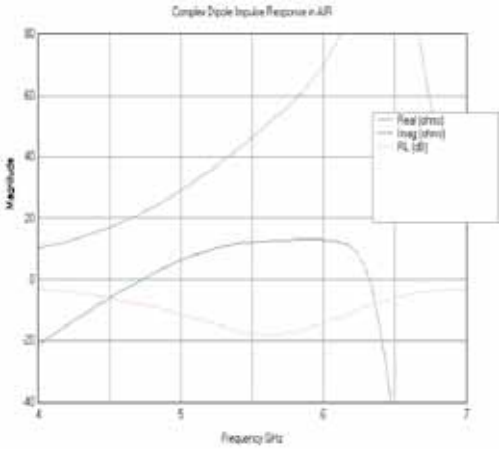

figure.11

Measurements

FREQUENCY	LENGTH	HEIGHT	GAP	DIAMETER	REAL	IMAGINARY	RL
MHz	mm	mm	mm	mm	ohms	ohms	dB
5200	22.8	20.7	1.8/3.0	3.6	47.1	0.5	-30.6
5800	22.8	20.7	1.8/3.0	3.6	52.8	-1.5	-29.5

figure.12

Conclusions

Our research demonstrates very good agreement between a theoretical numerical model and an actual physical dipole experiment. The interaction of the tissue properties on the dipoles electrical performance is well studied and repeatable. We have demonstrated the application of the Chebychev matching methods of previous research, and put them into practice. Results can be used for the determination of SAR target numbers related to exposure of simulated human tissue fluid specifically for the 5-6GHz frequency band.

Experimental studies were conducted using the physical model of the APREL Laboratories Universal Phantom *figure 7* which resulted from a study into methods for reducing errors for compliance assessment Wojcik & Harrington [9] and the development of the broad band dipole antenna. The tissue simulation fluids used within the experimental studies consisted of two mixtures, and the overall depth of tissue within the phantom was fixed at 10cm. The dipole was placed at a separation distance of 10mm (dipole centre to tissue). The dipole was connected to a Vector Network Analyzer and assessed using $^{S}11$ parameters for return loss, standing wave ratio, and impedance.

The computational modeling is based on the finite-difference time-domain analytic software (XFDTD) provided from Remcom Inc., which was used to derive the data for this report [8]. This paper demonstrates a viable method to evaluate the accuracy of numerical and experimental research with measurements and calculated data presented.

References

[1] Robert E. Collin, "Foundations for Microwave Engineering", McGraw-Hill, 1966, pp. 223-235.

[2] Theodore S. Saad, "Microwave Engineers Handbook", Volume 2, Artech House, 1971, Optimally Matched Compensated Balun, page 51.

[3] George Oltman, "The Compensated Balun" IEEE Transactions on Microwave Theory and Techniques, volume MTT-14 no. 3 March 1966, pp.112-119.

[4] A. Faraone, "Towards a Low-Power Exclusion" Motorola Labs, Presentation to IEEE SCC34-SC2, May22, 2003, page 19 (unpublished).

[5] A. Faraone, Q. Balzano and D. Simunic, "Experimental Dosimetry in a Sphere of Simulated Brain Tissue Near a Half-Wave Dipole Antenna," *IEEE Int. Symp. On EMC* , 1998, pp. 906-911.

[6] N. Kuster and Q. Balzano, "Energy Absorption Mechanism by Biological Bodies in the Near Field of Dipole Antennas Above 300 MHz." *IEEE Trans. On Vehicular Technology*, vol. 41, no.1, Feb. 1992, pp. 17-23.

[7] IEC 62209, IEEE1528.

[8] Kunz K S, and Luebbers R J, "The Finite Difference Time Domain Method for Electromagnetics", CRC Press, 1993.

[9] J.J. Wojcik and T. Harrington "Analysis of Head Phantom Dimensional and Shape Relative Errors in Wireless Specific Absorption Rate (SAR) Compliance Assessment. *2001 IEEE EMC Itnl Symposium PP 1158-1163*

Future Activities

As part of the ongoing research activities APREL Laboratories with support from the Spectrum Sciences Institute and in cooperation with Remcom (among others) will work on developing a new method for simulating anatomical tissues at frequencies in the 5-6GHz range. The data will be made public and be presented to other forums. The intention is to lead further developments of numerical evaluations for complex dipole and tissue models.

Further research is essential for the progress of international standards covering the frequency range of 5-6GHz so it is essential to have bi-lateral participation and input. Activities that need further attention through research include but are not limited to the following:

1. Creation of a defined methodology and set of guide lines for users of numerical code, where results may be used as a reference.
2. Investigation into the effects of RF sources on tissue at frequencies above 3GHz.
3. Define experimental homogeneous models based on research into the effects of RF on tissues above 3GHz.
4. The creation of stable tissue recipes for use in frequencies above 3GHz based on scientific research, traceable back to geometrically accurate heterogeneous anatomical models

EFFECTS OF DIPOLE LENGTH ON DOSIMETRIC PROBE SENSITIVITY

Alain Tran[1, 2], Mustapha C.E. Yagoub[1] Stuart Nicol[2]
[1]School of Information Technology and Engineering, Ottawa University,
Ottawa, Ontario, K1N 6N5
Canada
[2]APREL Laboratories 51 Spectrum Way, Ottawa, Canada K2R 1E6
Email: atran@site.uottawa.ca

ABSTRACT
Accurate measurements of electromagnetic radiation effects on human body require the use of very sensitive and highly miniaturized probes to improve spatial resolution. In this paper, the authors investigate the effect of smaller dipole-sensor on the sensor sensitivity to very small electric E-field magnitudes. Numerical simulations of various dosimetric E-field dipole lengths and two dielectric probe-protecting shells have been performed at 5.2 GHz and 5.8 GHz. Results show shorter dipole-sensors have lower sensitivity than longer dipole-sensors and the effect of shell dielectric constant is negligible.

KEY WORDS
Dosimetry, SAR, RF exposure, dipole-sensor, Finite element method.

1. Introduction

With the advances in microelectronic technology, leading manufacturers of dosimetric probes are currently developing 5–6 GHz probes with very small dipole-sensors. These dipole-sensors are typically less than 2 mm in length. The major benefit of highly miniaturized probes, at frequencies greater than 5 GHz, is to improve spatial resolution and over come small penetration depths. A proposal has been made to the IEC committee for inclusion into the *draft* standard 62209-2 [1] which recommends that the maximum probe-tip diameter be 16 / (freq in GHz) millimeters; thus determining that the largest tip-diameter for 5.8 GHz specific-absorption-rate (SAR) evaluations is 2.8mm.
The purpose of this paper is to investigate the effect of smaller dipole-sensors on the probe sensitivity, in particular, its performance in detecting very small electric-fields (E-field) using the finite-element-method [4]. Results will show that smaller sensors reduce the probe sensitivity by increasing the minimum-detectable field.

2. Background

The negative effect of reducing the probe size on its sensitivity has been analytically investigated by [2]. It has been found that, for a given incident E-field, when the physical dimensions of the probe is reduced by a given scale factor [k] (where k < 1), the minimum-measurable E-field detected by the sensor increases approximately by a factor [k^{-2}]. To reduce the dipole length by half would require the minimum source field to be four times larger so as to be detectable.
If the source frequency is much greater than the cut-off frequency ($\omega^2 >> \omega_c^2$), the detected voltage is frequency-independent [2]:

$$|Vo| \approx \beta_o \left(\frac{C_A}{C_A + C_j} \right)^2 \frac{h^2 |E_z^{inc}|^2}{2}.$$

Here V_o is the sensor output voltage, β_o is the diode current-sensitivity (20A/W for an ideal diode at 290K), C_A is the capacitive component of the electrically-short dipole input impedance, Cj is the parallel capacitance in a high-frequency equivalent circuit of the diode, *h* is the haft-length of the dipole, and $E_{z,inc}$ is the z-axis incident E-field. It is readily seen that the detected output voltage is proportional to the square of three parameters: dipole-length, incident field, and the capacitive ratio between the antenna and the diode. Note that the antenna capacitance C_A is proportional to dipole-length *h* and the effective relative permittivity of the substrate. Assuming the diode is mostly reversed-biased at high frequencies, C_j is essentially constant and independent of diode voltage and temperature [3]. A typical reversed-biased value for C_j is between 0.1pF and 0.4pF. Thus the length of the dipole is the most important parameter affecting the detected voltage thus reducing the length will significantly reduce this voltage.

3. Probe description

Miniaturized dosimetric E-field probes are generally used to measure electric fields induced in homogeneous tissues representative of biological body conditions by relatively low-level radio-frequency transmitters that cannot be detected by thermal methods. The rate at which RF

energy is absorbed in tissue is described in terms of Specific absorption rate (SAR). SAR is defined as [6]:

$$SAR = \frac{\sigma |E|^2}{\rho} \ (W/kg),$$

where σ is the electrical conductivity, |E| the RMS magnitude of the electric field strength vector, and ρ the mass density of the medium. Various radiation safety standards require that the maximum SAR not exceed a specified value at any localized point within the body of a person exposed to RF fields [5, 6].

To simplify the numerical study, the drawing of the probe used in the simulation has one single dipole. However, dosimetric E-field probes consist of an array of three orthogonally aligned electrically short dipole sensors. Each dipole sensor (probe) has the following components [5]: a diode detector, a dielectric substrate as mechanical support, a highly resistive balanced transmission line. E-Field probes are then connected to a differential amplifier, and a detected-signal processor. Sources such as dipoles or waveguides are generally used in laboratories during probe calibration and characterizations. In this numerical study, a dipole was used as the source-antenna.

In order to make the probes implantable in tissue or tissue-simulating liquid, they are housed within a protective cylindrical shell. The shell electrically and mechanically protects the fragile sensors. The HFSS simulation does not however take into account the zero-bias Schottky diode, which, is placed across the gap of each dipole to detect small E-fields of magnitude in the order of 1 mV per mW/cm^2 in free space, nor does it take into account the feed-lines. However, given the very high-impedance of these feed-lines and the small size of the diode, their effects are deemed to be negligible.

4. Numerical results

We simulated various lengths of the dipole-sensor to study how this affects the field intensity captured by the sensor.

Figure **1** illustrates the numerical simulation setup. It consists of a closed-end dielectric cylindrical shell (ε_r = 3.2 and 4.6) which surrounds the substrate and the sensor. The substrate is a thin dielectric strip (ε_r = 2.2) on which the sensor rests. The sensor is composed of two perfectly-balanced electric-conductor strips, each having dimension of (0.3 x 1.2) mm. The thickness of the sensor is 0.1 mm.

For the purpose of this simulation, the two arms are separated by a lumped-port length 0.4 mm. The source-dipole is composed of two perfectly-electric-conductor cylinders of radius 1.8 mm with a length of 14.4 mm (for the 5.2 GHz case) or 12.9 mm (for the 5.8 GHz case). The two arms are separated by a 11.3 mm-long lumped-port. The structure is immerged in a liquid whose electrical characteristics represent those presented in IEC for head..

Simulations were performed at 5.2GHz and 5.8GHz; then followed by a third simulation where the dipole length is reduced by 0.5 mm on each side. Results, shown in Figure **2**, demonstrate that shorter dipoles decrease the captured field magnitude, and thus decrease the sensor sensitivity.

To examine the influence of the protective cylindrical shell to the captured field, two dielectric materials were used.

Figure **3** shows that the probe shell has a negligible effect on the detected field. Here, the normalized distance (0 to 1) corresponds to the range [0.5mm, 15.5mm] from the source center. Noticeable effects only occur at very close distance, where the field is decreased by a few hundred(s) V/m. Likewise, the difference due to changes of the shell dielectric constant is insignificant, as shown in Figure 4.

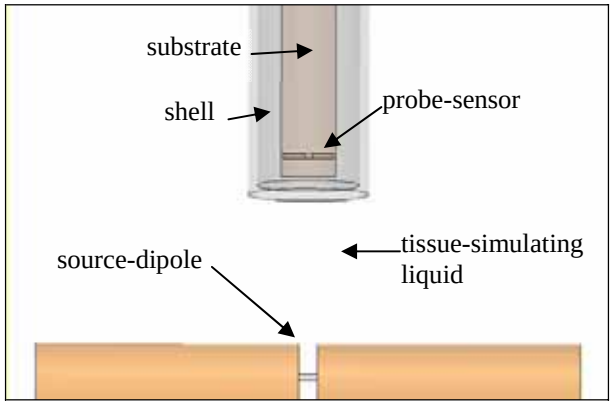

Figure 1: Sensor (top) and source (bottom) dipoles.

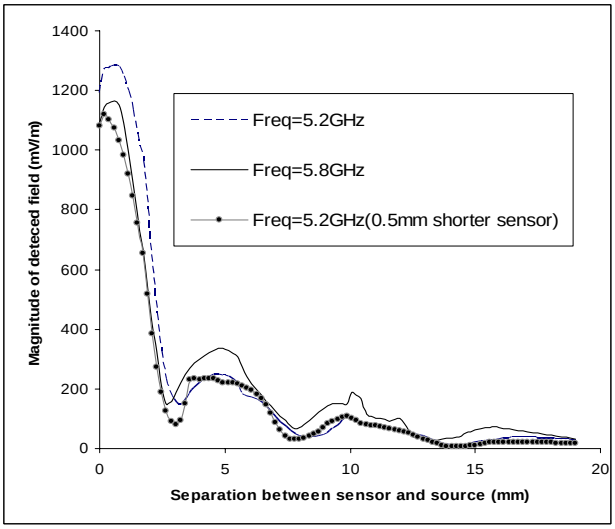

Figure 2: E-field magnitude captured by the sensors.

The distance between the protective shell and the dipole-sensors, or between the protective shell and the phantom surface, can be a major contributing factor in the boundary effect [7]. Boundary effect is defined as a

change in sensitivity of an E-field probe when the probe is located close to the phantom boundaries (less than one probe-tip diameter). It is caused by the external field being strongly perturbed by the superposition of a scattered field from the probe. Errors due to boundary effect can be reduced to less than 2% if the distance between the probe tip and the surface is kept greater than half the probe diameter [7].

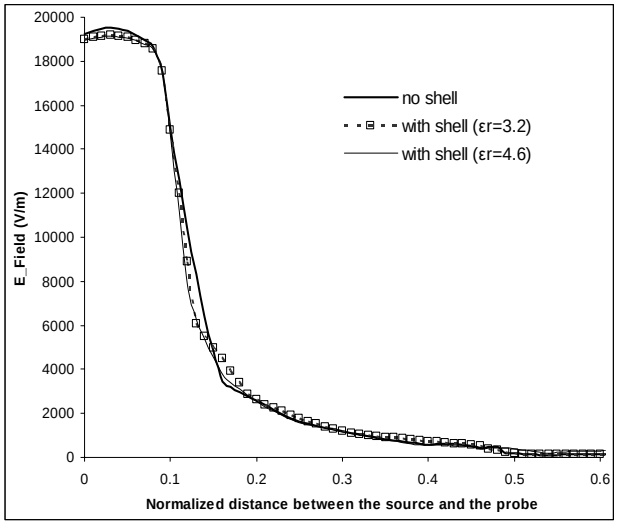

Figure 3: Cylindrical shell influence on E-field.

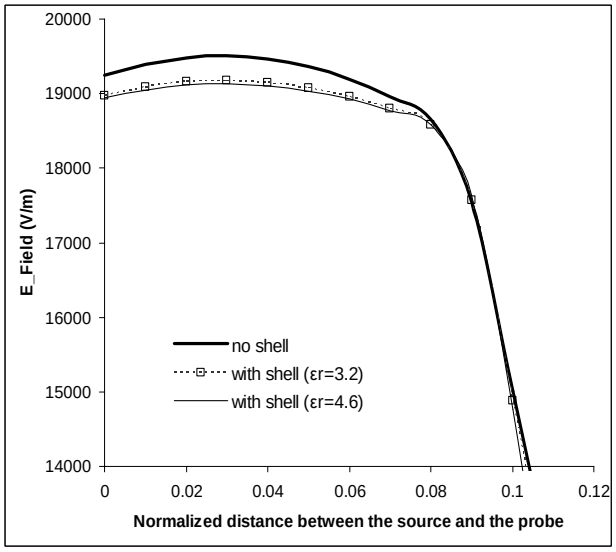

Figure 4: Zoom-in view of Figure 3.

Numerical regression of the results show that the received power decays exponentially with respect to the distance, at distances of [λ/50] or less from the source. At farther distance, the received power decays with a factor of [$x^{-1.5}$], where 'x' is the distance. This provides a more precise description of the field behavior in the immediate proximity of the source, in complement with the well-known description of the field behavior in the near-field and far-field regions.

5. Conclusion

Evaluation of the numerical values derived from our studies have been verified against previously determined simulation results, which utilized XFDTD, and experimental techniques executed using the ALSAS-10U (APREL Laboratories SAR Assessment System) and our new findings track extremely well with these previously derived values. We have presented a numerical investigation of various dipole-sensor lengths and the effect of two dielectric probe-protecting shells. The findings show that smaller sensors reduce the sensitivity of the probe by increasing the minimum-detectable field specification of the probe. In other words, the source power must be higher to be detected by the probe or spatial resolution and half diameter distances form the phantom boundary to sensor center be utilized in experimental measurements. We have also established that a higher dielectric constant of the probe-protecting shell also decreases the probe-sensitivity, although this effect is very small.

Further investigations will be needed to study other factors affecting the dosimetric probe sensitivity at high-frequency, such as sensor width, thickness, feed impedance, and protective cylinder size. Furthermore, as probes are getting smaller, mechanical positioning and minimum distance from the phantom surface can become dominant factors that influence SAR values. Actual dosimetric E-field probes consist of an array of three orthogonal electrically short dipole sensors, the next step of our work is to simulate the field behavior using the three-dipole configuration.

It can be assumed that the decrease in sensitivity would necessitate a need for improved spatial positioning within the electric field. However if a slightly larger sensor length is employed greater sensitivity would allow for reduced spatial resolution and greater half diameter boundary distances to be employed.

Acknowledgements

A brief acknowledgement section may be included between the Conclusion and References (optional). Do not include author biographies.

References

[1] IEC 62209-2 (Draft), "Human Exposure to Radio Frequency Fields from Hand-Held and Body-Mounted Wireless Communication Devices—Human Models, Instrumentation, and Procedures—Part 2: Procedure to Determine the Specific Absorption Rate (SAR) in the Head and Body for 30 MHz to 6 GHz

Hand-Held and Body-Mounted Devices Used in Close Proximity to the Body" (Geneva: International Electrotechnical Commission, unpublished).

[2] Glenn S. Smith, “Limitations on the size of miniature electric-field probes”, vol. MTT-32, no. 6, June 1984, pp. 594-600.

[3] B.R. Strickland, N.F. Audeh, “Diode-loaded dipole antenna modeling and design”, Antennas and Propagation, IEEE Transactions on Volume 41, Issue 3, March 1993 Page(s):333 – 337.

[4] *Ansoft*-HFSS v.9.x, Ansoft Corp., Pittsburg, PA.

[5] H. Bassen and G. Smith, “Electric Field Probes-A Review”, IEEE Transactions on Antennas and Propagation, vol. AP-31, no. 5, Sept. 1983, pp. 710-718.

[6] ANSI/IEEE, “IEEE recommended practice for the measurement of potentially hazardous electromagnetic fields, 3kHz to 300GHz”, ANSI/IEEE C95.3-1992.

[7] IEEE, “IEEE Recommended Practice for Determining the Peak Spatial-Average Specific Absorption Rate (SAR) in the Human Head from Wireless Communications Devices: Measurement Techniques” IEEE Std 1528-2003.

• CONSULTING • RESEARCH • TRAINING • CERTIFICATION TESTING SINCE 1981

Probe Calibration Module
WR159 Waveguide
Frequency Band (5-6)GHz

Presented By: Stuart Nicol

APREL Laboratories
51Spectrum Way,
Ottawa, Canada
K2R-1E6
1-613-820-2730
s.nicol@aprel.com
dan.brooks@aprel.com

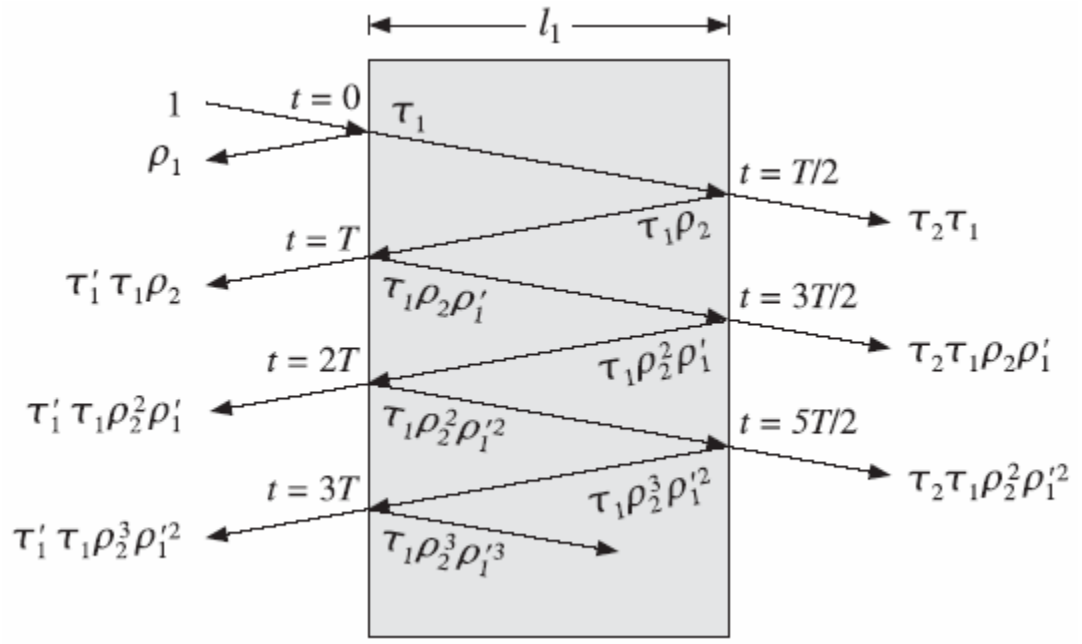

$$\Gamma_1(\omega) = \rho_1 + \sum_{n=1}^{\infty} \tau_1\tau_1'(\rho_1')^{n-1}\rho_2^n z^{-n} = \rho_1 + \sum_{n=1}^{\infty} \tau_1\tau_1'(\rho_1')^{n-1}\rho_2^n e^{-j\omega nT}$$

$$\Gamma_1(t) = \rho_1\delta(t) + \sum_{n=1}^{\infty} \tau_1\tau_1'(\rho_1')^{n-1}\rho_2^n \delta(t - nT)$$

Frequency vs Time Domain of Micro-reflection Impulse Response

WR159 Waveguide in XFDTD

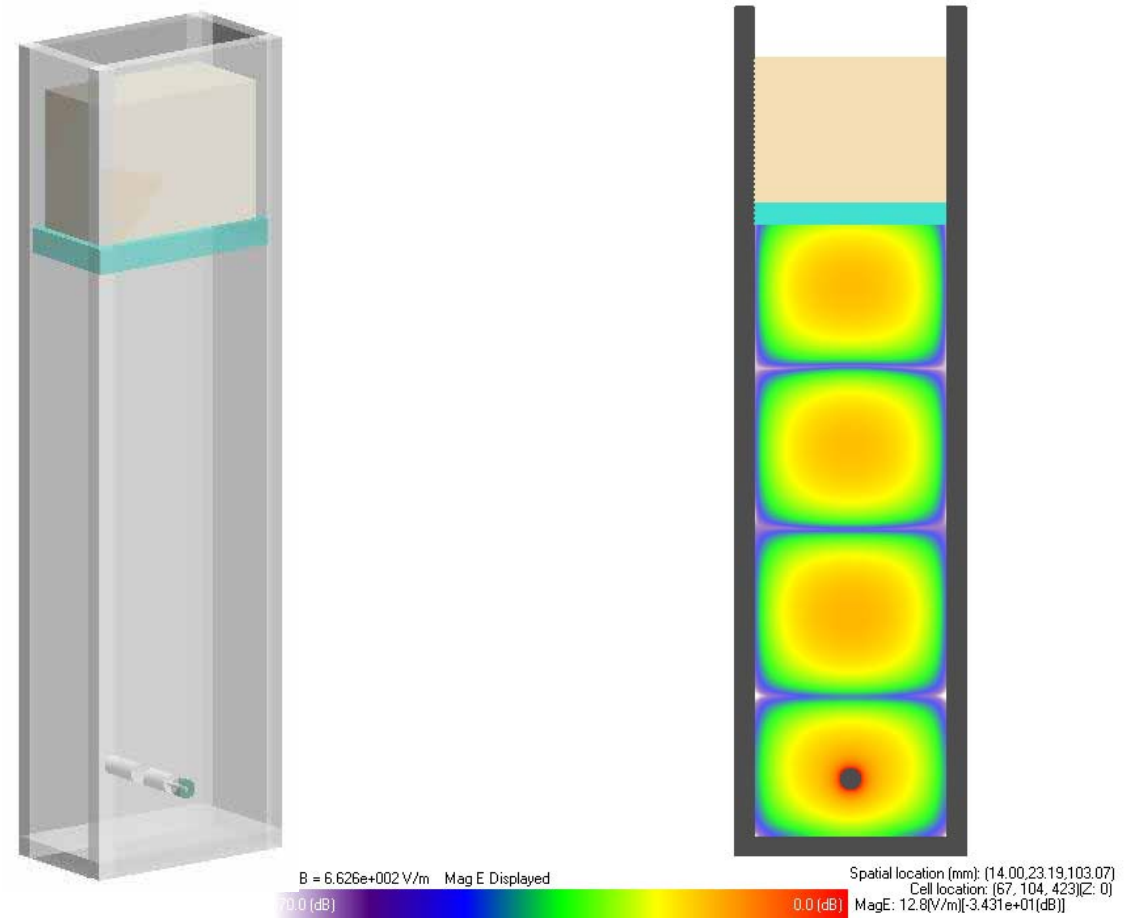

Functional Block Diagram Power Link Budget

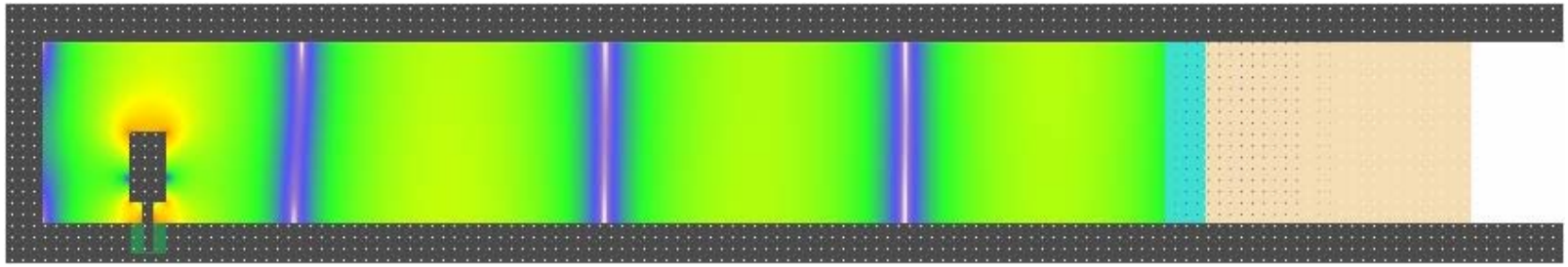

TE10 Propagating Wave

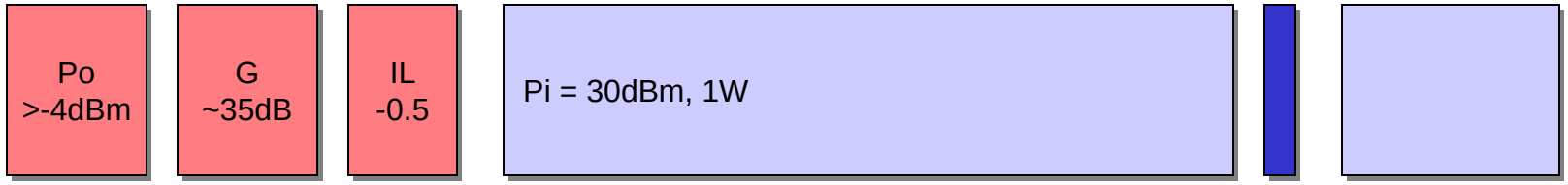

Source AMP Coupler WR159 Coaxial-WG Transition WR159 Window WR159 TEM

Electric Field Distribution 3D Solid View

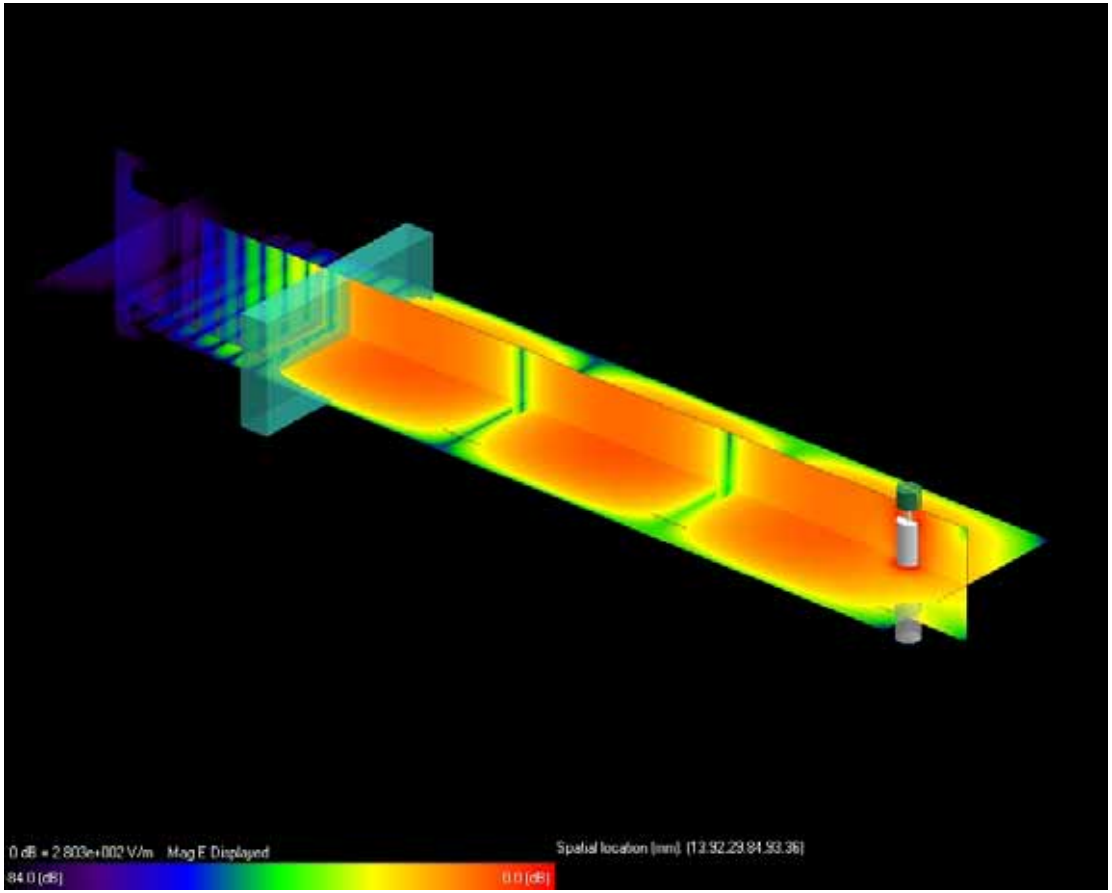

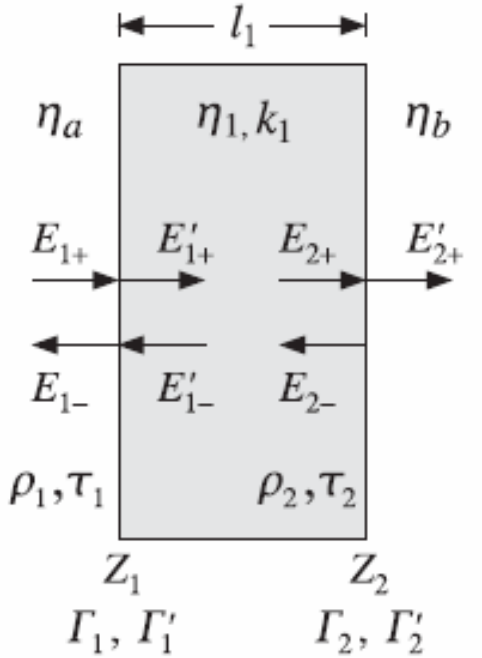

$$\Gamma_1(z) = \frac{\rho_1 + \rho_2 z^{-1}}{1 + \rho_1 \rho_2 z^{-1}} \quad where \quad z^{-1} = e^{-j\omega T} = e^{-2jk_1 l_1}$$

$$\Gamma_1 = \frac{\rho_1 - \rho_2}{1 - \rho_1 \rho_2} = \frac{\eta_1^2 - \eta_a \eta_b}{\eta_1^2 + \eta_a \eta_b} = \frac{n_a n_b - n_1^2}{n_a n_b + n_1^2}$$

$$\frac{\eta_b - \eta_1}{\eta_b + \eta_1} = \rho_2 = \rho_1 = \frac{\eta_1 - \eta_a}{\eta_1 + \eta_a} \quad \Leftrightarrow \quad \eta_1^2 = \eta_a \eta_b$$

quarter-wave: $l_1 = (2m+1)\frac{\lambda_1}{4}$, $\eta_1 = \sqrt{\eta_a \eta_b}$, η_a, η_b arbitrary

Dielectric Window Dimensional Formulation

S2P Ideal Match

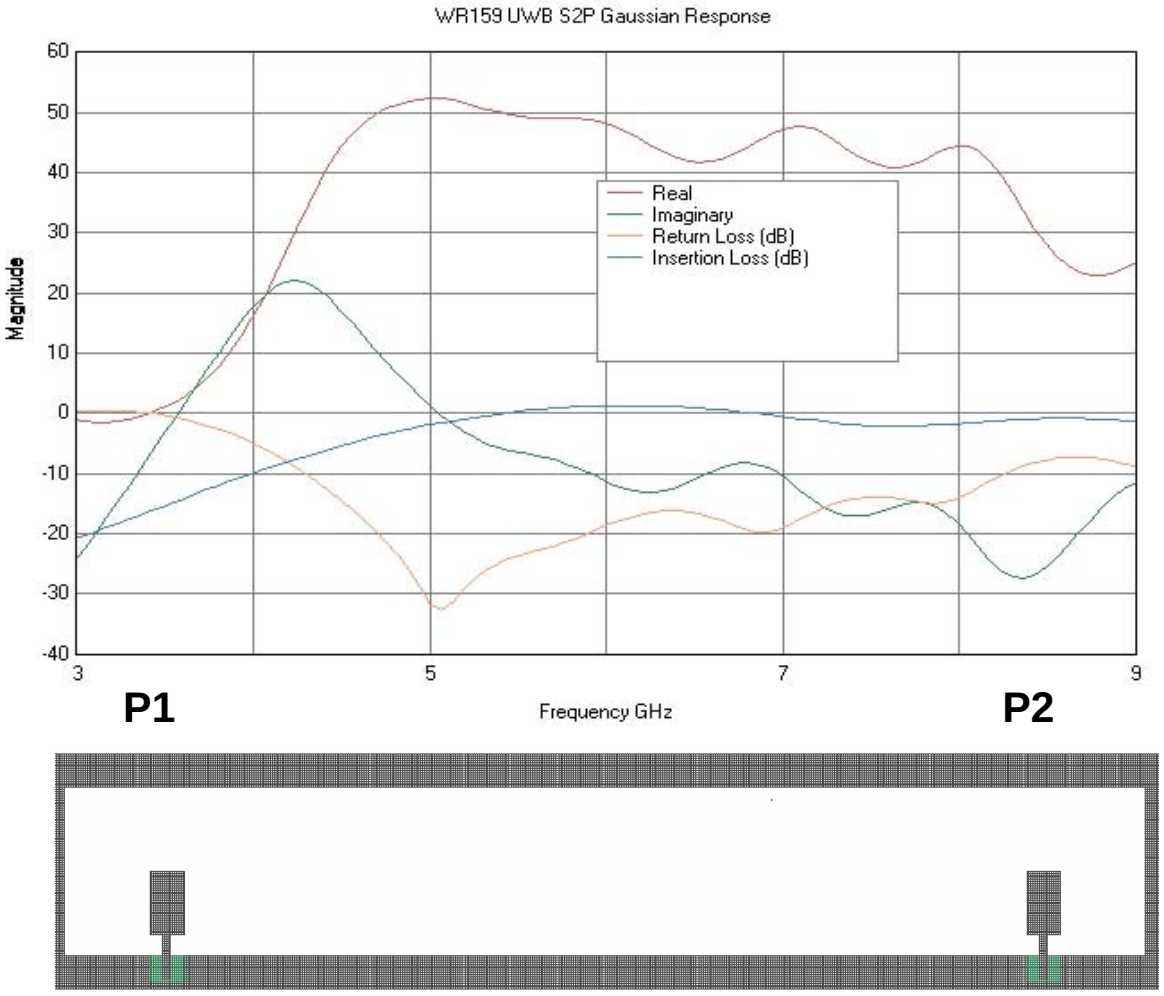

UWB S11 for 5.2GHz

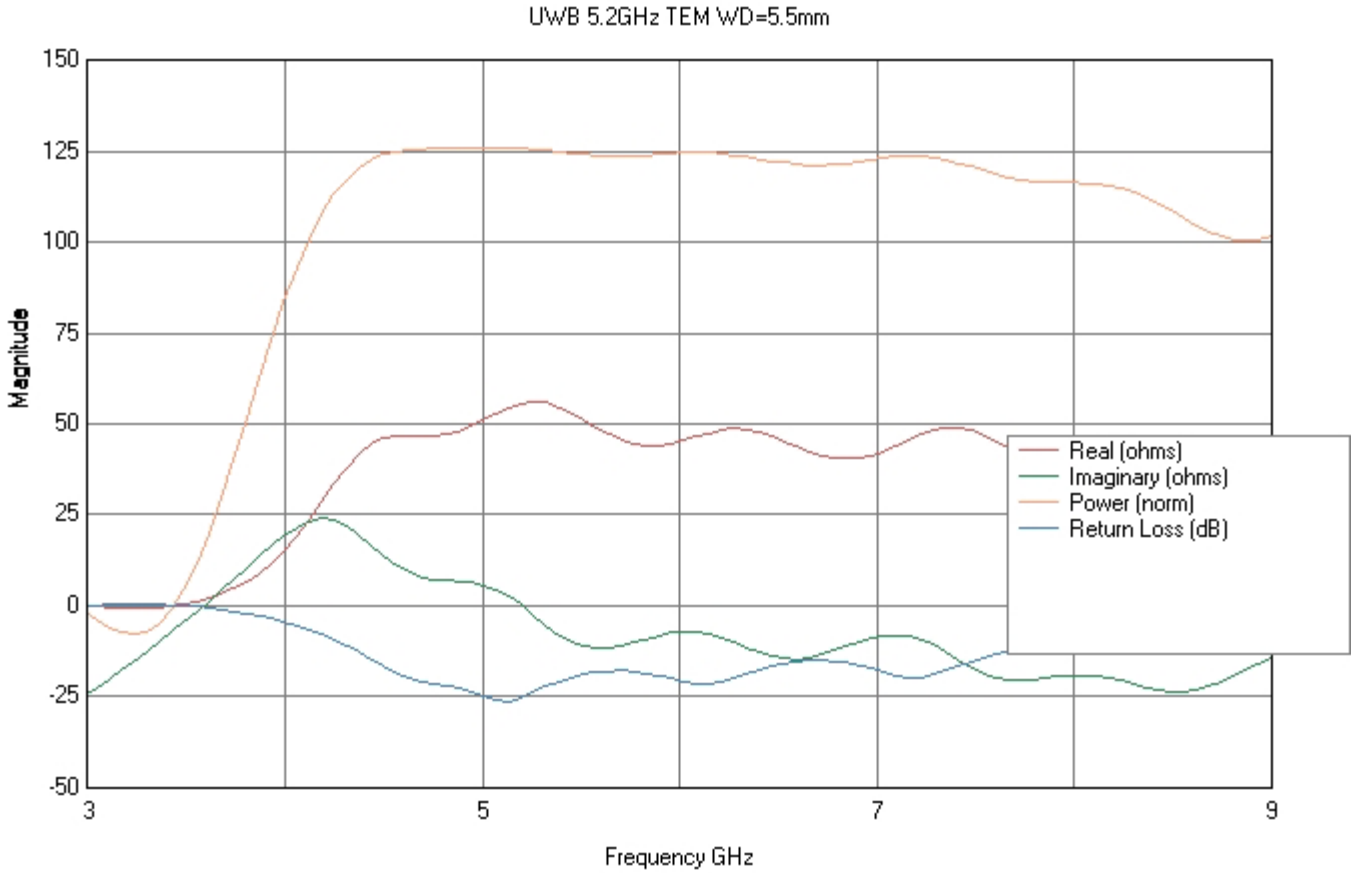

Steady State S11 for 5.2GHz

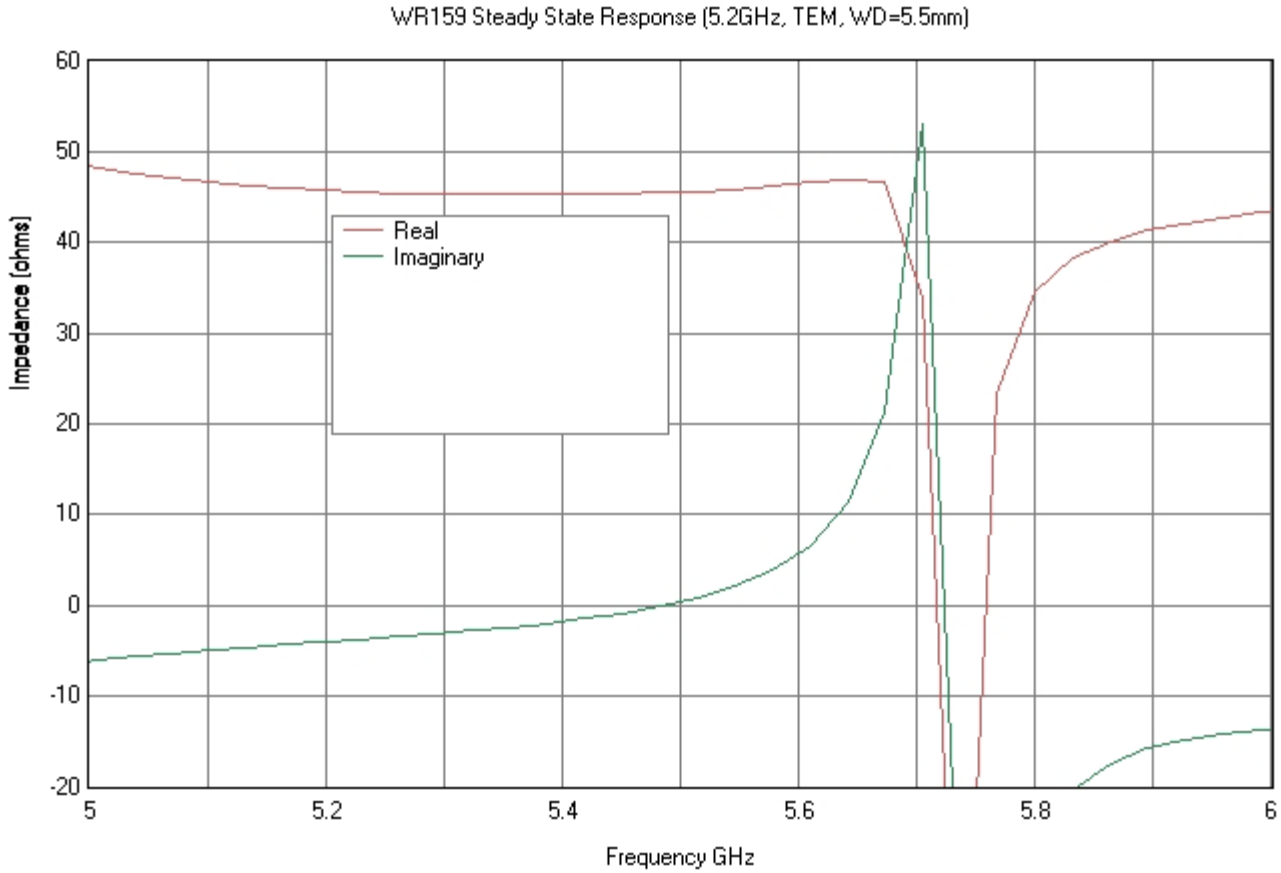

UWB S11 for 5.8GHz

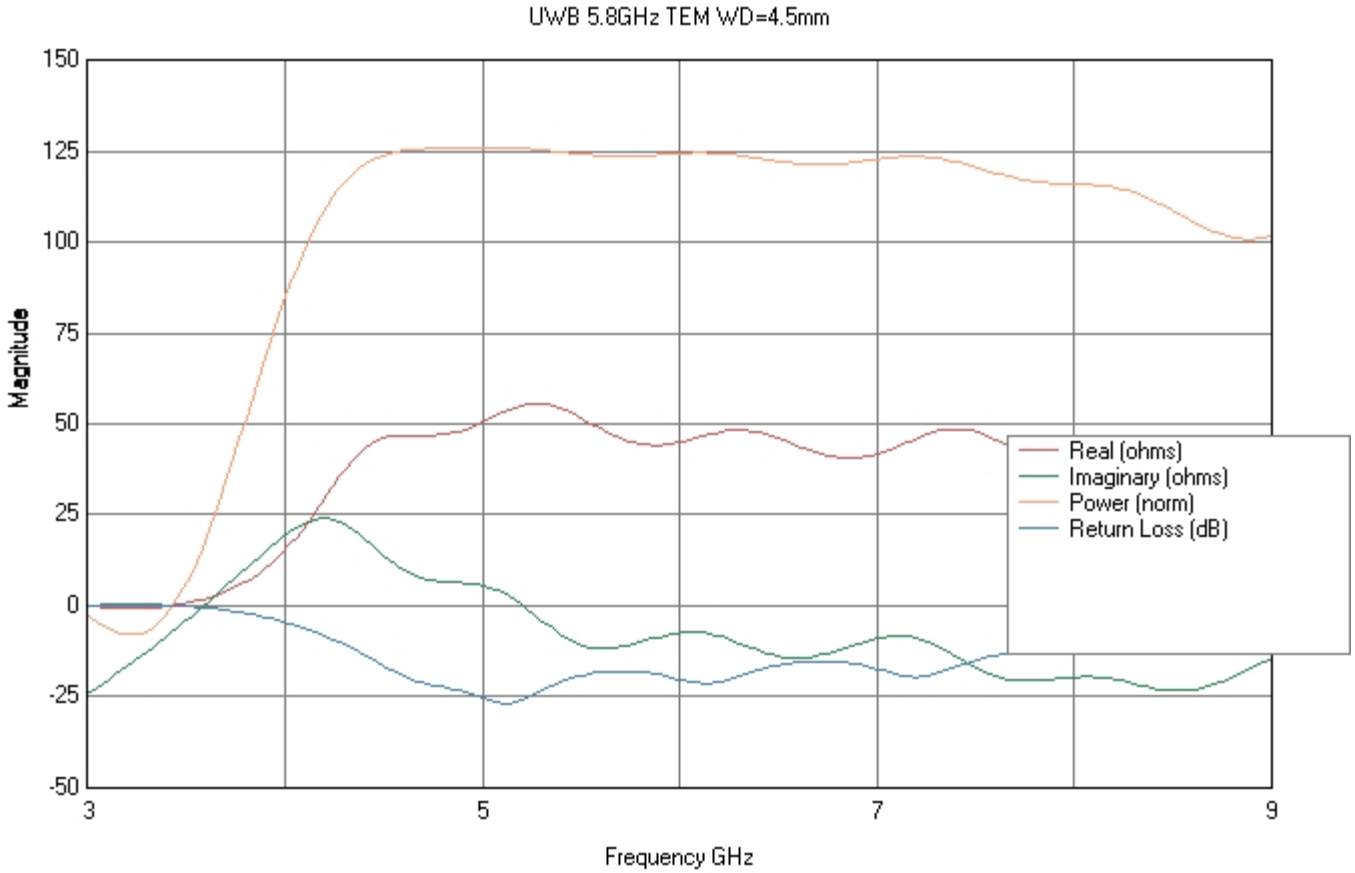

Steady State S11 for 5.8GHz

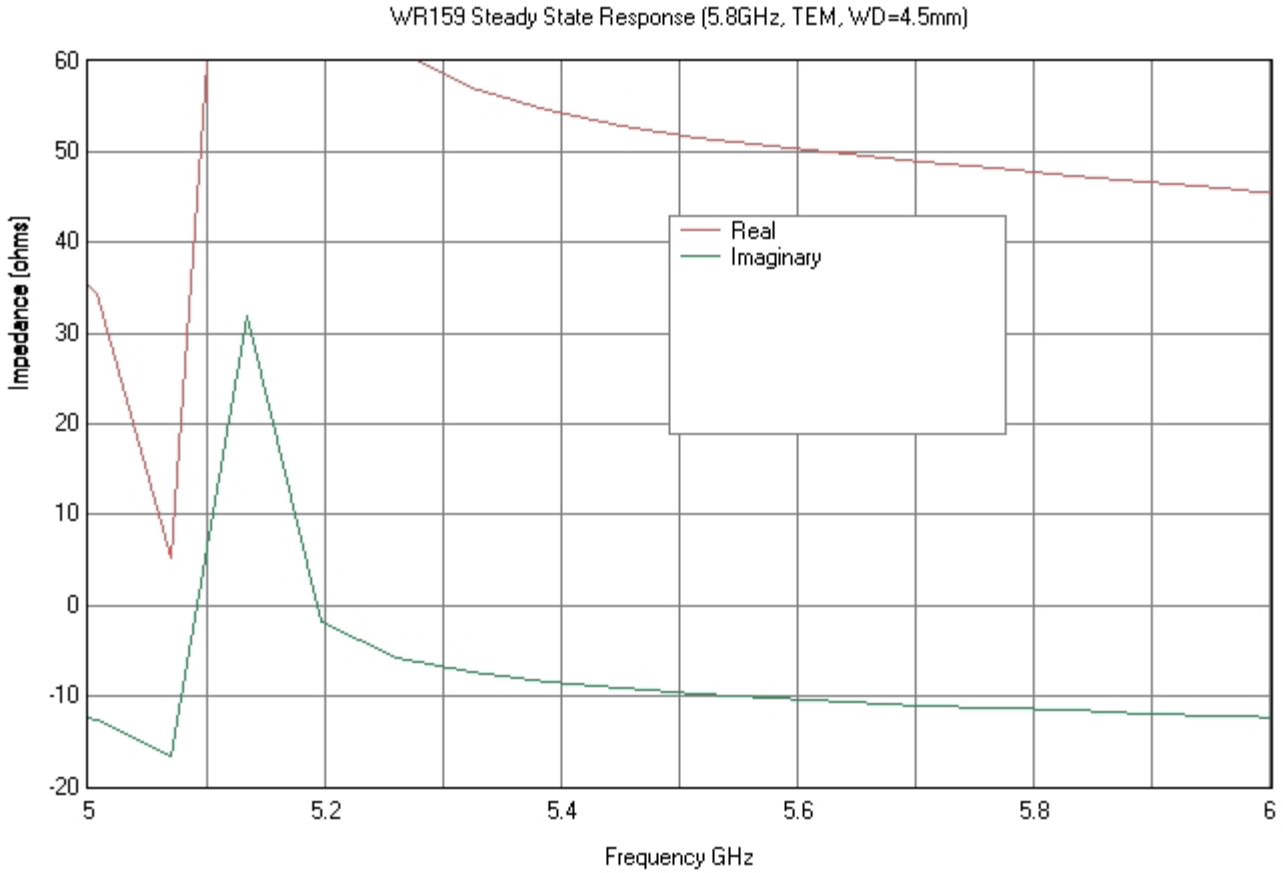

WR159 Adaptor-Window-Sleeve (4.93mm Dielectric Slab)

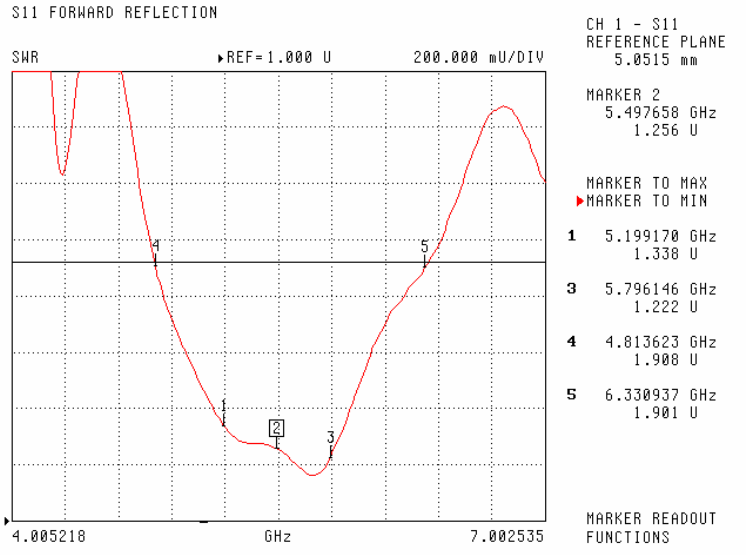

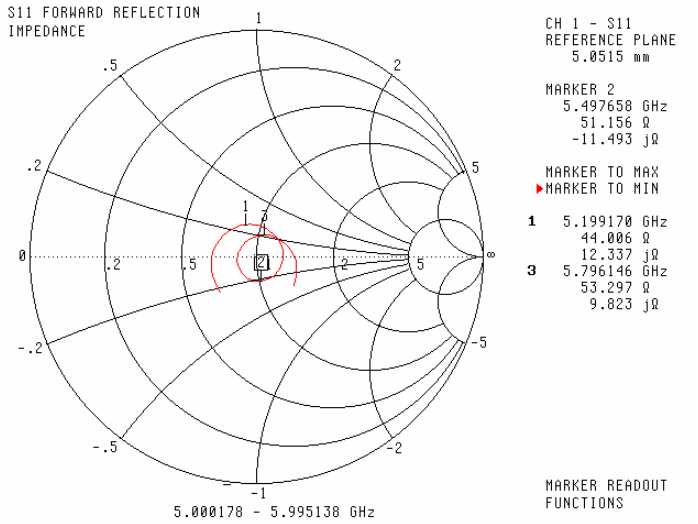

Appendix X Defines 28mm with εr' 3.2

Frequency	Thickness	Thickness	Length	width
GHz	mm	inch	inch	inch
5.2 & 5.8	4.93	0.194 +/- 0.001	1.658 +/- 0.03	0.862 +/- 0.03

WR159 Adaptor-Window-Sleeve (4.93mm) 5.2GHz Tissue

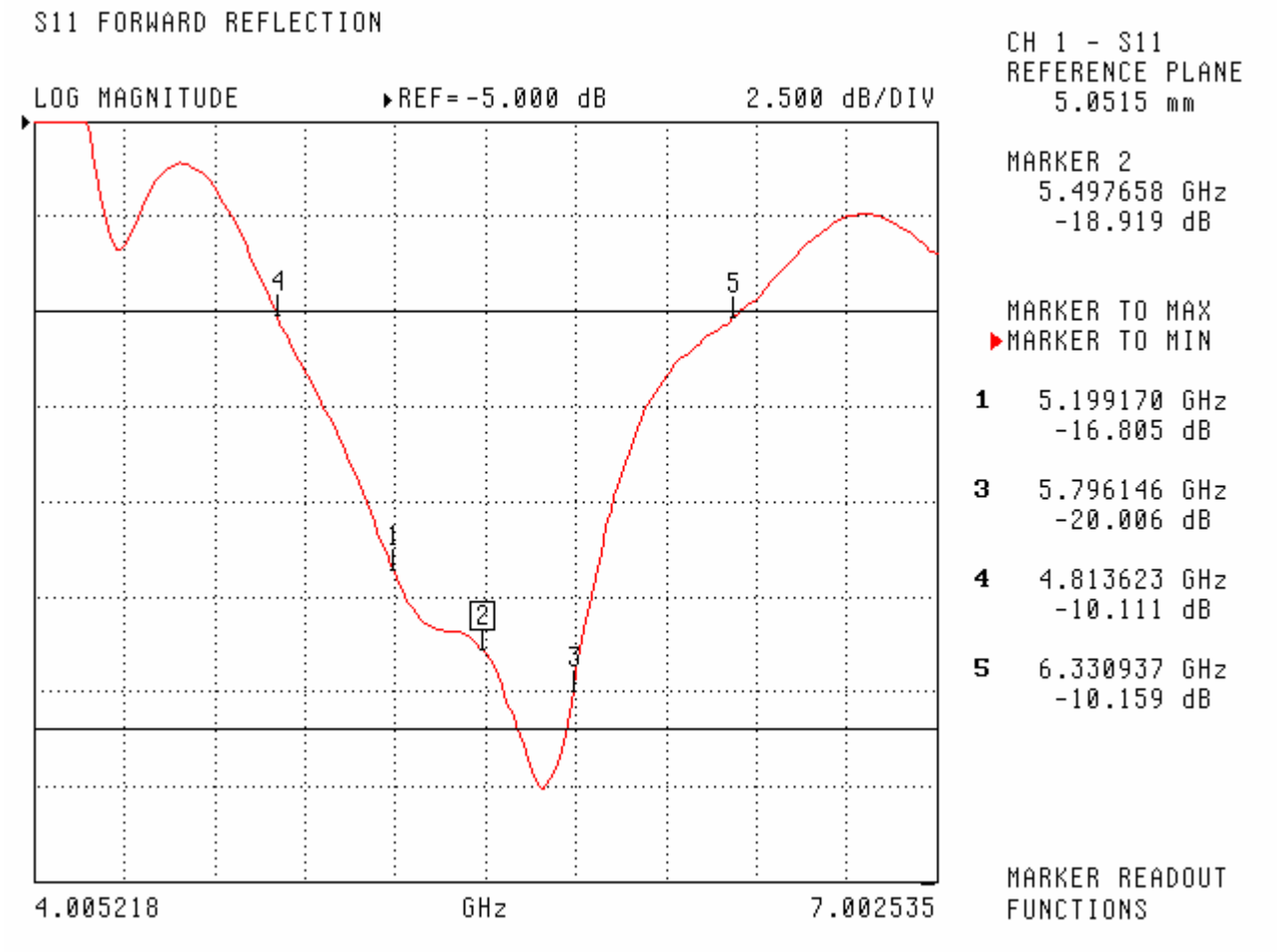

Relative Field Strength in the TEM Liquid

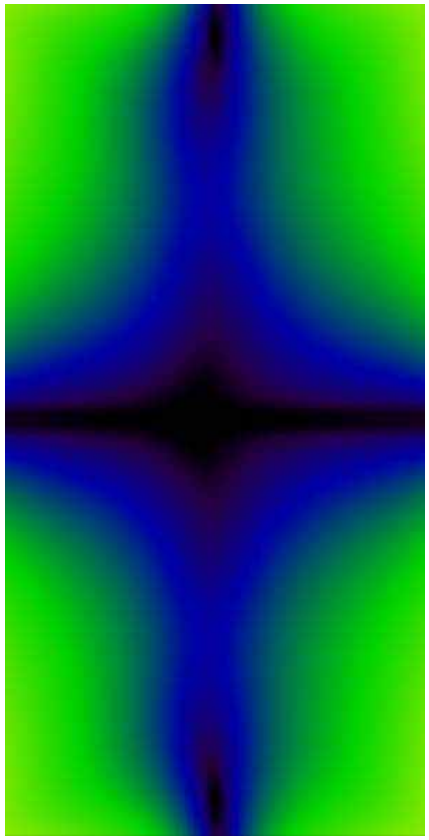

Ex

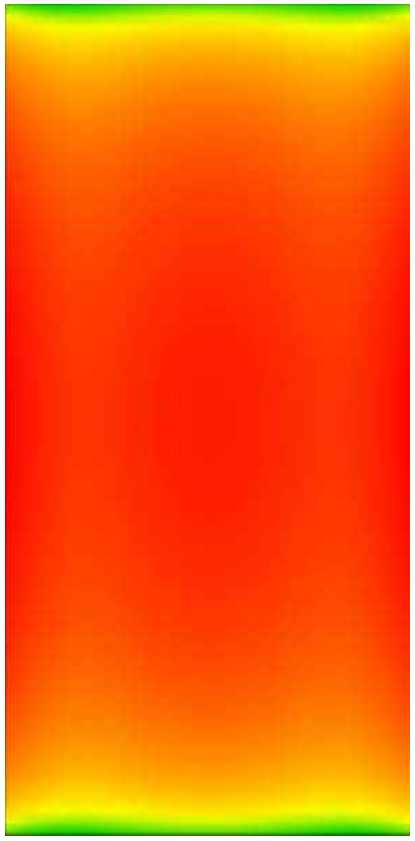

Ey

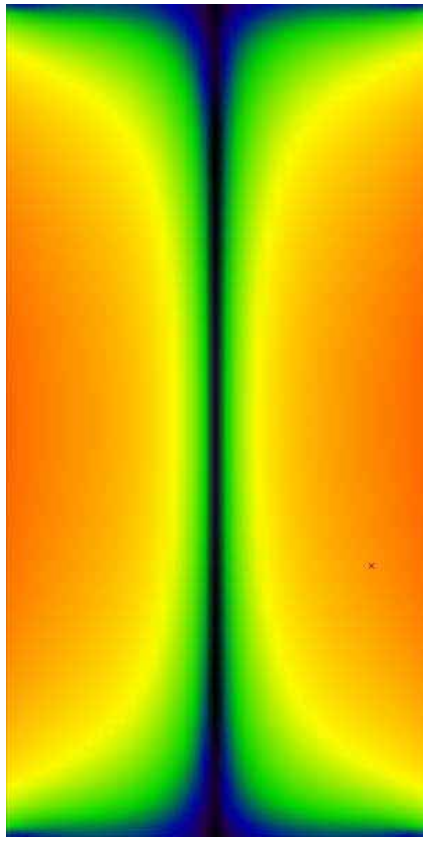

Ez

Electric Field Distribution 3D Ey Field Vector Linearity or Purity

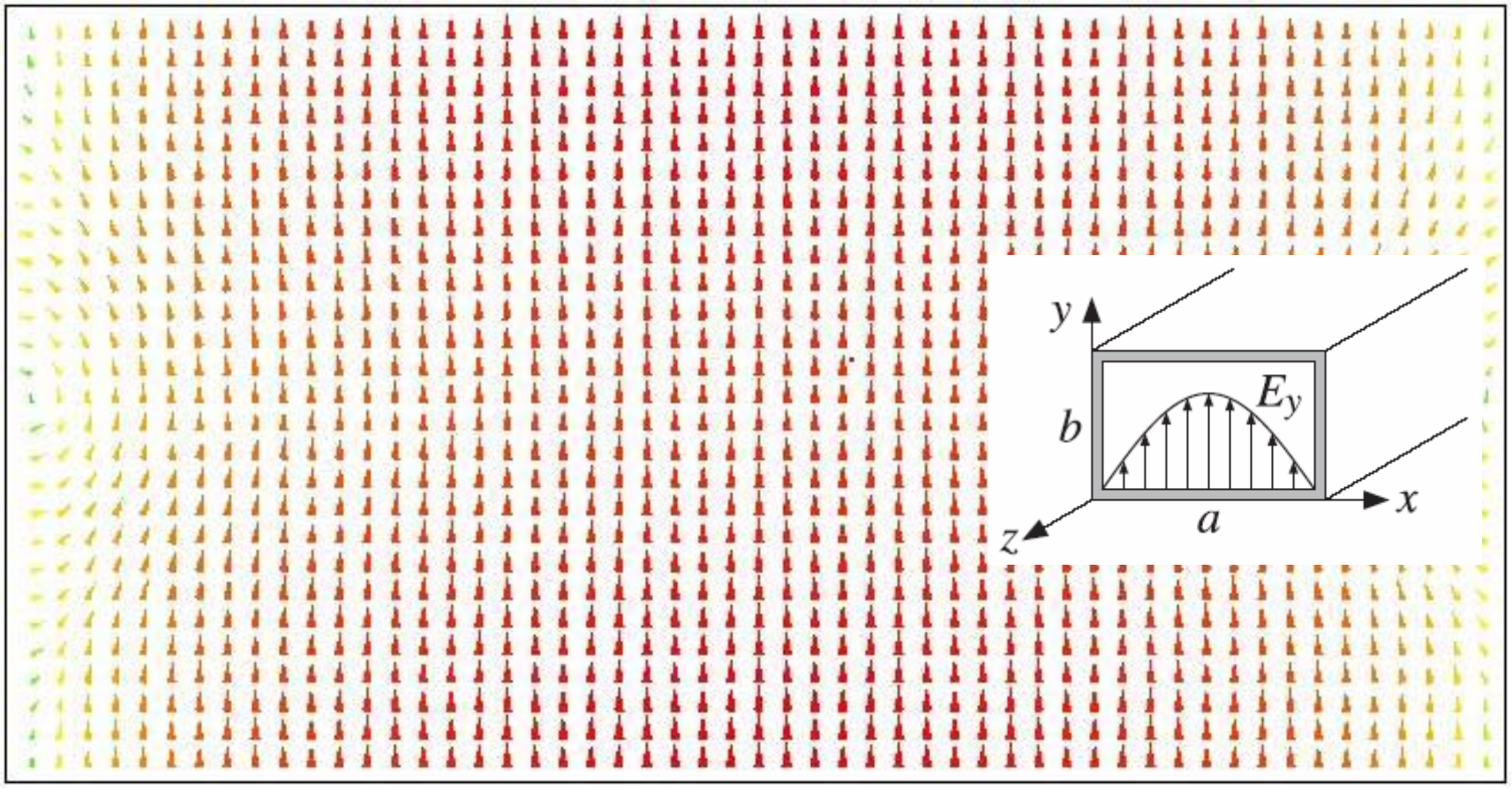

Analysis of Phantom Boundary Shell and the Resultant Matching Effect of Shell on SAR (Specific Absorption Rate) Values

Daniel Brooks, Stuart Nicol, Jacek Wojcik, APREL Laboratories

ABSTRACT **-** Finite Difference Time Domain (FDTD) methods were employed to develop the complete mechanical structure (complex) of the half-wavelength experimental dipole models used to conduct this research. This paper examines how the phantom shell dielectric boundary affects the Specific Absorption Rate (SAR) for simulations based on experimental system validation measurement protocols and the resultant calculations. Numerical calculations are made to determine complex electric and magnetic field magnitudes along with the SAR values within the APREL Laboratories universal phantom filled with tissue simulation fluid. Secondary calculations are made without the universal phantom shell (elimination of phantom shell boundary) being in place and compared against the prime phantom model data.

Introduction

Calculated values determine the basis for experimental Specific Absorption Rate (SAR) target numbers used for the determination of system conformity (validation) prior to experimental evaluation. Protocols used are well documented and widely accepted by standards creation bodies, including those referenced within this paper [1-3] and specifically for the (5 to 6) GHz frequency band. The generally accepted methods have been used to determine the affects of the phantom shell on conservative SAR.

Experimental laboratory measurements of the SAR level is the standard method of showing compliance with regulatory [6] RF safety limits for electromagnetic energy (EME) induced in the human body from near-field radio frequency (RF) emitting devices. Results are derived by applying the Finite Difference Time Domain (FDTD) method [4,5] which includes the creation of complex antenna characteristics in the near field so as to calculate the interactions within high-resolution numerical models. Research has already been conducted using numerical models of the human body for the evaluation of SAR levels under a wide range of exposure scenarios [7] extending our scientific knowledge of the subject.

Other examples contained within the listed literature are to model handheld transceivers [8] utilising wire and cylindrical antenna structures, using the method of moments (MOM) and coupled integral equations (CIE). These methods can be used to investigate the coupling phenomenon between a three-dimensional numerical human model and a dipole antenna with respect to variations of separation distances between the antenna and human model. Experimental results for the near field of dipole antennas and the SAR absorption mechanism of simulated brain tissue in a sphere [9] and phantom box [10] is also listed for reference.

Different types of antenna geometries operating in the close vicinity of human models have been examined [11-12] with the FDTD method, so as to identify an optimum circuit producing results for the SAR distribution relative to antenna performance and tissue parameters.

Our goal was to model the complete mechanical structure (complex) of a half-wavelength dipole antenna ***figure.1*** in order to gain new insight in providing a capacity to verify the accuracy of the experimental approach used to determine target SAR values.

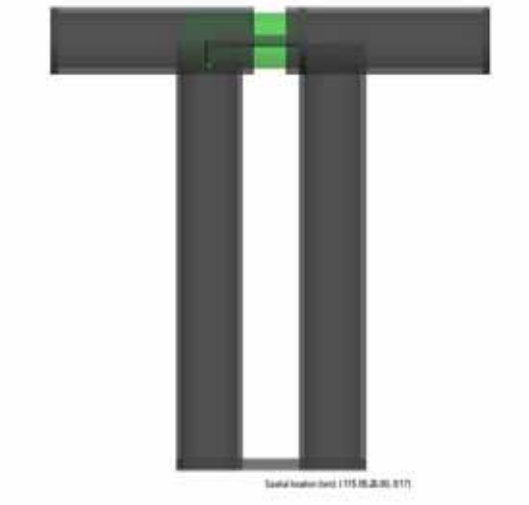

Figure.1 FDTD Model of Complete Mechanical Dipole Structure

Problem Geometry Formulation

Application of the FDTD method requires the determination of spatial and temporal aspects of the problem before commencing the calculation where the cell size should be λ/10 or less at the highest frequency of interest. For validation calculations, where λ/20 problems occur smaller cells are appropriate where the minimum cell size for 5.8 GHz in a medium with a relative permitivity of 40 should be:

$$Cell\ Size \le \frac{1}{20}\frac{c_0}{\sqrt{\varepsilon_r}\, f} \le 0.4\,mm \qquad eq.\ 1$$

The FDTD method is applied to determine the SAR values from the electric fields calculated inside the APREL Laboratories Universal Phantom (UP) together with the electrical characteristics at the antenna feed point. The dipole remains at a fixed distance of S=10mm between the dipole radial centre and the tissue equivalent liquid of the model ***figure.2***. The dipole is excited with a sinusoidal source at the resonant frequency and consequently the magnitudes of the field values are derived after performing a Discrete Fourier Transformation (DFT).

The alteration in the values of SAR and the values of the antenna's input impedance are presented with respect to the phantom shell being included and again with the phantom shell removed. The phantom shell is 2mm thick made from a low relative permitivity and conductivity plastic material (ε_r = 3.7, σ = 0.008 S/m). The interior of the phantom is filled with a tissue equivalent liquid with frequency dependant dielectric properties for the specific frequency to a depth of 100mm.

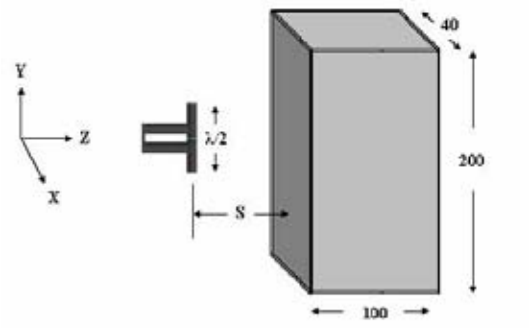

Figure.2 XFDTD Calculation Model

The complex (balun included) half wavelength dipole antenna is placed parallel to the length side of the model and is oriented along the y-axis also shown in ***figure.3***.

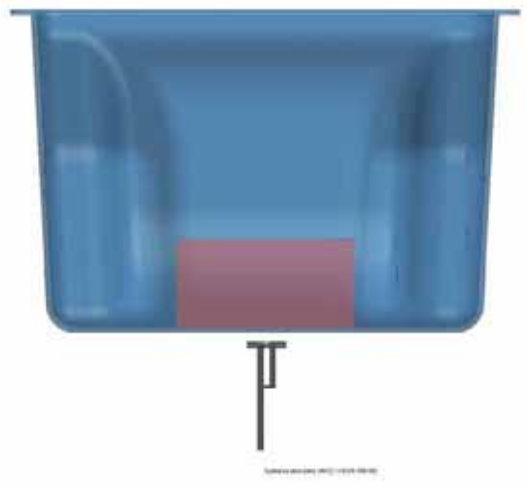

Figure.3 Universal Phantom and Dipole

Our dipole and phantom geometry is Cubically Meshed (CM) using a voxel size of 0.3mm and using an adaptive Variable Mesh (VM) using a 3:1 ratio and is surrounded with a Liao [13] absorbing boundary with 20 cells of separation from all geometry facets. The solution geometry dimensions and separation distance remain fixed and do not change for all the calculations. The only degrees of freedom is a change to the phantom shell thickness (0mm, 2mm, 4mm) the tissue dielectric parameters along with the dipole and balun length relative to the frequency of interest throughout the study.

The dipole antenna feed-point is excited with a sinusoidal stimulus of more than 20 cycles which equates to 8000dt time-steps or (–30dB) convergence to satisfy Courant stability ensuring that steady state is reached for proper calculation. The SAR (W/kg) can be determined (measured or calculated) at any point from the electric field at that same point. Where *E* is the electric field in (V/m), σ is the conductivity (S/m), and ρ is its mass density (kg/m^3) of the tissue in which the measurement is made. The calculated SAR values are normalized to 1watt of input power.

Discussion of Numerical Results

Case A) Phantom shell thickness is changed as shown in ***figure.4*** and ***figure.5*** for (0,2 and 4mm variations) for the frequency of 5.2GHz highlighting the effect on SAR and dipole resonance.

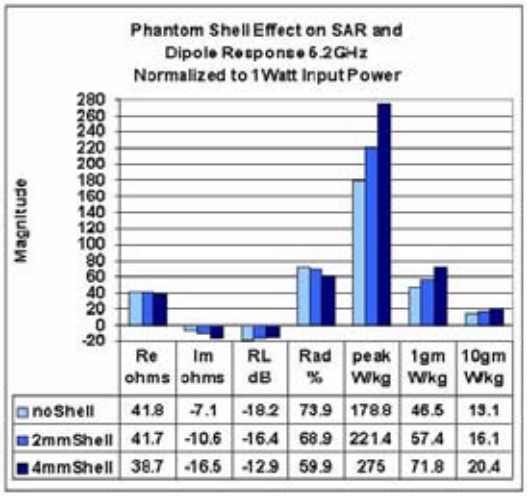

	Re ohms	Im ohms	RL dB	Rad %	peak W/kg	1gm W/kg	10gm W/kg
noShell	41.8	-7.1	-19.2	73.9	178.8	46.5	13.1
2mmShell	41.7	-10.6	-16.4	68.9	221.4	57.4	16.1
4mmShell	38.7	-16.5	-12.9	59.9	275	71.8	20.4

Figure.4 SAR and Dipole Analysis for 5.2GHz

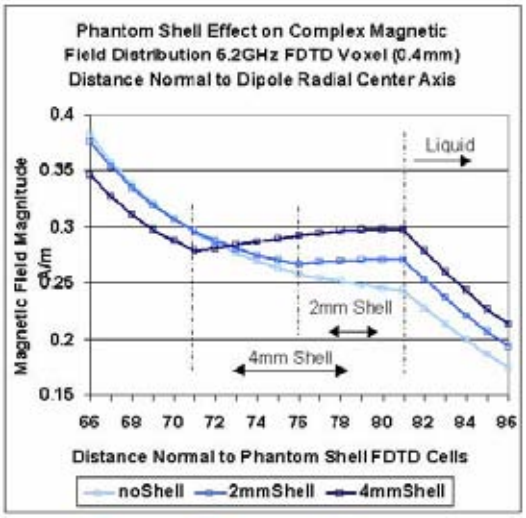

Figure.5 Shell v.s. HFM for 5.2GHz

The phantom shell boundary is located between FDTD cells (71 and 81 for a 4mm shell and 76 to 81 for 2mm shell) with tissue boundary located at 81. Considering the results in ***figure.4*** and looking at the magnetic field distribution across the shell in ***figure.5***, it is shown that a stronger magnetic field exists at the human tissue simulant boundary as the shell thickness increases.

Higher SAR values are calculated with the phantom shell inserted as depicted in ***figure.4*** where the tissue simulant begins at the phantom boundary FDTD Cell location (81) extending out to the truncation cell.

Case B) Phantom shell thickness changes are shown for the frequencies (3, 4.5, 5.8GHz) in ***figure.6*** where the comparison is made relative to shell versus no shell problem.

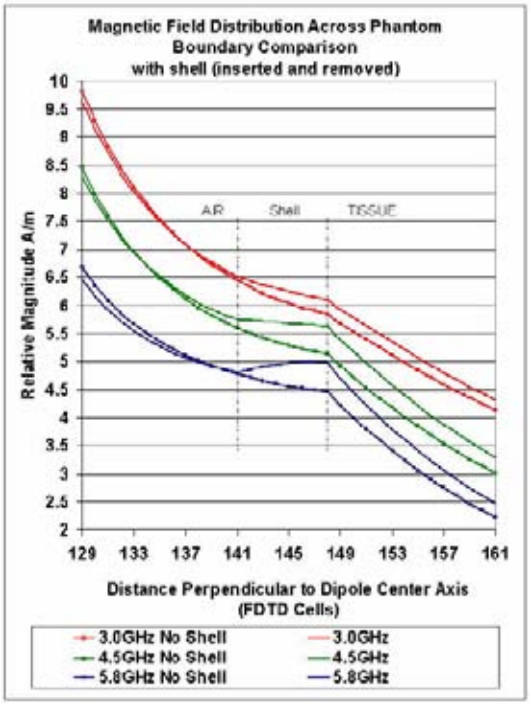

Figure.6 Shell v.s. HFM for Frequency Octave

It is apparent the shell has an effect which increases the magnitude of the magnetic field distribution across one frequency octave.

Case C) Phantom shell thickness changes are evaluated at 500MHz frequency steps shown for the frequencies (2.45 to 5.8GHz) in ***figure.7*** where the comparison is made relative to shell versus no shell.

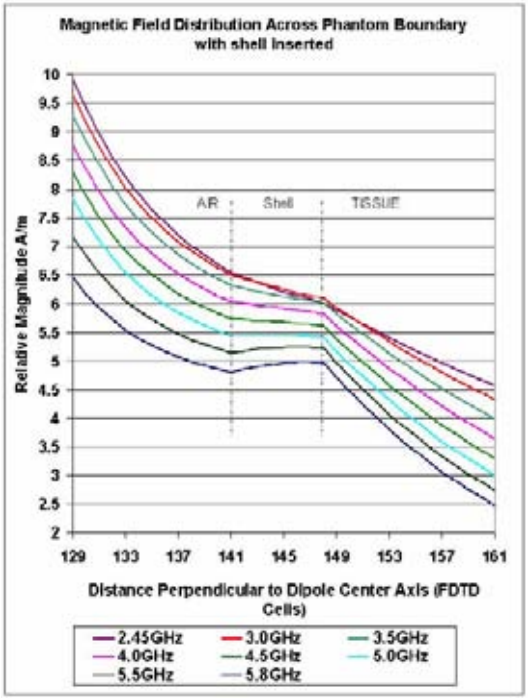

Figure.7 Shell v.s. HFM for 500MHz Frequency Steps

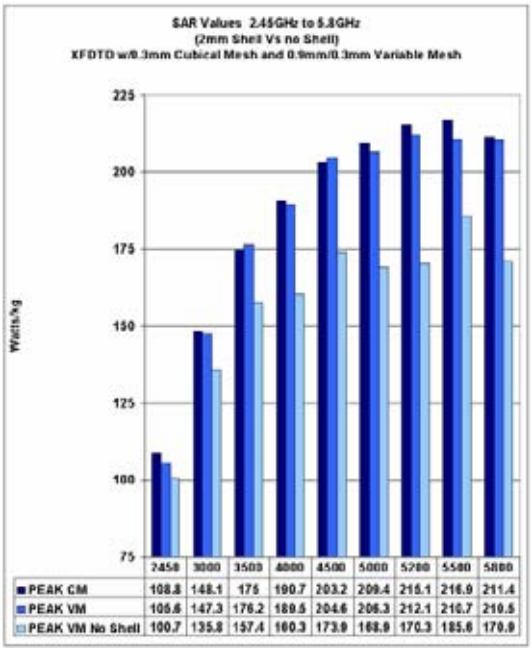

Figure.8 Shell v.s. SAR peak for 500MHz Frequency Steps

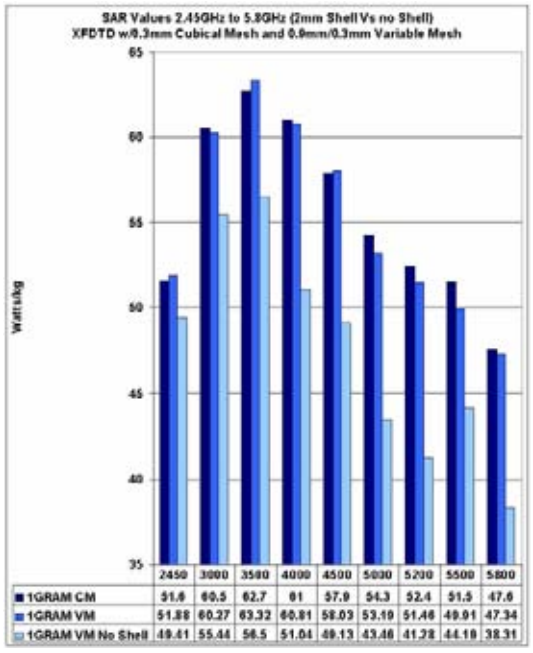

Figure.9 Shell v.s. SAR 1gram for 500MHz Frequency Steps

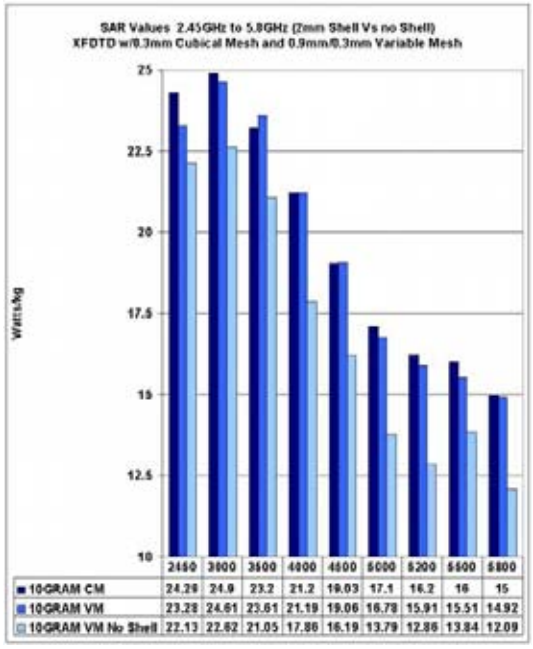

Figure.10 Shell v.s. SAR 10gram for 500MHz Frequency Steps

Problem Analysis

We begin our analysis by defining our phantom shell as a multiple interface problem as described with the help of a single dielectric shell outlined in ***figure.11***.

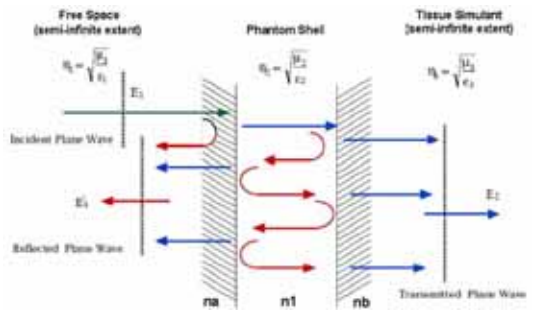

Figure.11 Single Dielectric Shell Equivalent Model

This two-interface equivalent diagram of the phantom shell has a dielectric shell η1 separating the semi-infinite tissue simulant ηb from free space ηa. Our boundary conditions define the tangential components of **E** and **H** fields and intrinsic impedance's (in the direction normal to the boundary) are continuous ***figure 12***.

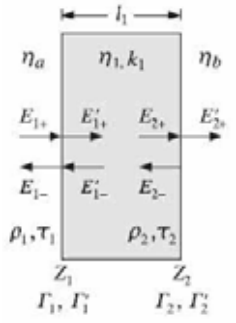

Figure.12 Single Dielectric Shell

Let l_1 be the width of the shell, $k_1 = \omega/c_1$ the propagation wave number, and $\lambda_1 = 2\pi/k_1$ the corresponding wavelength within the shell. We have $\lambda_1 = \lambda_0/n_1$, where λ_0 is the free-space wavelength and n_1 the refractive index of the shell. We assume the incident field is from the left medium η_a, and thus, in medium η_b there is only a forward wave. Let ρ_1, ρ_2 be the elementary reflection coefficients from the left sides of the two interfaces, and let τ_1, τ_2 be the corresponding transmission coefficients:

Energy conservation states that the energy flux into medium η1 must equal the energy flux out of it. It is equivalent to the following relationship between Γ and T, thus we call $|\Gamma_1|^2$ the reflectance of the shell representing the fraction of the incident power that gets reflected back into medium ηa as the transmission of the shell.

$$\frac{\mathcal{P}_{\text{transmitted}}}{\mathcal{P}_{\text{incident}}} = \frac{\frac{1}{2\eta_b}|E'_{2+}|^2}{\frac{1}{2\eta_a}|E_{1+}|^2} = \frac{\eta_a}{\eta_b}|\mathcal{T}|^2 = 1 - |\Gamma_1|^2 \qquad \text{eq. 2}$$

Conclusions

It is evident from the results ***figure 8, figure 9*** and ***figure 10*** that the phantom shell when used in a numerical problem as described within this paper is conservative where more of the available radiated incident power transfers across the boundary into the tissue simulant. Thus it can be assumed that this phenomenon of power transfer will be applicable to experimental SAR exercises where one can assume that the phantom shell adds to the conservative method for SAR evaluation. The phantom shell allows for a more efficient '*power transfer'* mechanism across the boundary into the tissue simulant liquid resulting in higher calculated SAR values ***figure 8, figure 9*** and ***figure 10***. The increase in SAR values from less available radiated power is brought on by a change in the dipole's input power efficiency factor.

Further Research and Considerations

The phenomenon as described within this paper shows that existing methodologies used for experimental SAR evaluations have met with a conservative mandate. Additional studies have been made which have led to claims of the need to enhance SAR values by post processing factors. When one takes into consideration the results of this study addition to the experimental SAR values at frequencies above 3GHz due to post processing factors are not needed as a phantom shell adds to the conservative nature of experimental SAR methods. Within this pilot project studies on electrical field effects on high resolution MRI FDTD models have been made where the goal has been to identify the effects of standing waves within complex heterogeneous tissues on final calculated SAR, and the results

of this shall be published in a later paper. By identifying a tissue layer where SAR can be seen to be more conservative one can assume homogeneous models can be derived which provide worst case SAR conditions. At this time Remcom and the Hershey medical institute as part of this pilot project which was sponsored by the WiFi Alliance have derived complex heterogeneous models based on high resolution MRI data sets, and have begun to expose these models to RF conditions similar to those as discussed in this paper.

The next series of problems will look at the following scenarios, and present the findings for use in experimental analysis with resultant publication of results and findings.

a) Create a numerical problem based on conservative heterogeneous tissue compositions, and expose to RF fields as described within this paper.

b) Create numerical problems based on homogeneous tissue composition resulting form the worst case data set as described in problem (a) and expose to RF fields as described within this paper.

c) Create numerical problems based on the homogeneous tissue composition resulting from the problem described (b) and include the APREL Laboratories Universal Phantom then expose to RF fields as described within this paper.

d) Compare all data and specify experimental protocols for final verification.

It can be assumed that if conservative values are shown to have a relationship with heterogeneous (a), and homogenous (b) results, then when the APREL Laboratories Universal phantom is introduced to the numerical problems (c) conservative SAR shall increase for both of the numerical problems and experimental investigations.

Thanks

The authors of this paper would like to acknowledge the WiFi Alliance for their help in sponsoring the research which led to this paper being written and published.

References

[1] Gabriel C, "Compilation of the Dielectric Properties of Body Tissues at RF and Microwave Frequencies", Brooks Air Force Base, report no. AL/OE-TR-1996-0037, 1996.

[2] Federal Communications Commission (FCC), http://www.fcc.gov/fcc-bin/dielec.sh, FCC web site on Tissue Dielectrics.

[3] Hurt W D, "Radiofrequency Radiation Dosimetry Workshop", Brooks Air Force Base report no. AL/OE-SR-1996-0003, 1996.

[4] Kunz K S, and Luebbers R J, "The Finite Difference Time Domain Method for Electromagnetics", CRC Press, 1993.

[5] Remcom, Inc., "XFDTD, The Finite Difference Time Domain Software for Electromagnetic Calculations", Version 6.05.25 October 2003 from Remcom, Inc. http://www.remcom.com.

[6] ANSI/IEEE, "IEEE Standard for Safety Levels with Respect to Human Exposure to Radio Frequency Electromagnetic Fields, 3 kHz to 300 GHz", ANSI/IEEE C95.1-1992.

[7] IEC 62209 TC106 revision(2), IEEE1528 and IEEE1529.

[8] H. R. Chuang, "Human Operator Coupling Effects on Radiation Characteristics of a Portable Communication Dipole Antenna," *IEEE Trans. on Antennas and Propagation*, vol. 42, no. 4, April 1994, pp. 556-560.

[9] A. Faraone, Q. Balzano and D. Simunic, "Experimental Dosimetry in a Sphere of Simulated Brain Tissue Near a Half-Wave Dipole Antenna," *IEEE Int. Symp. On EMC* , 1998, pp. 906-911.

[10] N. Kuster and Q. Balzano, “Energy Absorption Mechanism by Biological Bodies in the Near Field of Dipole Antennas Above 300 MHz.” *IEEE Trans. On Vehicular Technology,* vol. 41, no.1, Feb. 1992, pp. 17-23.

[11] M. A. Jensen and Y. Rahmat-Samii, “EM Interaction of Handset Antennas and a Human in Personal Communications,” *Proc. IEEE,* vol. 83, no. 1, Jan. 1995, pp. 7-17.

[12] D. Brooks, S. Nicol, Jacek Wojcik, “Wideband Complex Dipole Antenna Design for Reference measurements in the Human Body from RF Frequencies in the 5-6GHz Band” EMC Zurich, 2005, pp.97-102.

[13] Z. P. Liao, H. L. Wong, B. Yang, and Y. Yuan, ``A transmitting boundary for transient wave analysis," *Sci. Sin., Ser. A*, vol. 27, pp. 1063-1076, 1984.